Holographic investigation of visual circuits : Proof-of-concept of a new flexible two-photon microendoscopy system for all-optical interrogation of neuronal circuits for freely-moving animals

Florence Bui

THESE DE DOCTORAT DE SORBONNE UNIVERSITE

Spécialité :

NEUROSCIENCES

Ecole doctorale ED158 Cerveau Comportement Cognition
Préparée au Laboratoire Wavefront Engineering microscopy – Photonics Department
Institut de la Vision - Paris, France

Présentée par

Florence BUI

Pour obtenir le grade de

DOCTEUR DE SORBONNE UNIVERSITE

Sujet de la thèse :

HOLOGRAPHIC INVESTIGATION OF VISUAL CIRCUITS

"Proof-of-concept of a new flexible two-photon microendoscopy system for all-optical interrogation of neuronal circuits for freely-moving animals"

Dirigée par

Dr. Valentina EMILIANI -Directrice du laboratoire

Co-supervisée par

Dr. Valeria ZAMPINI – Biologie
Dr. Nicolo ACCANTO – Physique

Présentée et soutenue publiquement le 26 Novembre 2021

Devant le jury composé de

Dr. Valentina EMILIANI – Directrice de thèse
Dr. Anna BEYELER – Rapportrice
Dr. Amanda FOUST – Rapportrice
Dr. Alberto BACCI – Examinateur

To all humans and heroes, smiles and mice,
who did, do, and will nurture our brains, merci.

Sincerely,

FBI.

Acknowledgments

I would like to deeply thank my jury committee for accepting to read my manuscript and evaluate my thesis project. Thank you Dr. Anna BEYELER from Neurocentre Magendie in Bordeaux and Dr. Amanda FOUST from Imperial College London in United Kingdom for being my duo of evaluators and Dr. Alberto BACCI from Institut du Cerveau et de la Moelle Epinière in Paris for being my examinator. A warm thank to you and Dr. Christoph SCHMIDT-HIEBER from Pasteur Institute in Paris for your advice during my follow-up committee, for your encouraging reports, I had a real pleasure to discuss with you about Neuroscience.

My doctoral work was done in the laboratory of Dr. Valentina EMILIANI, head of Wavefront Engineering Microscopy Laboratory and director of the Photonic Departments. My thesis journey was co-supervised by Dr. Valeria ZAMPINI, Research Engineer in Neurobiology and Dr. Nicolo ACCANTO, awarded Researcher in Optic Physics. I would like to deeply thank all of you! Some years ago, I chose to join your interdisciplinary group for your strong implication in the development of new microscopes and optogenetics for Neuroscientists. Then during my first PhD year, we moved from St-Pères in the chic district St-Germain-des-Prés to the place of my very first lab experience: Institut de la Vision near Bastille: *grazie mille* Valentina! It was a blast organizing all celebrations for you and seeing the lab growing. Valeria, thank you for your empathy, for introducing me to patch, for your supervision and guidance in Biology. Nicolo, there are not enough words to express my gratitude to you. You teach me about everything! From imaging treatment to basis in optics and analysis. I know it was a challenge to translate it to a young biologist, thank you for your patience. You were a great mentor! I was happy to be part of the 2P-FENDO adventure, thank you for giving me this opportunity. You will always be an inspiration and congratulations for your career.

Christophe TOURAIN, notre Monsieur Géo Trouvetou, merci d'avoir accepté de designer et fabriquer mes demandes les plus farfelues, du support 3D pour les tranches de cerveau, aux souris miniatures et implants en tout genre… C'est toujours un plaisir de travailler avec toi, ton atelier est une vraie mine d'or, j'espère que je pourrais toujours passer admirer tes oeuvres. Ta gentillesse et ton savoir-faire m'impressionneront toujours ! Vincent DE SARS, l'inventeur du logiciel Wavefront, tu es l'un des premiers que j'ai rencontré un matin d'été 2016, merci pour ton accueil et bon courage pour les versions 10.0. Imane BENDIFALLAH, je te remercie pour ta joyeuse compagnie en culture cellulaire, d'avoir continué le projet scanning/holography et montré les coulisses organo'. Bon courage pour ta these! Aysha LAFIRDEEN, a warm thanks for handling the organotypic culture and viruses, above all thanks for supporting my obsession for organization in the lab. It was fun to do it with a friend. Antonio LORCA, I am happy you arrived in the lab for your PhD, it was a pleasure to finish the experiments with a clever graduate in Optics. François BLOT, the French man from Netherlands, it was a real pleasure to meet you those last months. Thank you for our meaningful discussions about Science, I wish we met earlier and wish you now the best. To Serge CHARPAK and Marine TOURNISSAC, thank you for your help about whisker stimulation, it was a pleasure to work with you. Thanks to Noam BADT and Ori KATZ from Weizmann Institute for the collaboration. To Manuela ALLEGRA from Pasteur and Joanna SCWHENKGRUB from Gif, thank you showing me your implant surgeries. Merci à toute l'équipe de l'animalerie, Manuel SIMONUTTI, Julie DEGARDIN, Quénol CESAR et au matinal Andrei ; à Stéphane FOUQUET de la plateforme confocale et Marie-Laure NIEPON en histologie. Thanks to all suppliers I did deal with and provided us (Mr Montagne & Eric Marty from Phymep, Harvard App, Stoelting, Olympus, Nightsea EMS, JanvierLab, Addgene etc.) and airports! Merci Zober et Romuald d'avoir tout réceptionné.

Eirini PAPAGIAKOUMOU, I am honoured you gave me the first lesson in Optics when I arrived in the group, and I will always admire your bravery, sense of aesthetics and scientific rigour. Emiliano RONZITTI, it was a pleasure to organize the internal "WEMinar" with you. Grazie a Dimitrii TANESE e Giulia FAINI per la vostra compagnia durante le lunghe serate in laboratorio. I-Wen CHEN, thank you for showing your viral injection procedure and sharing the *in vivo* setup for my preliminary experiment needs. Ruth SIMS, what a nice melody to my ears to listen to your beautiful British speaking! I will deeply miss your foolproof enthusiasm, literally "fan" of it! Osnath ASSAYAG, thank you for sharing your desk and super coffee machine, I am glad to have met such an impressive woman as the director of *3i* France!

I would like to thank all lab members, past and present from EMILIANI's and TESSIER's teams, including Gilles, Abeer, Tengfei, Haithem, Fabio, Fabrice and co. Bravo to the former PhD, now Doctors and much more. Special thanks to Alexis PICOT, I was happy to be your copilot for 2 years and thanks for your unconditional support and engagement with the PhD society, I am glad to call you my friend. To Marta GAJOWA for your kind listening, Marco PASCUCCI for your cuccina love, Minh Chau NGUYEN and Chang LIU for your kindness and all former graduates for your works, we never met but you were part of it. To Massilia HAMDANI, Joe CHAN and Cécile TELLIEZ, good luck for your PhD. To Pr. Benoît FORGET and Pr. Robert KUSZELEWICZ, it was always a nice surprise or great lesson to be with you. To Verena TODDE and Elisa PREIRA, thank you for replying so fast to our regular "urgent" orders. Danke schön Chrissy GRIMM, die Viren sind jetzt in guten Händen! To Pascal BERTO, thank you for your enthusiasm, you are the sunniest person I have ever met! To all the people I have met at St Pères & IDV, you participated in some way. To all amazing Scientists I had the chance to meet, special thanks to Ben SCHOLL from USA for your positive energy, Sophie BOUCCARA from Israël and Sculpted Light Brain conf' for their impressive work and insightful discussions.

Parce que ce n'est pas juste quelques années de thèse. Ce sont les rencontres et les expériences du passé qui m'ont forgé et m'ont permis d'aboutir à ce travail. Je pense particulièrement à Emilie MACE qui m'a donné envie de rejoindre les Chercheurs, merci de m'avoir fait confiance si tôt ! A Olivier MARRE, nous n'avons finalement jamais travaillé ensemble mais tu as toujours trouvé le temps de me conseiller, merci. A Deniz DALKARA pour ta gentillesse. A Valérie FRADOT pour m'avoir encouragé si tôt pour les chirurgies fines. A Serge PICAUD, je suis fière d'avoir croisé ton chemin et partagé ton bureau, bravo pour ta récente nomination comme Directeur de l'Institut de la Vision. Au fondateur José-Alain SAHEL, merci pour votre grande idée ! Je suis heureuse d'avoir fêté les 10 ans avec vous et Emmanuela DE LUCA, Alvaro RENDON, Arnault BRICOUT. To Michael HÄUSSER, Adam PACKER, Lloyd RUSSELL and Henry DALGLEISH, my "Cor Blimey" crew, thank you for giving me the opportunity to work with you before my thesis. To my big sister Zoe, thanks for bringing spark in my life! A Gaëlle CHAPUIS, ma Suisse préférée, merci de m'avoir appris à coder dans le métro londonien ! A tous mes collègues de fac à Jussieu et ma marraine Anaïs A., j'ai grandi avec vous, merci ! A Gaël ORIEUX et Gregory GAUVAIN and co, merci pour les cours sur la vision ! A Dr. J. LE GOASTER, merci de m'avoir appris à ne jamais abandonner et toujours viser plus haut. A mon cher Romain B., merci pour la relecture du manuscrit ! Never give you up de Rick Astley, retentit même de l'autre côté de la Manche ! Aussi, une pensée pour mes amis de l'association Symbiose6, passés et futurs. A la directrice du Master Biologie, Patricia SERRADAS, le Directeur de l'Ecole Doctorale Cerveau Cognition Comportement Alain TREMBLEAU et tous mes professeurs de la Sorbonne Université qui m'ont fait confiance, merci !

A mes camarades du MBA de la promotion Science & Management, particulièrement à Antoine A, Koudedja C, Etienne C, je pense à vous, merci pour vos encouragements. Merci au fondateur du Collège des Ingénieurs Philippe MAHRER pour la double expérience en or ; à Bruno BOULAY, Anne MOTTE, Alain DERIEZ pour votre bienveillance. Grâce à vous, j'ai rencontré des scientifiques, entrepreneurs et PDG hors pair !

A ma maman, la vraie docteur, pour ton soutien et ta patience, à ces jours et nuits blanches où tu es restée à mes côtés puis à tes bons plats, sans quoi, je n'aurais pas eu l'énergie de me lever, cảm ơn Mẹ ! A mon papa, le vrai héros, pour ton écoute et ton dévouement, tu m'as permis de faire mes études jusqu'au bout, tu m'as suivi dans mes projets fous avec tes astuces par milliers et tu as toujours répondu à mes SOS, merci ! A mon petit frère, mon graphiste attitré, merci pour ton talent pour la mise en page de ce manuscrit. Je te souhaite le plus beau des futurs, qui s'annonce prometteur ! A toute ma famille, tous mes cousins, Pascal & Dominique, Jeannine, mes haut-savoyards puis Denis & Erika, qui même si vous ne compreniez pas mon travail, m'avez soutenu à votre manière, des 4 coins de la France et du Monde. Spécial merci à ma grand-mère Bà Nội Rose pour m'avoir tant gâtée avec ta cuisine toujours excellente et à ma tante Eida pour avoir gardé un œil sur moi ! A feu Ông Nội, Ông Ngoại, Bà Ngoại, Ông Lan, je pense fort à vous.

A mes Princesses, à ma Mélou, Aurélien, Cédric, Thibault pour ta cuisine d'amour[2], Jkl & Térence mes colocs de toujours, et tous mes amis, merci d'avoir supporté mes humeurs et essayé de me faire sortir de mon mode ermite ! A Clément MOLINIER, mon roc, merci ! Ton ingéniosité et enthousiasme me surprendront toujours. Merci de m'avoir supporté tous les jours, soutenu quoi qu'il arrive et redonné le sourire à toutes les épreuves, je dis bien toutes. A l'Avenir !

Enfin, à toutes les héroïnes et tous les héros dont je garde précieusement les visages et les prénoms dans mon cœur, vous m'avez littéralement sauvé la vie et cette thèse par la même occasion, MERCI !

Acronyms & abbreviations

1P	one-photon
2P	two-photon
3P	three-photon
GFP	green fluorescent protein
Ca^{2+}	calcium
AP	action potential
GECI	genetically encoded calcium indicator
GEVI	genetically encoded voltage indicator
SNR	signal noise to ratio
ChR2	channelrhodopsin 2
AAV	adeno-associated virus
NA	numerical aperture
IR	infrared
CGH	computer generated holography
SLM	spatial light modulator
PSF	point spread function
TF	temporal focusing
GRIN	gradient refractive index
AO	adaptive optics
FWHM	full width at half maximum
WF	widefield
SC	scanning
FOV	field of view
L2/3 of V1	layer 2/3 of the primary visual cortex
GL1	GRIN lens #1 GT-MO-070-016-ACR
GL2	GRIN lens #2 GT-MO-080-032-ACR-VISNIR-08CG-20
2P-FENDO	two-photon flexible microendoscopy

Préface

1. Contexte

Comprendre comment le cerveau code l'information est l'un des grands défis scientifiques de notre époque. Dépeindre le processus neuronal signifie déchiffrer et mieux comprendre les circuits neuronaux qui donnent naissance à la perception et guident le comportement. En d'autres termes, décoder la communication entre les multiples neurones et les signaux qui sous-tendent le fonctionnement et le dysfonctionnement du cerveau est au cœur des grandes quêtes scientifiques. Au cours des dernières décennies, les neurosciences ont fait des progrès exponentiels dans l'enregistrement et l'imagerie de la communication entre les neurones. En outre, les généticiens ont récemment développé la capacité de manipuler les neurones avec la lumière grâce à l'expression de protéines microbiennes activées par la lumière, appelées "opsines". Ce nouveau domaine révolutionnaire, désormais appelé optogénétique, transforme la recherche en neurosciences et promet de permettre aux neuroscientifiques de piloter et de lire les circuits neuronaux et de déterminer comment ils donnent naissance aux sensations, à la perception et aux fonctions cognitives. Pour déchiffrer le code neuronal, il est désormais nécessaire d'examiner de plus près comment les neurones individuels des circuits collaborent pour établir le comportement. Pour atteindre une résolution aussi fine et imiter l'activité neuronale rapide à l'échelle de la milliseconde, le laboratoire dirigé par Valentina Emiliani a développé des outils optiques de pointe basés sur des approches de mise en forme du front d'onde (comme l'holographie générée par ordinateur (Papagiakoumou *et al.* Optic Express 2008)) pour la manipulation optogénétique de plusieurs neurones (Hernandez *et al.* Nature Com. 2016; Accanto, Molinier *et al.* Optica 2018, Chen *et al.* JNeuro. 2019).

2. Motivation

L'activité cérébrale est à la base du comportement ; elle détermine notre perception et la façon dont nous réagissons à l'environnement extérieur. Pour déchiffrer la fonction de circuits neuronaux complexes, nous devons donc les étudier dans des conditions qui ressemblent de près au comportement naturel. La mise au point d'un nouveau microendoscope optique permettant de contrôler avec précision les neurones au niveau de la cellule unique et son extension à l'étude d'animaux se déplaçant librement pourraient donc fournir la clé pour élucider le lien entre l'activité neuronale et le comportement. Le développement, l'optimisation et le test d'un tel microendoscope *in vivo* est au cœur de mon projet de thèse. Des systèmes de microendoscopie ont été précédemment développés principalement pour imager l'activité neuronale chez des rongeurs se déplaçant librement (Ghosh *et al.* Nature Methods 2011, Szabo *et al.* Neuron 2014, Aharoni *et al.* Front. Cell Neuro. 2019, Helmchen *et al.* Cold Spring Harb. Protoc. 2013, Zong *et al.* Nature Methods 2017, Ozbay *et al.* Sc. Reports 2018) avec des approches d'imagerie à un (1P) et deux (2P) photons. Néanmoins, elles présentaient certaines limites. Par exemple, les microendoscopes 2P actuels sont limités en vitesse d'imagerie à 3-40Hz. Pour citer l'inconvénient le plus important, aucun microendoscope 2P n'a été développé jusqu'à présent avec la capacité d'effectuer une photostimulation 2P au niveau de la cellule unique. Pour une exploration complète des fonctions cérébrales, des mesures précises et, surtout, la capacité d'induire avec précision l'activation des neurones, préalablement identifiés, sont essentielles.

3. *Projet de thèse*

NOUVEAU MICROENDOSCOPE FLEXIBLE POUR L'IMAGERIE FONCTIONNELLE À HAUTE VITESSE ET LA PHOTOSTIMULATION *IN VIVO* POUR L'ANIMAL MOBILE

Ce projet de recherche a évolué au sein d'une équipe multidisciplinaire et un nouveau microendoscope 2P flexible (2P-FENDO) a été développé grâce à la collaboration de physiciens et de biologistes dans le but de surmonter les limitations susmentionnées de la microendoscopie, à savoir la faible vitesse d'imagerie et l'absence de photostimulation précise des cellules. La première validation des performances du système a été effectuée *in vivo* chez des souris dans une configuration où la tête est fixée. Avec cette approche, nous avons réussi à démontrer l'imagerie morphologique de neurones uniques avec une haute résolution axiale. De plus, nous avons pu réaliser une imagerie bicolore (GFP et TdTomato) jusqu'à une profondeur de ~200µm dans le cerveau de la souris. Grâce à l'indicateur calcique le plus récent (Dana et al. Nature Methods 2019), nous avons obtenu une imagerie rapide de l'activité des neurones exprimant GCaMP7s en utilisant l'imagerie 2P (50-100Hz) dans un grand FOV (250*250*200 µm3). Après avoir identifié les neurones spontanés et évoqués visuellement, la photostimulation à la résolution d'une cellule unique d'un groupe de neurones exprimant l'opsine a été accomplie en utilisant l'approche holographique 2P. 2P-FENDO est maintenant prêt à être utilisé dans la configuration où les animaux sont mobiles et ces expériences sont toujours en cours dans le groupe. L'application ultérieure des systèmes peut également impliquer des implants chroniques du système de microendoscopie dans le cerveau des animaux afin d'accéder à des régions cérébrales plus profondes et de permettre des enregistrements et des stimulations répétitifs chez les mêmes animaux. Pour préparer des études similaires, nous avons commencé à développer des implants pour les souris et à mettre au point des préparations chirurgicales. Nous pensons que 2P-FENDO contribuera à l'étude des mécanismes régulant la connectivité fonctionnelle et le traitement des signaux, par exemple, dans l'ensemble du système visuel ou des études neuronales impliquant la nécessité de disposer d'animaux libres de leurs mouvements, en combinant ces méthodes innovantes de sculpture de la lumière avec de nouvelles opsines. Pour résumer, de l'ensemble préliminaire *in vitro* aux techniques optimisées *in vivo*, j'ai participé au développement et établi la preuve de concept d'un nouveau système de microendoscopie flexible 2P pour l'étude tout-optique des circuits neuronaux chez la souris agile. Nous avons démontré que notre innovation surpasse les microendoscopes précédents en termes de vitesse d'imagerie et de capacité de photostimulation des neurones. Nous pensons que ce nouveau microendoscope pourrait être utilisé pour étudier les circuits cérébraux des animaux agiles et mobiles.

Preface

1. Context

Understanding how the brain encodes information is one of the scientific grand challenges of our times. Depicting the neuronal process means to decipher and gain more insights in neural circuits to give rise to perception and guide behaviour. In other words, decoding the communication between multiple neurons and signals underlying the brain function and dysfunction is at the heart of major scientific quests. Over the past decades, Neuroscience has made exponential progress towards recording and imaging communication between neurons. In addition, geneticists have recently developed the capability to manipulate neurons with light through the expression of light-activated microbial proteins called "opsins." This new revolutionary field, now called optogenetics, is transforming neuroscience research with the promise of enabling neuroscientists to drive and read neural circuits and determine how they give rise to sensation, perception, and cognitive function. To decipher the neuronal code, it is now necessary to have a closer look at how individual neurons in the circuits collaborate together to establish behaviour. To reach such fine resolution and to mimic fast neuronal activity at the millisecond scale, the laboratory led by Valentina Emiliani has been developing cutting-edge optical tools based on wavefront shaping approaches (such as computer generated holography (Papagiakoumou *et al.* Optic Express 2008)) for optogenetic manipulation of multiple neurons (Hernandez *et al.* Nature Com. 2016; Accanto, Molinier *et al.* Optica 2018, Chen *et al.* JNeuro. 2019).

2. Motivation

Brain activity is at the basis of behaviour; it determines our perception and the way we react to the external environment. For deciphering the function of complex neuronal circuits, we thus need to study them in conditions that resemble closely natural behaviour. Developing a new optical microendoscope to precisely control neurons on the single cell level and extending it to the study of freely-behaving animal could therefore provide the key to elucidate the link between neuronal activity and behaviour. The development, optimization, and test of such microendoscope *in vivo* is at the heart of my thesis. Microendoscopy systems were previously developed mainly to image neuronal activity in freely-moving rodents (Ghosh *et al.* Nature Methods 2011, Szabo *et al.* Neuron 2014, Aharoni *et al.* Front. Cell Neuro. 2019, Helmchen *et al.* Cold Spring Harb. Protoc. 2013, Zong *et al.* Nature Methods 2017, Ozbay *et al.* Sc. Reports 2018) with single- (1P) and two-photon (2P) imaging approaches. Nevertheless, they presented some limitations. For example, current 2P microendoscopes are limited in imaging speed to 3-40Hz. To cite the most important drawback, no 2P microendoscope was so far developed with the capability of performing 2P photostimulation at the single cell level. For the complete exploration of brain function, precise measurements and above all, the capability to precisely induce spiking activity in selected neurons are essential.

3. *Thesis project*

NEW FLEXIBLE MICROENDOSCOPE FOR HIGH-SPEED FUNCTIONAL IMAGING AND PHOTOSTIMULATION *IN VIVO* FOR FREELY-MOVING ANIMALS

This research project evolved in a multi-disciplinary team and a new flexible 2P microendoscope (2P-FENDO) was developed thanks to the collaboration of physicists and biogists with the objective of overcoming the aforementioned limitations in microendoscopy, i.e., the low imaging speed and the absence of cell-precise photostimulation. The first validation of the performances of the system were done *in vivo* in mice in a head-fixed configuration. With this approach, we managed to demonstrate morphological imaging of single neurons with high axial resolution. Besides, we were able to carry out two-colour imaging (GFP and TdTomato) until a depth of ~200µm in the mouse brain. With the newest engineered calcium indicator (Dana *et al.* Nature Methods 2019), we achieved fast activity imaging of GCaMP7s expressing neurons using 2P imaging (50-100Hz) in large FOV (250*250*200 µm3). After identifying both spontaneous and visually evoked neurons, the photostimulation at the single cell resolution of a group of opsin expressing neurons was accomplished using 2P holographic approach. 2P-FENDO is now ready to shift to a freely-moving configurations and experiments are still ongoing in the group to reach such goal. Further application of the systems can also involve chronic implants of the microendoscopy system in the animal brain to gain access to deeper brain regions and to allow repetitive recordings and stimulations within the same animals. To prepare for similar studies, we have started to develop implants for mice and debug surgical preparations. We believe that 2P-FENDO will help to investigate the mechanisms regulating functional connectivity and signal processing, for example, across the visual system or neural studies implying the necessity of freely-behaving animals, by combining these innovative light-sculpting methods with engineered new opsins. To put in a nutschell, from the preliminary set *in vitro* to optimized techniques *in vivo*, I participated in the development and established the proof-of-concept of a new 2P flexible microendoscopy system for all-optical investigation of neuronal circuits in mice. We demonstrated that our innovation outperforms previous microendoscopes in the imaging speed and the capability of photostimulating neurons. We believe that this new microendoscope could be used for interrogating brain circuits for freely-behaving animals.

Table of contents

I. INTRODUCTION

Contents

I.1 All-optical manipulation with 2P optogenetics

Shedding light on neuronal circuits at the single cell resolution to understand the mechanisms of the animal and human brains has been the dream of most scientists for a century. Neural circuits dynamics and their relations are at the base of behaviour, but these relations and how information relevant to behaviour are processed are still poorly understood. In particular, the order of neuronal connectivity should be considered: the firing order of neurons in a circuit reflects the organisation of connections between presynaptic and postsynaptic neurons. The series, the order and the timing of firing patterns are essential, and they should be considered to understand the operational principles of neuronal circuits. To decipher neuronal circuits, one should ideally be able to play with the notes (cells) of the brain partition (circuit). Hence, the holy grail is to perform in concert, both recording neuronal activity by imaging and "replaying" it by manipulating neurons one by one or in patterns, by maintaining high precision in time and space.

Aiming at this complete experimentation scheme, optogenetics (Boyden *et al.* **Nature Neuro.** 2005) has paved the way to all-optical approaches. Without the need of relying on most hand-demanding skills during the experimentation and overcoming the limitations of electrophysiological techniques (the limited number of cells that can be monitored simultaneously, and the exact location and identification of them), optical methods represent new powerful tools for observing and manipulating brain circuits. Two photons optogenetics enables simultaneous recording and manipulation of neuronal activity with the possibility to precisely deliver light on one or multiple cell-targets (Packer *et al.* **Nature Methods** 2012). It is a less invasive approach that can maintain intact the connections between neurons while allowing manipulation of single cells also in *in vivo* preparations.

This "all-optical" readout and manipulation of activity in neural circuits relies on genetically encoded sensors and actuators. The all-optical technique is a breakthrough method that improves continuously thanks to developments in optical microscopy and in molecular tools (Emiliani *et al.* **J. Neuro.** 2015). From the first experiments of cell imaging, countless discoveries have seen the light in various fields including physics, chemistry, and biology to enable reading of neuronal activity with genetic calcium indicators or voltage sensors.

This introduction aims to tell the fascinating story from the onset of microscopy to the latest high-resolution microendoscopy and to expose all principles needed to understand the physical and the biological concepts. I will describe a new microendoscope that we developed for in depth investigation of neuronal circuits in freely moving animals using an all-optical method.

I.1.1 Reading with genetically encoded calcium indicators

History of microscopy

The first microscopes appeared in the 17th century with Anton van Leeuwenhoek, and enabled the description of bacteria, yeast, microbes, and the circulation of blood corpuscles. In 1665, Robert Hooke, first coined the term "cell". Two centuries later, the term "neuron" came forth. Starting with Ramon Y Cajal in 1899, with the first meticulous drawing of a neuron in a silver-stained tissue through a microscope (**Fig.I.1**), the fields of neuroscience and microscopy have tremendously evolved towards the current concept of all-optical manipulation of neurons. Awarded the Nobel Prize of Medicine and Physiology with Camillo Golgi in 1906, the founder of modern neuroscience, brought two brilliant insights: he discovered that every neuron in the brain is a separate unit, and that neurons communicate across synapses. Nevertheless, the Golgi's method (the silver staining technique) to visualize neurons under light microscopy, used a tissue fixed in paraformaldehyde, impregnated of potassium dichromate and silver nitrate, and sliced with a thickness of 20-100 µm. Afterwards, new techniques for visualizing alive cells and their connections were developed in the late 20th century for both *in vitro* and *in vivo* experiments. Cell imaging became a fundamental aspect of most cell biology projects and is still in continuous development. Some techniques include the scanning and spinning disk confocal microscopy, multi-dimensional live-cell imaging systems and multi-photon excitation microscopy.

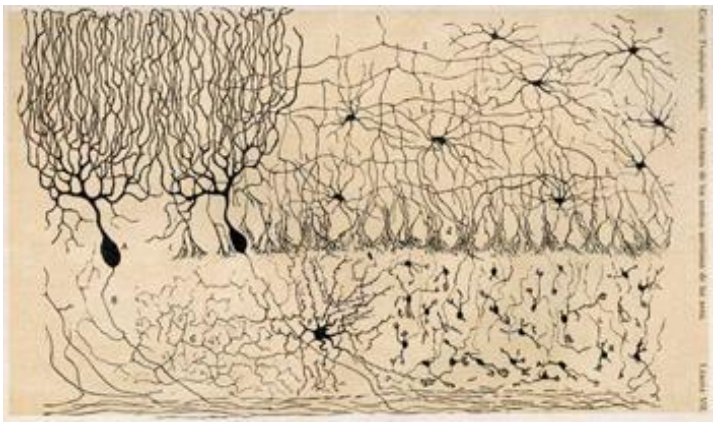

Fig.I.1. First drawing of neurons by *Ramon Y Cajal*
based on silver staining technique on fixed brain tissue (1899)

Genetically encoded calcium indicators

To selectively detect cells and their functional activity, fluorescent biomarkers present an undeniable advantage. In 1962, the discovery, cloning and application of green fluorescent protein (GFP), purified from the Pacific Ocean jellyfish *Aequorea victoria,* had a transformative impact in biological research (Shimomura *et al.* **J. Microsc.** 2005), and leading to the Nobel Prize in Chemistry in 2008 to Roger Tsien and his colleagues Osamu Shimomura and Martin Chalfie (**Fig.I.2.**). Engineering GFP expression in living organisms has spread its use as a reporter of gene expression and as a fusion tag to mark protein localisation and dynamics (Pracher *et al.* **Gene** 1992). The numerous genetically encoded fluorophores now comprise multiple spectral forms of

the GFP protein, such as cyan (CFP) and yellow fluorescent protein (YFP) and other red versions (mScarlet, mRuby etc).

Genetically encoded calcium indicators (GECI) are protein-based fluorescent indicators for calcium. The first prototype dates from 1997 (Romoser *et al.* **J. Biol. Chem.** 1997). Its design is modelled on Low Molecular Mass (LMM) organic compounds in which a fast calcium-binding molecule is structurally combined with a bright fluorescent protein that would result in a change of fluorescence output upon binding of calcium (Grynkiewicz *et al.* **J. Biol. Chem.** 1985). I will focus on the GCaMP family of GECI as the most widely used protein calcium sensors. Initially developed in 2001 by Junichi Nakai, GCaMP structure consists of circularly permuted green fluorescent protein (cpGFP) fused with the calcium-binding protein calmodulin (CaM) and the CaM-interacting M13 peptide, a domain of myosin light-chain kinase. The complex CaM/M13 is next to the chromophore. The conformational change following calcium binding would cause an increase of brightness, ensuring a large modulation of fluorescence with the increase in calcium concentration (Knöpfel, **Nature** 2012). (**Fig.I.3.**). Protein-based reporters can be either a single fluorescent protein or a pair of fluorescent proteins suitable for Förster Resonance Energy Transfer (FRET). The mechanism consists in energy transfer from a donor chromophore in its electronic excited state to an acceptor chromophore. The ratio of the fluorescent signals from the donor and acceptor component is interpreted as a measure of calcium concentration, independently of indicator concentration, excitation light intensity, and absorption in the optical path.

GECI are used to perform functional calcium imaging, a method widely used to optically record Ca^{2+} concentration changes linked to cell activity. Indeed, the neuronal action potential activity can be inferred from the fluorescence measurements. $Ca^{2+}$is a second messenger for numerous somatic, dendritic and axonal events, from the neurotransmitter release to the regulation of neuronal excitability, plasticity and gene expression (**Fig.I.4.**). Essentially, cytoplasmic Ca^{2+} concentration at rest is maintained at about 50–100 nM, but when a neuron fires an action potential, its plasmatic concentration increases via multiple routes, due to Ca^{2+} influx into the cell through voltage-gated calcium channels. Immediately after the action potential, Ca^{2+} extrusion from the cytoplasm occurs via Na+/Ca2+ exchangers or ATP-driven pumps. In cortical neurons during an action potential, the intracellular Ca^{2+} rises of about 150-300 nM within 10 ms, showing a half decay time of 50–70 ms (Helmchen *et al.* **Biophys. J.** 1997).

The characteristics of Ca^{2+} dynamics in a cell, combined with the brightness of optimized indicators, make calcium indicator responses advantageous in terms of photonic output and thus easier to detect. For example, a single AP can be initiated and completed within 3–5 ms, before the calcium transient even reaches its peak (Lin and Schnitzer, **Nature Neuro**. 2017). Therefore, the fluctuations of fluorescence from GECI, as indirectly linked to variations in calcium concentration, are reflecting the activity of neurons. The slower kinetics of the resulting calcium transients allow them to be detected at sampling intervals of 30–60 ms (Chen *et al.* **Nature** 2013). To date, many variants of GECI have been engineered to tune specific applications, such as subcellular or class-specific neuronal targeting, faster kinetics for fast events detection, different excitation/emission wavelengths for multicolor imaging, or improved brightness for single action potential detection. (Tian *et al.* **Nature Methods** 2009 ; Akerboom et al. **J.Neuro** 2012 ; Chen *et al.* **Nature** 2013 ; Dana *et al.* **PlosOne** 2016, **Nature Methods** 2019 ; Subach *et al.* **Int. J. Mol. Sci.** 2020) **(Fig.I.5.)**

Fig.I.2. Painted Petri dish by *Roger Tsien* with palette of fluorescent proteins (2004)

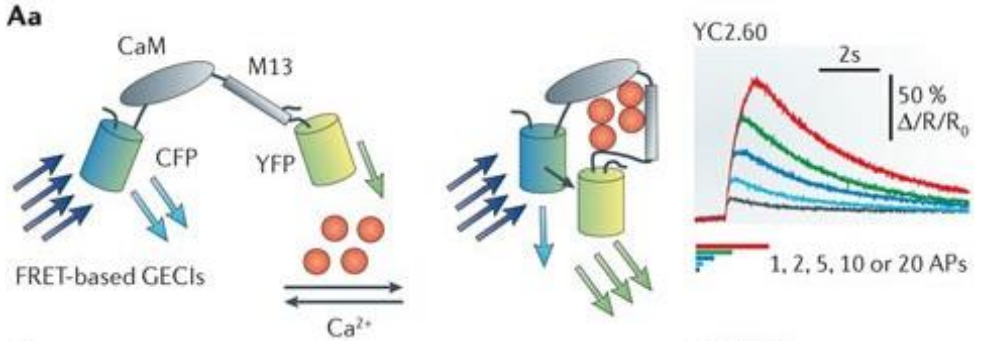

Fig.I.3. Genetically encoded calcium indicator basics (from Knöpfel, **Nature** 2012)

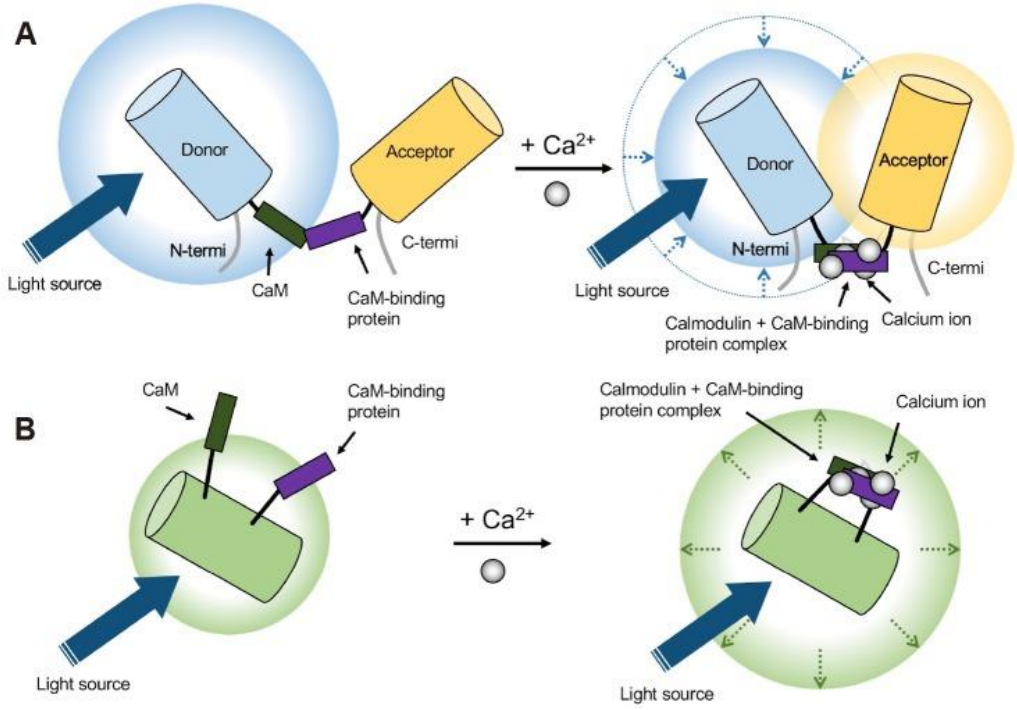

Fig.I.4. GECI, FRET and GCaMP principles (from Oh *et al.* **Korean J Physiol Pharmaco.** 2019)

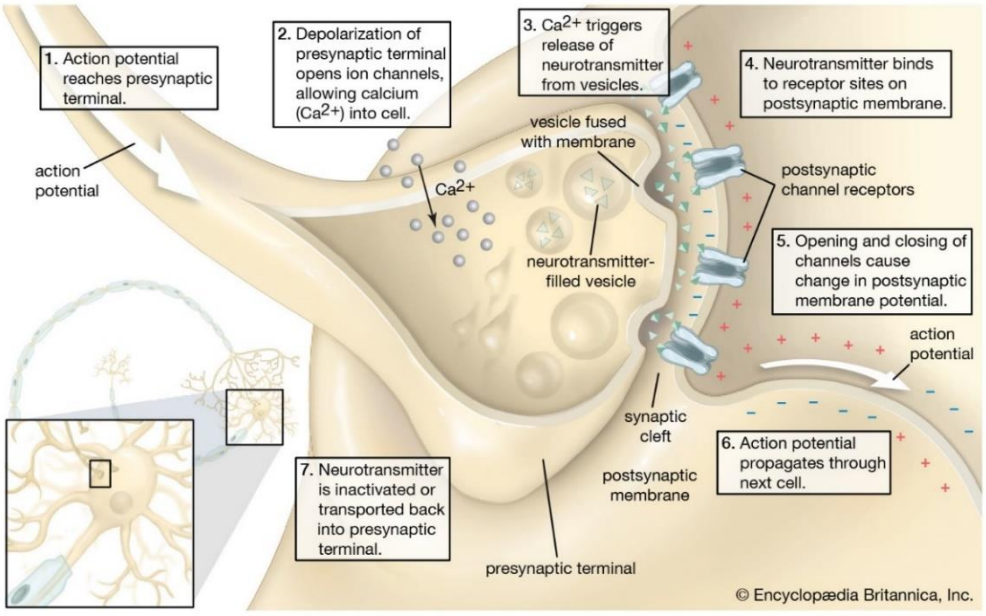

Fig.I.5. Action Potential mechanism with Ca2+ increase in pre- and post-synaptic neuron

Advantages and drawbacks of GECI

Optical monitoring of neuronal circuits activity has been successfully applied for behaviour investigations (Russell *et al.* **bioxriv** 2019; Dalgleish *et al.* **eLife** 2020; Robinson *et al.* **Cell** 2020 (Michäel Häusser Lab)), for local synaptic connectivity studies (Ko *et al.* **Nature** 2011; Carillo-Reid *et al.* **Science** 2016, **Current Op. Neurobio.** 2020 (Rafael Yuste Lab); Cossart **Current Op. Neurobio.** 2014), and for dissection of mechanisms involved in sensory-motor integration, perception, and memory formation. (Möser *et al.* **Cold Spring Harb. Perpect. Bio** 2015 (May-Britt and Edward Möser Lab); Forli *et al.* **Cell Rep.** 2018 (Tommaso Fellin Lab); Allegra *et al.* **Neuron** 2020 (Christoph Schmidt-Hieber Lab); Schwenkgrub *et al.* **Science Advances** 2020 (Brice Bathelier Lab)). Imaging through brain tissue results in a loss of spatial resolution due to light scattering, and this as we will see below can be improved by using two-photon excitation which enables reaching cellular resolution imaging at depths up to about 800 μm, using a spot with a point spread function of less than 1 μm diameter. (Helmchen *et al.* **Nature** 2005).

The combination of GECI with two-photon (2P) microscopy has been often the method of choice to perform *in vivo* brain imaging. One of the advantages of the use of GECI is that they allow imaging of hundreds of neurons simultaneously in living animals with a micrometer spatial resolution. Action potentials in hundred cells (up to 500 cells) can be monitored for periods of high- or low-frequency firing (Katona *et al.* **Nature Methods** 2012) and recently many more (up to 50k cells, Stringer *et al.* **Cell** 2021). Although all studies are not single action potential detection due to the limitations of GECI kinetics. One great advantage of GECI is also that subpopulations of cells can be selected by expressing the reporter only in a specific set of neurons. Expression is in general very stable, and studies can be conducted over a large range of time, following the timing of processes like learning and development. Thereupon, GECI are a key tool to read and record the action potentials activity from identified cell populations at single cell resolution.

Newer generations of GECI (see below) provide large changes in measured light intensity and hence a higher SNR. Signal to noise ratio (SNR) is defined as the ratio between the signal amplitude

and measurement noise. Since for optical signals, the maximal achievable SNR is proportional to the square root of number of sampled photons (Hires *et al.* **Brain Cell Biol.** 2008), one way to improve SNR is to increase the number of photons captured by using a brighter illumination source.

Some drawbacks of GECI rely on the fact that they are indirect reporters of neuronal activity, and spike rates and spike timing must be inferred from the measured fluorescence emerging from the noise. Therefore, correlating spikes and fluorescent transients is not trivial and several approaches have been developed over time. The best algorithm achieved 40-60% accuracy for high frequency events (Theis *et al.* **Neuron** 2016).

Other limitations of GECI concern the fact that they cannot report hyperpolarizations of the cell membrane nor, in most cases, subthreshold depolarizations. At last, GECI, as exogenous actors, may not express homogeneously over a population of cells or they can overexpress over time, especially when they are delivered through viral injections. On the other side, transgenic animals expressing GECI might not express enough calcium reporter, or they can have some unwanted expression in a cell type or a brain region.

Characteristics of GCaMP

In the mouse visual cortex, GCaMP6 reliably detects single action potentials in neuronal somata, and orientation-tuned synaptic calcium transients in individual dendritic spines (Chen *et al.* **Nature** 2013). GCaMP imaging was used to show that most neurons from the primary visual cortex (V1) can be driven to fire action potentials in response to drifting grating visual stimuli over multiple weeks (Dana *et al.* **Nature Methods** 2019). The most recent variants are the jGCaMP7 (j for Janelia) (Dana *et al.* **Nature Methods** 2019) and jGCaMP8 sensors (Zhang *et al.* Janelia Research Campus. Online resource. 2020). The performances of those calcium sensors are unprecedented so far. The jGCaMP7s version ("s" for slow and sensitive) produces larger fluorescent signals in response to action potential trains (1-10) the DF/Fo response to one action potential is five-fold larger in amplitude and faster in rise time than GCaMP6s. The version "b" (for bright) shows three-fold larger DF/Fo amplitude for one action potential and 50% increase in resting fluorescence compared to GCaMP6s; the "c" (for contrast) exhibits lower resting fluorescence; the "f" (for fast) has three-fold larger DF/Fo amplitude for one action potential than GCaMP6f, with 27±2 ms half-rise time and 265±20ms half-decay time **(Fig.I.6.).** High-performance of those calcium sensors was demonstrated in drosophila and mice (Dana *et al.* **Nature Methods** 2019).

Those mentioned GECI can be used for two main types of experiments: either to track activity in large populations of soma or to follow some calcium dynamics associated with action potential activity in subcellular components such as axons, dendrites, and individual synaptic terminals.

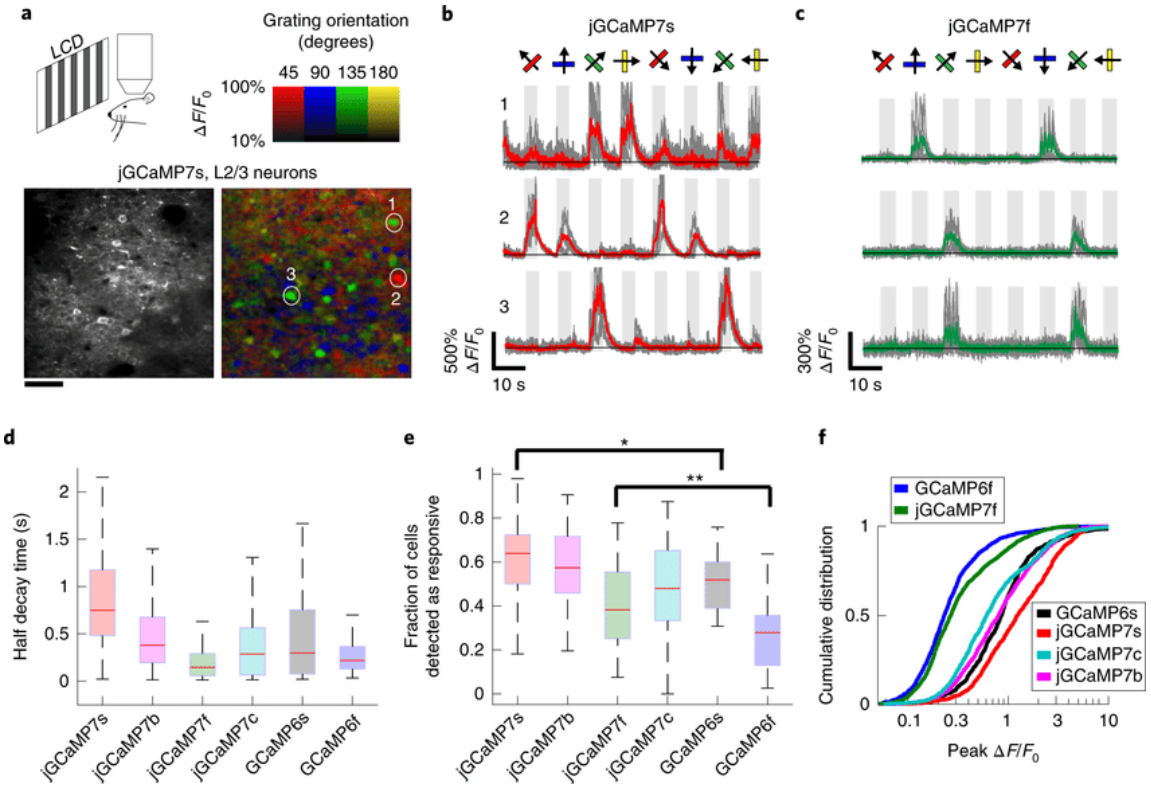

Fig.I.6. jGCaMP7 performance in the mouse primary visual cortex (from Dana et al. **Nature Methods** 2019)

I.1.2 Writing with optogenetic actuators

History of optogenetic actuators

Controlling the neurons with light sounds like something out of a science fiction movie. It has clearly met the reality over a decade ago with the release of the first publication about optogenetics (Boyden *et al.* **Nature Neuroscience** 2005). It described the use of high-titer viral vector injections in the mammalian brain as a delivery strategy for light-sensitive microbial opsins expression, to activate or inhibit neural systems by shining light on them. (**Fig.I.7.**) Nevertheless, the concept dates back to 1988, when a photoreceptor protein (bovine visual rhodopsin) was used to activate currents in *Xenopus* ovocytes upon blue-light illumination (Khorana *et al.* **Proc Natl Acad Sci USA** 1988). Historically, four main opsin protein-based were discovered: (1) bacteriorhodopsin in the beginning of the 70's, i.e., a proton pump which converts light to energy; (2) halorhodopsin in the late 70's, i.e., a chloride pump; (3) sensory rhodopsin 1 in the 80's which reacts to orange light by phototactism; (4) sensory rhododopsin 2 in 2003 which reacts to the blue light. Several years later, opsins were expressed in cultured hippocampal neurons (Zemelman *et al.* **Neuron** 2002). The breakthrough came with the discovery of channelrhodopsin (ChR), which acts as a light-gated ion channel derived from the sensory photoreceptors of a unicellular green algae, the *Chlamydomonas rinhardtii* (Nagel *et al.* **Proc Natl Acad Sci USA** 2003). Expressed in HEK cells and ovocytes, it allowed depolarization of cells with light. In 2005, Ed Boyden, Karl Deisseroth and their colleagues proved that ChR2 could be expressed and activated in neurons, and the current induced by ChR2 activation was sufficient to evoke action potentials. Followed by peers, the results were confirmed within a year in brain slices by Yawo and

colleagues, in spinal cord by Herlitze and Landmesser, in retina by Pan and colleagues. In 2007, halorhodopsin allowed the inhibition of neurons. New microbial opsins including bacteriorhodopsins, halorhodopsins, sensory rhodopsins, and channelrhodopsins, are still under development, leading to availability of myriads of optogenetic actuators (**Fig.I.8.**).

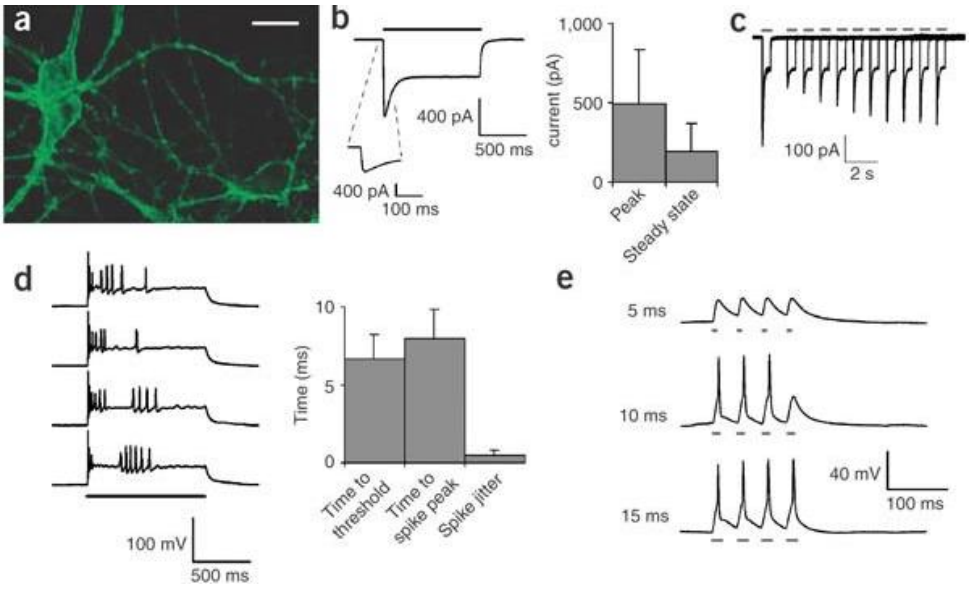

Fig.I.7. Optogenetic revolution with ChR2
enabling light-driven neuron spiking (from Boyden *et al.* **Nature** 2005)

Principle of optogenetic actuators

Their structure consists of seven-transmembrane domains, and includes the light-isomerizable chromophore all-*trans*-retinal (a derivative of vitamin A). Whereas most 7-transmembrane proteins are G protein-coupled receptors that open other ion channels indirectly via second messengers (i.e., they are metabotropic) or channelrhodopsins directly form ion channels (i.e., they are ionotropic). In cation-selective ChRs, photons absorption (lambda=420nm) triggers retinal isomerizations and conformational changes, where multiple *trans*- and *cis*- retinal isomers coexist within the protein. This triggers a modification in the 3D structure that leads to a transient opening of the channel pore, allowing trans-membrane flux of H^+, Na^+ and Ca^{2+} (Scheider *et al.* **Annual Rev. Biophysics** 2015). This behaviour is generally explained by a four-states photocycle model, comprising two closed non-conductive states and two open states with different conductances (Ernst *et al.* **J. Biol. Chem.** 2008; Nikolic *et al.* **Photochem Photobiol.** 2009).

As an example of opsins properties, ChR2 has fast opening (τ_{on} ~ 1 ms) and closing (τ_{off} ~ 13 ms) kinetics (Lin, **Exp. Physiol.** 2011); desensitization is observed upon repetitive activation of ChR2 by brief light pulses, with a recovery time of about 30 s (Feldbauer *et al.* **PNAS** 2009). Over the last decade, plenty of optogenetic actuators were engineered, covering a large range of different properties (faster kinetics, larger current amplitudes, different wavelengths sensitivities) (**Fig.I.8.**). Optogenetic actuators combined with optical methods aim to "achieve gain or loss of function of well-defined events in specific cells of living tissue" (Deisseroth, **Nature Methods**

2010). To this end, optogenetics permits to depolarize and hyperpolarize subpopulations of neurons with high spatial and temporal resolution with light beams.

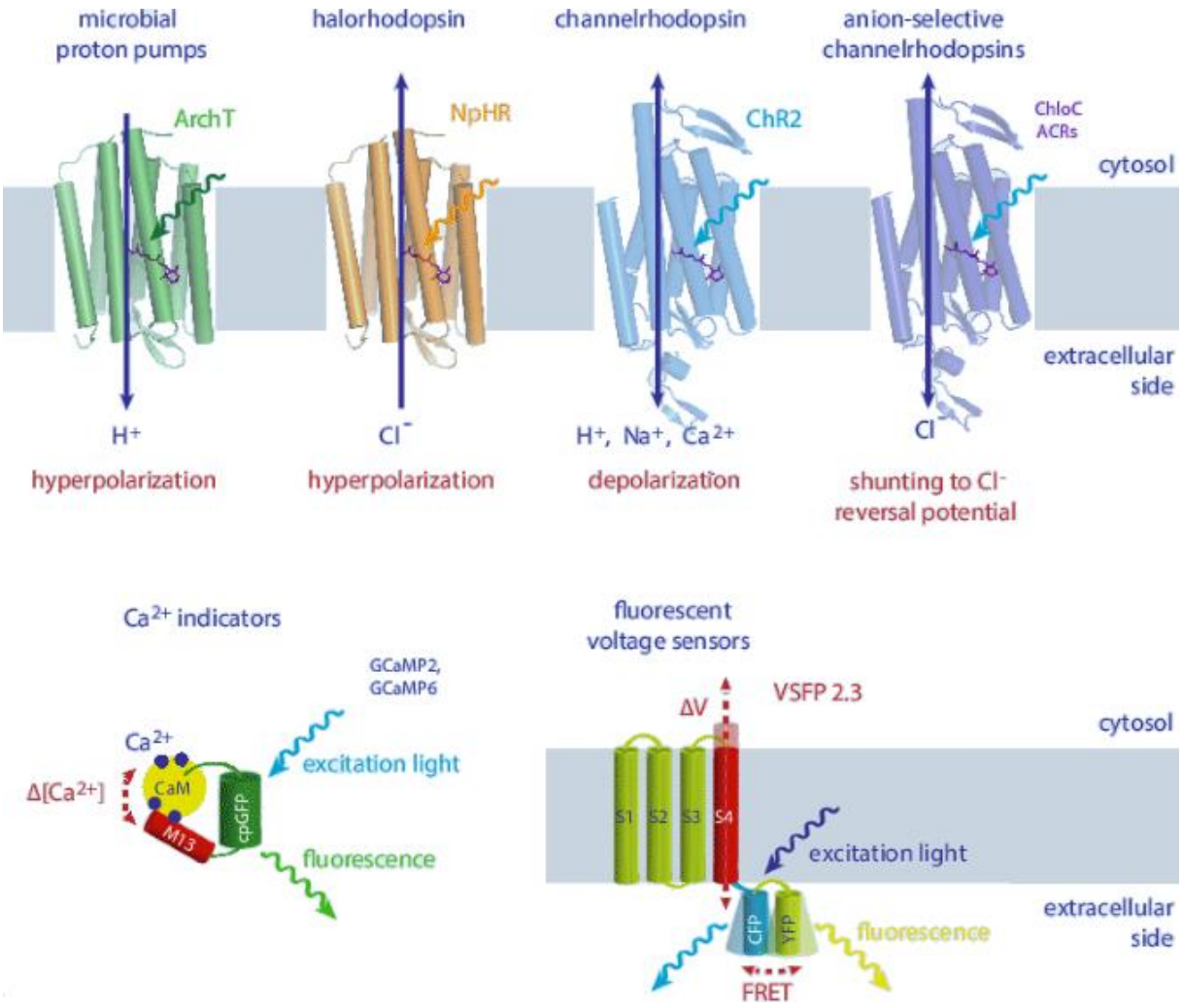

Fig.I.8. Myriad of optogenetic probes (from Schneider-Warme, **Elektrophysiologie** 2018)

Advantages of optogenetic actuators

Optogenetic actuators elicit or suppress electrical activity in neurons. The unprecedented advantages include: the access of a wider region and a larger number of neurons relative to the limited number of cells that can be simultaneously approached with conventional electrophysiological techniques, maintaining a single cell resolution ; second, the specificity of cell targeting based on the possibility of genetically target the cells of interest to express the opsin; third, the possibility to easily perform imaging and manipulation of brain circuits on the same animal sample over time with minimal invasiveness. Indeed, with the traditional patch-clamp technique to record neuronal activity, the all-optical method guarantees less invasiveness, and the possibility to retrieve the same cell in the same FOV. For instance, all this would not be possible once a cell is patched. With all-optical methods, the brain can be imaged several days during several months without causing cell-damaging (unless a high temperature threshold is reached,

Picot *et al.* **Cell Rep.** 2018). Above all, optogenetic actuators now allow the activity of neurons to be controlled with millisecond precision (Emiliani *et al.* **J. Neuro.** 2015).

Several methods can be used to induce opsins expression in living cells, including DNA transfection, electroporation, and gene-transfer techniques (**Fig.I.9.**). Since 2005, viral-mediated gene delivery has become the method of choice for opsin expression. The viral vectors commonly used are lentiviruses, adeno-associated viruses (AAV), canine adenoviruses, herpes viruses and rabies viruses. The smallest option is the AAV (22 nm size, about 4.5 kb packaging capacity), mainly used in intact tissues. It is characterized by a gene expression time-window of a few weeks. After receptor-mediated endocytosis at the somatic compartment and transfer into the nucleus, the transgene-encoded proteins are synthetized, trafficked and integrated into the membrane of the soma or neurites, including the axon terminals. (Thompson and Towne, **Neuromethods** 2018).

Strategies for opsin targeting include a combination of classical genetic tools, such as Cre/loxP and Flp/FRT technologies, the use of cis-regulatory elements, targeted knock-in transgenic mice and gene delivery by AAV or other viral vectors (Haery *et al.* **Frontiers in Neuro.** 2019; **Fig.I.10.**). Cre-expressing transgenic mouse lines also allow to specifically target specific sub-populations of cells. However, the cost of cre line is more expensive and time-consuming for maintenance, handling and selection of the transgenic breeding (>5000€, 4 months to get the first breeding) than injecting virus in wild-type animals (~200€, 2 weeks for animal delivery and hosting habituation period and about 3 weeks for viral expression). To specifically target a cell population and control expression, the choice of the right gene promoter and the viral serotype are crucial (Watakabe *et al.* **Neuro. Res.** 2015; **Fig.I.11**.). To identify neuronal connections with distinct anatomical inputs or outputs, the trafficking ability of retrograde and anterograde vectors are advantageous (Beier *et al.* **Proc Natl Acad Sci USA** 2011). To precisely control neurons without activating surrounding neurites, several constructs for soma-targeting of opsins or calcium reporters are available (Baker *et al.* **eLife** 2016, Shemesh *et al.* **Nature Neuro.** 2017, Shemesh *et al.* **Neuron** 2020).

As a last remark, several characteristics need to be taken into account, among opsin kinetics and illumination methods with high spatio-temporal precision in the readout and in the manipulation of the intact brain. Ideally, stimulation and readout should be free of crosstalk between imaging and photostimulation (Emiliani *et al.* **Journal of Neuroscience** 2015).

In conclusion, optogenetic actuators is a powerfool tool to control the neuronal activity with high precision in space and time.

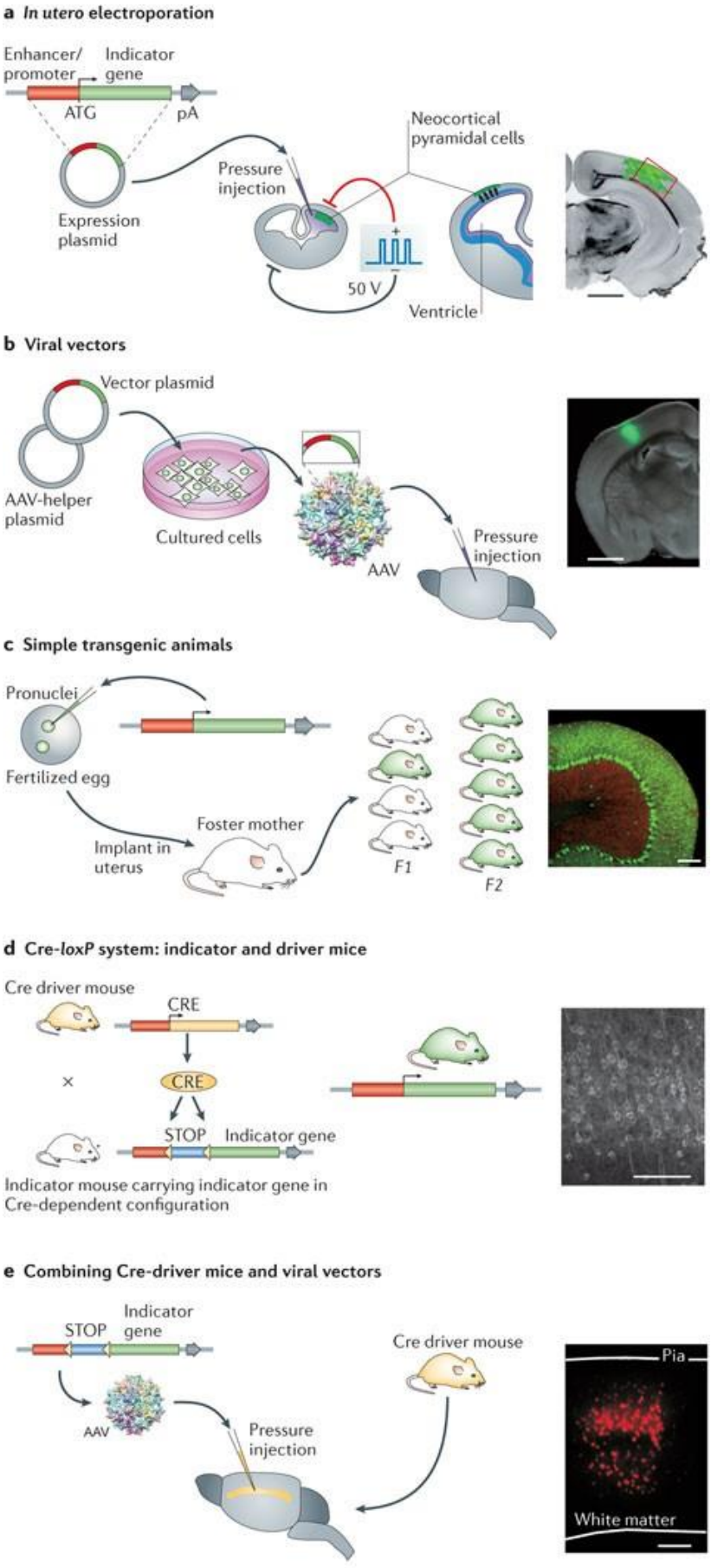

Fig.I.9. Strategy to express opsin in neurons (from Knöpfel, **Nature Review** 2012)

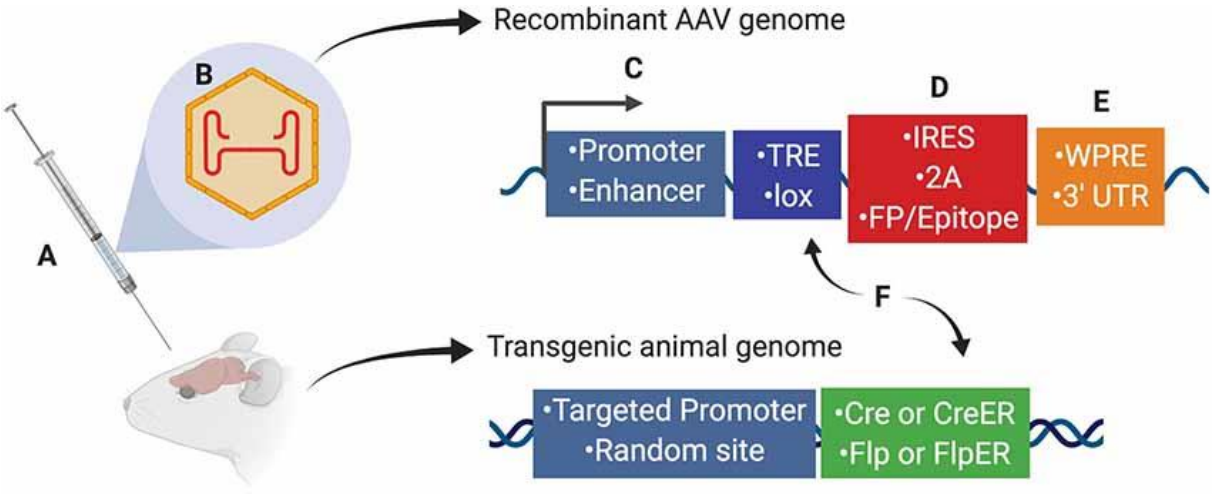

Fig.I.10. Viral construct schema (from Haery *et al.* **Frontiers in Neuro.** 2019)

		AAV1	AAV2	AAV5	AAV6	AAV6.2	AAV7	AAV8	AAV9	rh.10
Adult	Cortex	+			+	+	++	++	+++	++
	Hippocampus	+			+	+	++	++	+++	++
	Thalamus	+			+	+	++	++	++++	+++
	Hypothalamus	+			++	+	+++	++	++	+++
	Cerebellum	+			++	+	++	+++	+++	++++
	Brain Stem	+			++	+	++	++	++++	+++
	Cervical	+++			+	+	+++	+++	++++	+++
	Thoracic	+++			+	+	+++	+++	++++	+++
	Lumbar	+++			+	+	+++	+++	++++++	+++
Neo-Natal	Cortex	++	+	-	++	+	+	+++	++	++
	Hippocampus	+	+	-	-	-	+++	++	+	+
	Thalamus	+	+	-	-	+	++	+	+	+
	Hypothalamus	++	-	-	+	+	++++++	++++++	+	+
	Cerebellum	++	-	-	+	-	+	+	+	+
	Brain Stem	++	-	-	+	-	++	+	+	+
	Cervical	-	-	-	+	++	++	+++	++	+++++
	Thoracic	+	-	-	+	++	+++	++	++	++
	Lumbar	+	-	-	+	++	++	+	+	++

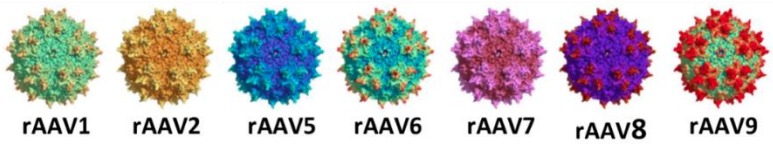

Primary receptor	N-linked sialic acid	HSPG	N-linked sialic acid	N-linked sialic acid; HSPG	unknown	unknown	N-linked galactose

Fig.I.11. Viral serotype AAV1to9 regarding cells tropism (from Vance *et al.* **IntechOpen** 2015)

I.1.3 Single-photon (1P) vs two-photons (2P) imaging

Linear and nonlinear fluorescence microscopy: 1P vs 2P

The observation of fluorescent biological tissues mainly relies on high-resolution microscopy alongside highly specific targeting of fluorescent biomarkers. Fluorophores can **absorb** photons of a certain wavelength (**excitation**) and quickly re-emit photons at a slightly different wavelength, a process that is referred to as fluorescence (or **emission**). A fluorophore is then characterized by its spectra of absorption and emission (**Fig.I.12.**). **In one photon (1P) excitation, fluorescence** occurs when a photon is absorbed by a fluorophore, raising an electron to an excited energy state, from which it relaxes to the electronic ground state and emits a lower energy photon therefore at longer wavelength. For absorption to occur, the energy of the exciting photon must match the energy difference between some excited state and the ground state (definition from Oheim *et al.* **Advanced Drug Deliv. Reviews** 2006). It is sketched by the **Jablonski diagram** (**Fig.I.12.**). The phenomenon where the emitted fluorescent photon is of lower energy than the photon originally absorbed, is called **Stokes shift.** In linear fluorescence, the probability of absorption (P) of the electron by the tissue is linearly dependent on the intensity (I) of the light (P proportional to I). In two-photon (2P) nonlinear excitation instead, P is proportional to I^2 (quadratic relation). In three-photon (3P) scenario, P is proportional to I^3. The two-photon excitation process (2P) was first described by Maria Goeppert-Mayer in 1931. According to that, two photons (instead of only one) are absorbed quasi simultaneously to complete the transition into the excited state. When the electron decays to the ground state, it emits one photon with slightly less energy than the sum of the two initial photons. In this way, 2P uses photons of roughly half the energy and double the wavelength with respect to 1P excitation of the same fluorophore. As a consequence, 2P excitation is normally performed using infrared lasers (wavelengths of 800 to 1000 nm), which is beneficial for a better penetration in scattering tissues (Oheim *et al.* **J. Neuro. Methods** 2001; Papagiakoumou. **Biology of the cell, Wiley** 2013).

Because two photons need to interact with a fluorophore quasi simultaneously (within ~0.5 fs, Helmchen, Denk **Nature Methods** 2005) to be absorbed, in general, 2P excitation has a much lower probability to occur with respect to 1P excitation. This in turn means that 2P absorption requires photons to be highly concentrated both in space and in time. Indeed, 2P absorption is normally performed by tightly focusing a laser beam in space using a high NA objective. Additionally, 2P excitation requires ultrashort laser pulses (in general, shorter than 500 fs). The light source is called pulsed laser or mode-locked but not continuous. In fact, multiphoton excitation requires extremely high photon flux: 10^{12} to 10^{30} photons (cm/s^2) (Book: Xu and Webb, **Topics in Fluorescence Spectroscopy** 2002). The pulsed laser emits photons intermittently in high-intensity pulse trains rather than in a continuous beam. Compared to a continuous beam, pulsed light lasers permit to generate picoseconds (10^{-6} second) to 100 femtoseconds pulses ($100*10^{-12}$ second) with high peak power.

As a consequence, the key benefit of two-photon microscopy is its ability to restrict excitation to a tiny focal volume. The objective focal point is the only place with a high enough photon density to ensure simultaneous absorption of two photons by the fluorophore. This technique permits a more precise excitation profile to focus beams on individual cells and greater penetration depth (Helmchen and Denk **Nature Methods** 2005; Bègue *et al.* **Biomedical Optic Express** 2013).

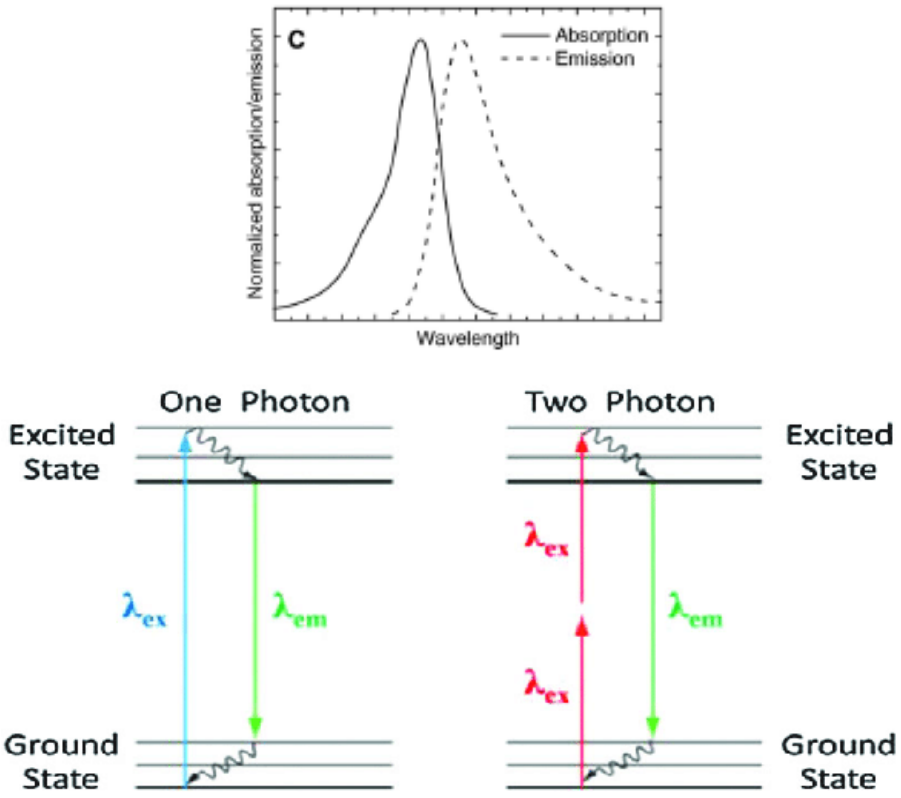

Fig.I.12. ***Upper:*** Absorption and emission spectra.
Lower: Jablonski diagram for 1P and 2P.

Advantages of 2P

In short, for performing two-photon illumination, specific parameters from the laser are required: (1) wavelength (2) ultrashort pulses (3) fast repetition rate. (Denk *et al.* **Science** 1990: principles and first application; Oheim *et al.* **J. Neuro. Methods** 2001: 2P principles; Zipfel *et al.* **Nature Biotech.** 2003: 2P principles and spatial resolution of 2P; Helmchen and Denk **Nature Methods** 2005: a review on 2P imaging in depth and the use of longer wavelengths in 2P).

Although 2P require costly mode-locked laser, the multiphoton excitation fluorescence microscopy shows several advantages over single-photon microscopy: (1) the capability of imaging in depth in scattered tissues; (2) the focalization of the absorption volume. Firstly, 2P microscopy is suitable for deep-tissue imaging because it involves the use of longer wavelength (IR) light, and those are less subject to absorption and scattering than the visible wavelength used in 1P microscopy. Hence, excitation penetrates more deeply in the brain tissue. Secondly, 2P microscopy permits precise targeting of single cells, getting rid of unnecessary out-of-focus fluorescence. Widefield excitation would lack optical sectioning with a large illumination volume, while the fluorescence would not be confined at the focal plane (z), whereas multi-photon excitation such as 2P confines fluorescence excitation to a small volume at the focus of the objective (**Fig.I.13**.). Since 2P is localized, no pinhole is needed, as it is for example in 1P confocal microscopy. Since there is no pinhole, most of the emitted photons can be collected. Thirdly, the reduced volume of excitation, out of the focal plane. The 2P technique is suitable for long *in vivo* imaging in intact or semi-intact brain (**Fig.I.14.**). Moreover, as 2P requires a higher wavelength

(700 to 1040nm), most used fluorophores can be excited at the longer wavelength range (**Fig.I.15**.). The development of multiple-photon microscopes is still ongoing from 2P to 3P (Wang *et al.* **Optica** 2020): to image brain areas in vivo at higher depths (>1mm), the three-photon (3P) imaging technique has been successfully applied in vivo (Wang *et al.* **Nature** 2019). In this study, we focus on 2P technique. In general, about half of the incident photons are scattered every 50–200µm (Oheim *et al.*, **J. Neuro. Methods** 2001; Yaroslavsky *et al.*, **Phys. Med. Biol.** 2002; Kleinfeld *et al.* **Proc. Natl. Acad. Sci. USA** 1998). Although 2P permits to reach deeper tissues, the imaging is limited to 1mm from the surface. Then neuroscientists are limited to the studies of the brain regions near the surface, optically accessible, i.e., mostly the cortex (Helmchen, Denk **Nature Methods** 2005; Horton *et al.* **Nature Photon.** 2013).

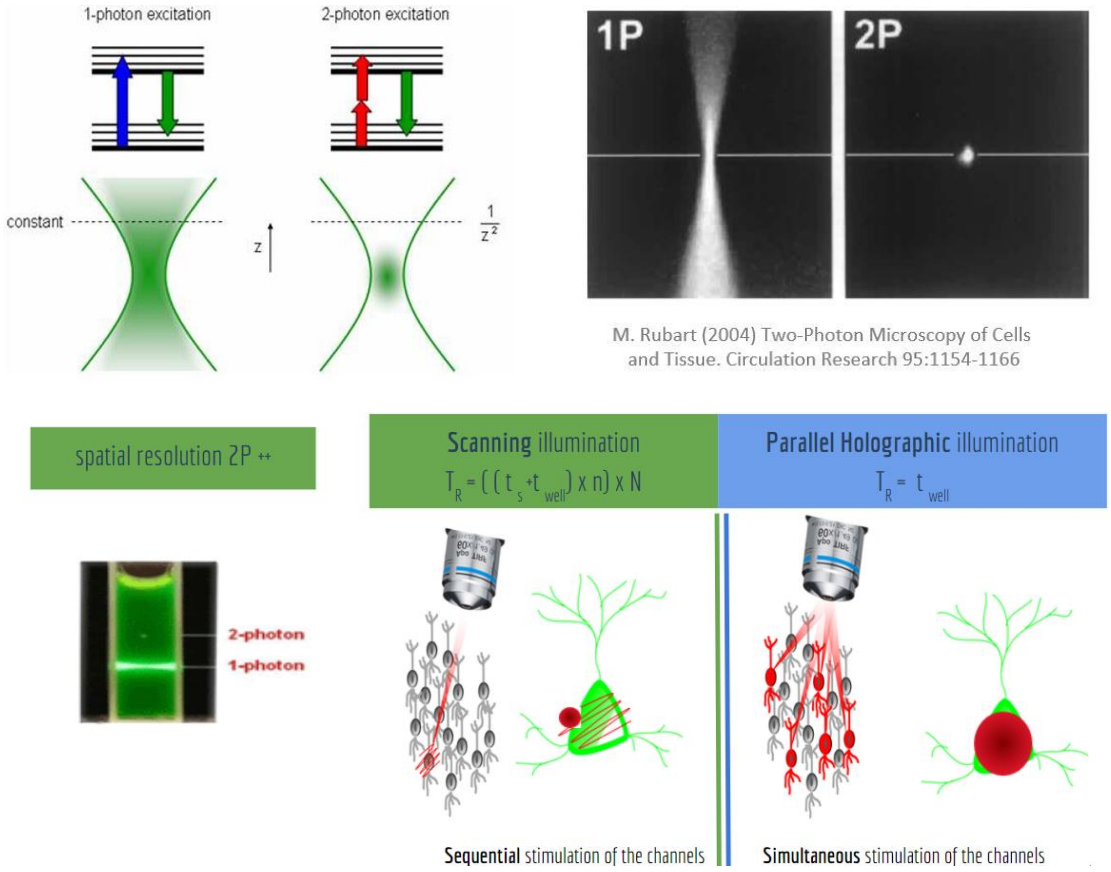

Fig.I.13. 1P vs 2P and scanning vs holographic illumination approaches (adapted from Rubart **Circ. Research** 2004)

I.1.4 1P vs 2P photostimulation

High spatial precision

Stimulating cells with precise light delivery is also necessary in the optical manipulation of neuronal activity *in vitro* and *in vivo*. A neuron is basically structured as a cell body or somata, an elongated axon and numerous dendrites and spines. To shine light on small or large structures with high precision, targeting only at the site of interest, requires high spatial precision. Multi-photon excitation is a promising optical stimulation method that provides single-cell resolution (**Fig.I.14**).

To efficiently activate opsins at single cell resolution, 2P microscopy is preferable for its spatial precision relative to 1P excitation (Papagiakoumou *et al.* **Nature Methods** 2010). Even though the 1P wide-field illumination enables millisecond temporal resolution and activation of a large population of neurons, the 2P illumination has the advantage of a more focused beam and a greater light penetration in depth. Although using optical fiber and blue light allow us to get information on the link between specific brain regions and behaviour (Aravanis *et al.* **J. Neural Eng. 2007**, Adamantis *et al.* **Nature** 2007, Iwai *et al.* **Neuro. Research** 2011, Huber *et al.* **Nature** 2008).

Understanding the mechanisms regulating neuronal circuits, require more precise targeting approaches, enabling to control single or multiple targets, independently in space and time. This has required to move from 1P wide field illumination to 2P patterned light. Patterned photostimulation with two-photon can be obtained with two main types of optical approaches: scanning and parallel, which have been proved to be both efficient for opsins excitation (Packer *et al.* **Nature Methods** 2012; Prakash *et al.* **Nature Methods** 2012, Papagiakoumou et al. **Nature Photon.** 2013, Ronzitti et al. **J. Neuro.** 2017).

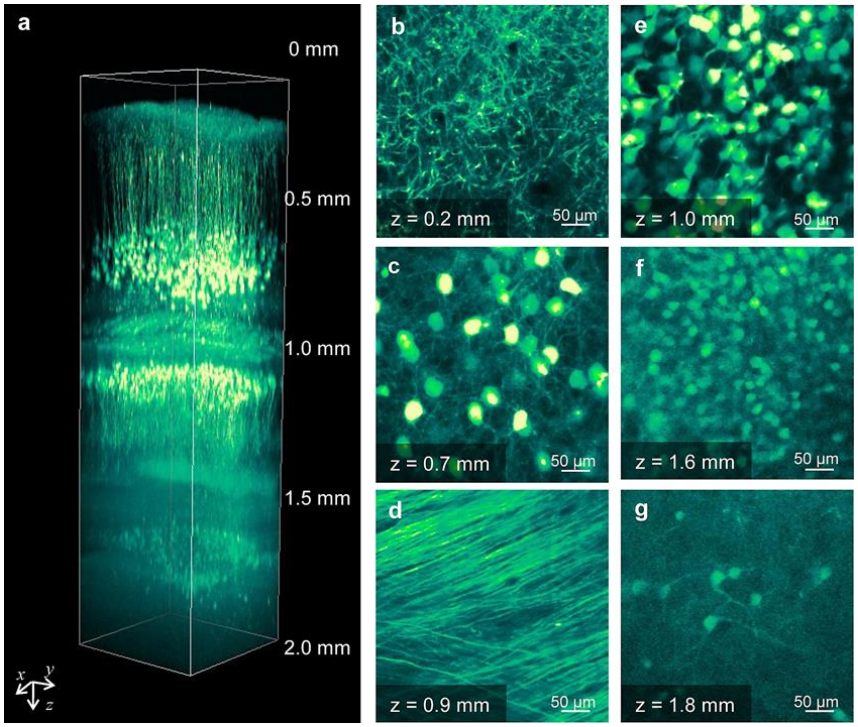

Fig.I.14 2P excitation in the mouse cortex (from Aoyagi *et al.* **PlosOne** 2015)

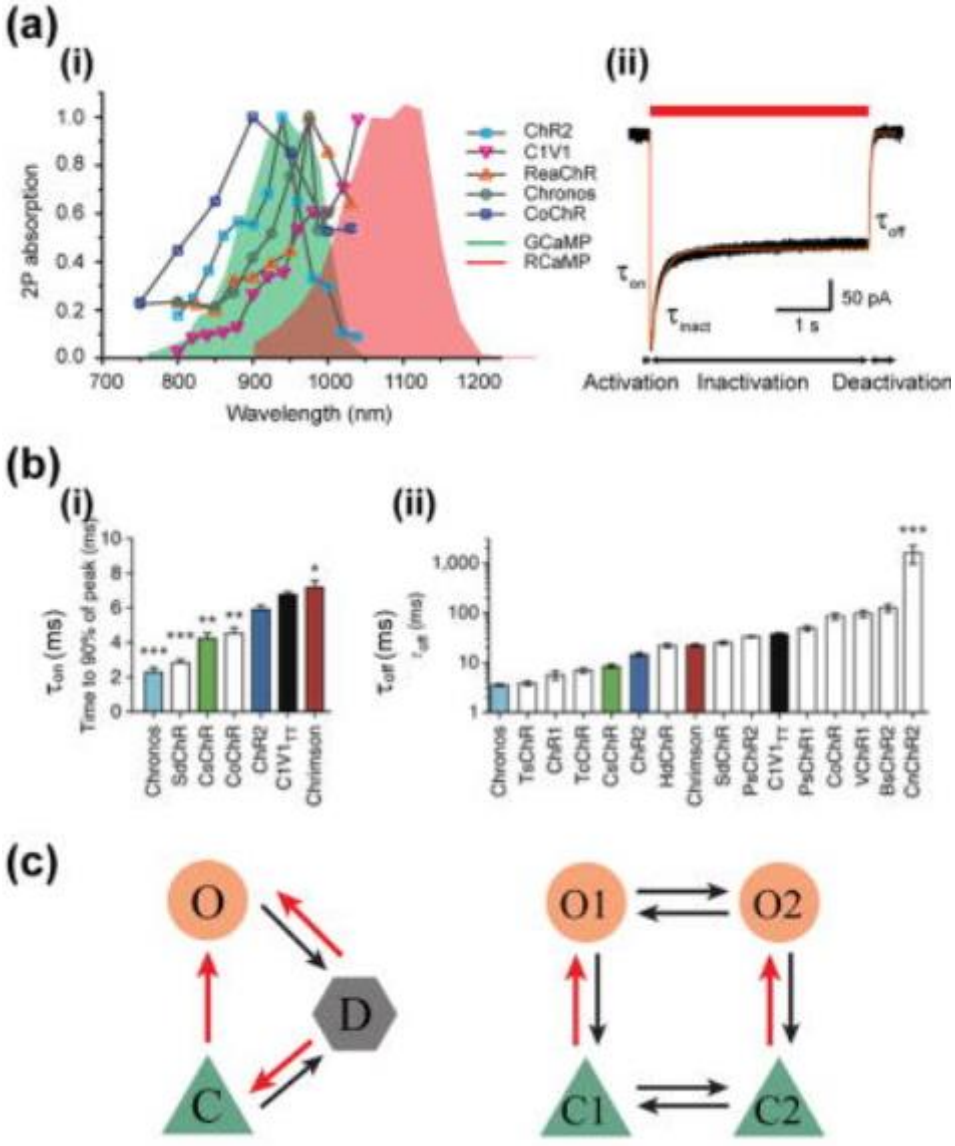

Fig.I.15. Opsins action spectra (2P) underlining relevance of optimized virus combination (Chen *et al.* **Current Op. Neurobio.** 2018)

Scanning approach

The first method used to photostimulate cells was the scanning method using spiral scanning on a cell soma. With scanning approaches, the temporal resolution for the photostimulation of N cells can be expressed as Ts = [(n * Rt) + St] * N, where n is the number of positions visited within each cell, and Rt and St are the dwell and scanning times, respectively (Emiliani *et al.* **J. Neuro.** 2015). The first demonstration of action potential generation with two-photon excitation was shown in cultured cells with 30ms temporal resolution in 2009 (Rickgauer and Tank, **PNAS** 2009). Then simultaneous imaging and photostimulation were performed in the mouse *in vivo* (Packer *et al.* **Nature Methods** 2012; Prakash *et al.* **Nature Methods** 2012). It enabled single cell excitation ranging between 5 and 70ms illumination time in neurons expressing the opsin actuator C1V1 and GCaMP6s calcium indicator in the primary visual cortex.

For a specific opsin, the efficiency of the photostimulation process is a trade-off of a series of parameters: the total scanning time (Ts) and the scanning speed, which determine the summation rate of the photoevoked-current; the illumination intensity on the cell membrane, which determines the quantity of light-gated channels activated; and the illumination power (Ronzitti *et al.* **J. Neuro.** 2017). Hence, fast delivery of patterned light would permit to open the largest possible number of light-sensitive channels on the targets.

To increase the number of achievable cells, this approach has been combined with holographic multiplexing to scan multiple spirals simultaneously.

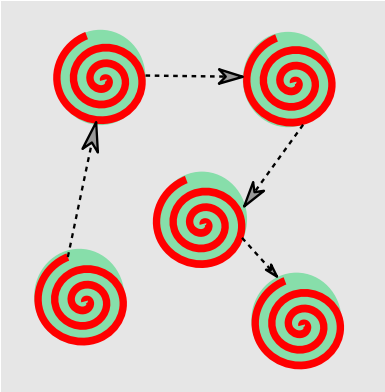

Fig.I.16. Spiral scanning schema

Parallel approach

Parallel techniques, as computer generated holography (CGH), Generalised Phase Contrast (GPC) or low NA gaussian beam, permit to simultaneously excite all selected targets at the same time. In this case, the temporal resolution of photoactivation is independent of the number of stimulation targets Ts = Rt. In that sense, the temporal resolution of the holographic illumination is only due to the dwell time of photostimulation (Lutz *et al.* **Nature Methods** 2008; Papagiakoumou *et al.* **Nature Methods** 2010, Pégard *et al.* **Nature Com.** 2017, Reutsky-Gefen *et al.* **Nature Com.** 2013).

Originally described by Gabor in 1947, holography is known as a technique that enables us to generate with light the shape of a predefined 3D object, in absence of the object. Today, this approach has evolved into CGH (Lohmann, Paris 1967). In this case the object can be a custom-made image template (the target) drawn by computer that becomes the input source to a Fourier transform-based algorithm (Gerchberg and Saxton, 1972). The so calculated interferogram (or phase-profile or phase-hologram) is converted into a grey-scale image and sent as input to a liquid crystal spatial light-modulator (LC-SLM). (**Fig.I.17.** Papagiakoumou *et al.* Optogenetic Roadmap, **Neuromethod - Springer Protocols Edition** 2018) That modulation of light, so called phase modulation, enables to recreate the shape of the target at the focal plane with the laser (**Fig.I.17.**). Hence, the exact morphology and size of the targeting cell can be photostimulated in 2D or 3D with a precise light delivery (**Fig.I.13)**.

There are three types of approaches for light delivery with CGH: (1) parallel-scanning (2) scanning-parallel (3) parallel-parallel. In parallel-scanning, the light is shaped on the target at

once, and for illumination of several cells, those will be illuminated in a sequential manner with a holographic pattern that will match the cell shape (Rickgauer *et al.* **Nature Neuro.** 2014). In scanning-parallel, several spiral scans are performed on multiple cells at the same time (Packer *et al.* **Nature Methods** 2012). In (3) parallel-parallel, one of multiple cellular targets are illuminated simultaneously (Papagiakoumou *et al.* **Nature Methods** 2010; Bègue *et al.* **Biomed. Opt. Express** 2013; Papagiakoumou *et al.* **Biology of the cell. Wiley** 2013; Szabo *et al.* **J. Neuro.** 2014).

The holographic approach uses devices that modulate the phase (e.g., spatial light modulator, SLM) in order to shape light and illuminate all targets simultaneously. While covering large targets (multiple somatas), the axial resolution would be quickly deteriorated, proportionally to the lateral spot size. Fortunately, in 2P excitation, by working on the temporal aspect of the laser pulse, the two quantities can be decoupled, as for example with temporal focusing. Indeed, to address this limitation, CGH can be combined with temporal focusing (TF) to stretch laser pulses outside of the focal plane, which, combined with 2P nonlinear intensity dependence, axially confines fluorescence regardless of lateral extent. (Papagiakoumou *et al.* **Optic Express** 2008).

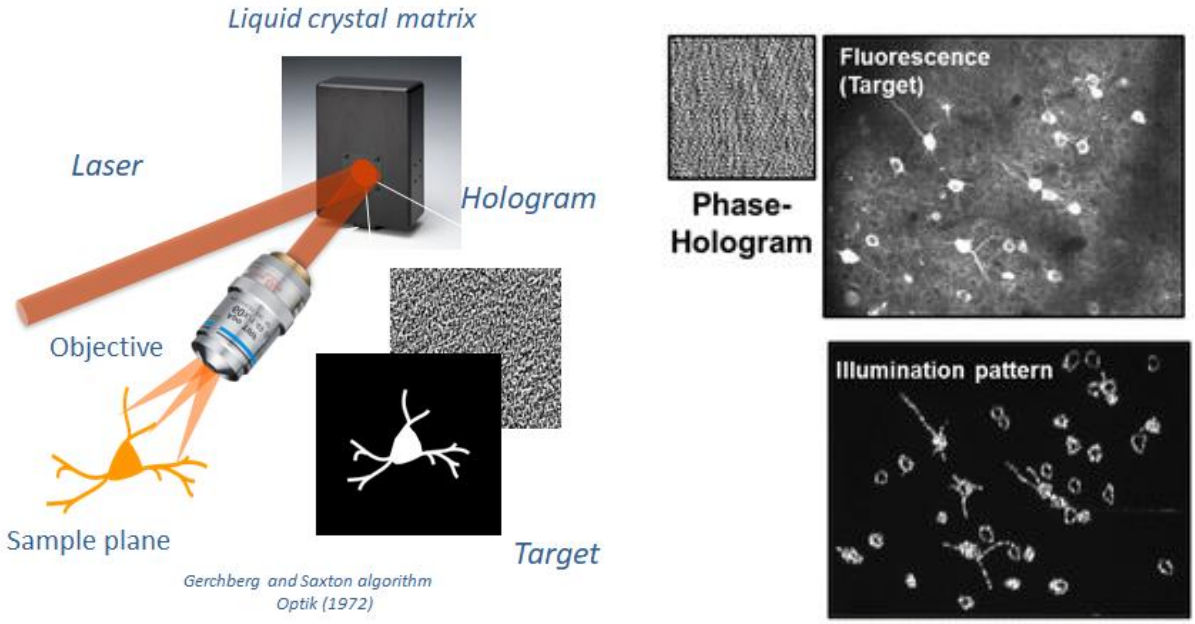

Fig.I.17. Computer Generated Holography approach
(from Papagiakoumou *et al.* **Springer Protocols** 2018)

Temporal focusing

The temporal focusing (TF) can be thought of as a way to focus the ultrafast laser pulse in time at the sample plane (Oron *et al.* **Opt. Express** 2005, Zhu *et al.* **Opt. Express** 2005). TF permits to enhance optical sectioning and reduce out of focus excitation. Briefly, by using a diffraction grating, TF disperses the laser pulse in its different wavelengths, which are then recombined together at the sample plane after the microscope objective (**Fig.I.18.**). Consequently, the 2P fluorescence is decreased away from the focal plane, thus maintaining good axial resolution even for laterally extended excitation spots. (Oron and Silberberg, **Cold Spring Harb. Protoc.** 2015). As

an example, in the first demonstration of high-speed selective control of neuronal activity in ChR2 expressing hippocampal slices using the technique of temporal focusing, sculpted light distributions that are axially and laterally confined to the target neurons were generated and used for inducing single cell firing with 2 ms temporal resolution and 40 µm axial resolution. (Andrasfalvy *et al.* **Proc Natl Acad Sci USA** 2010).

Computer generated holography combined with temporal focusing offers therefore in principle high spatial resolution together with the flexibility of spatially shaping the light to the targets of interest, although it may require higher total excitation power relative to scanning based approaches (Ronzitti *et al.* Review **Journal of Optics** 2017). To obtain a customized temporally focused illumination pattern, the excitation beam is shaped using a spatial light modulator (SLM) and a diffraction grating is positioned after a lens, in the plane where the holographic patterns appear. (**Fig.I.19**) (Papagiakoumou *et al.* **Optics Express** 2009).

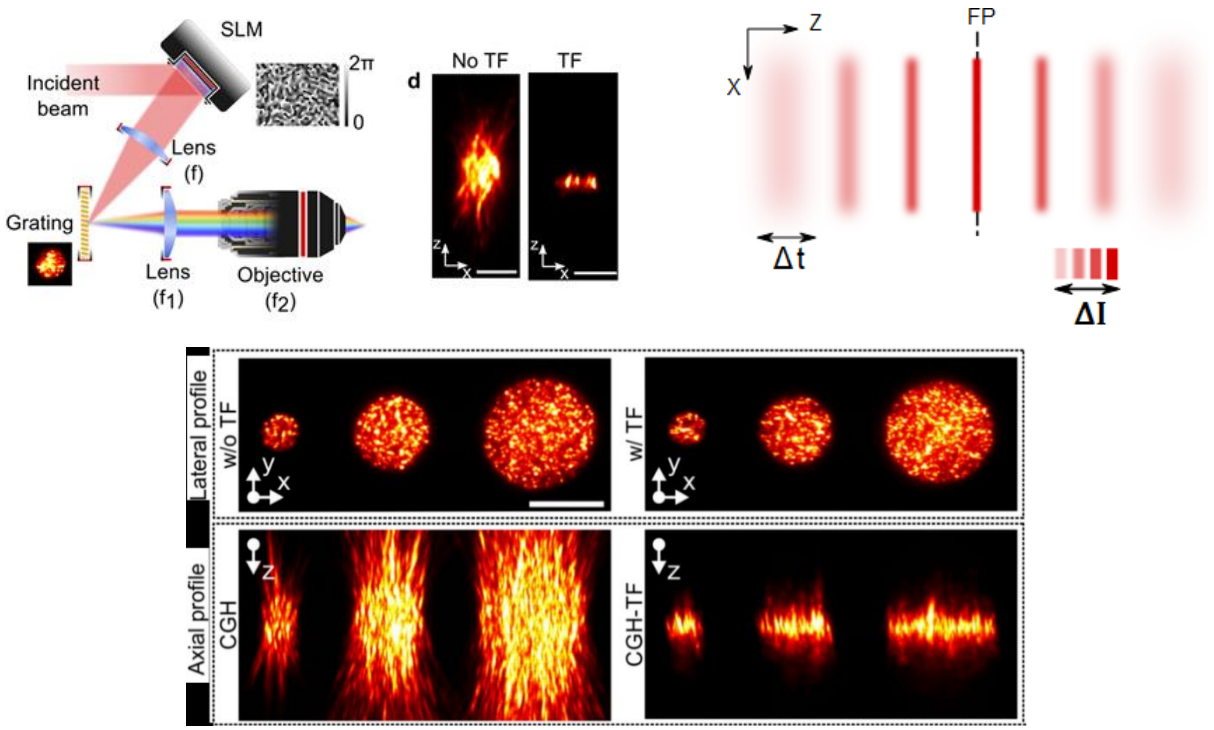

Fig.I.18. Temporal focusing (adapted from Papagiakoumou *et al.* **Nature Methods** 2020)

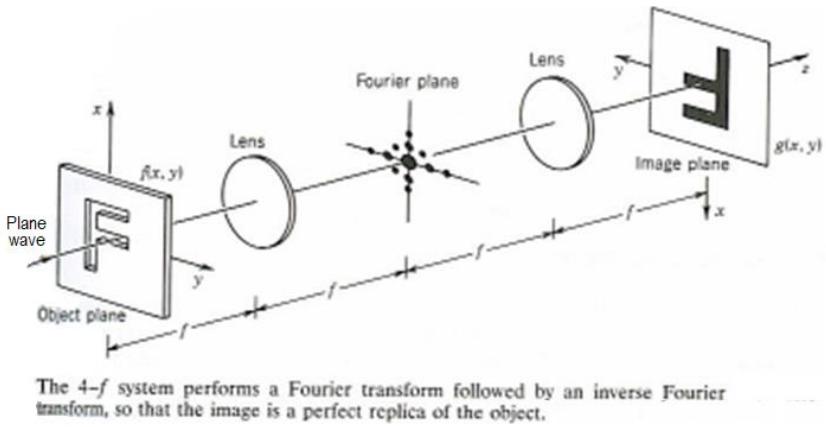

Fig.I.19. Fourier plane (from Faculty Washington Edu)

I.2 Micro-endoscopy for all optical investigation in deep brain areas & freely-moving animals

There are at least two reasons why optical microendoscopes are gaining importance in Neuroscience: a minimally invasive microendoscope could be implanted to gain access to deep unreachable regions of the brain; a miniaturized, portable, or flexible micorendoscope could be used to record neuronal activity during natural behaviour, i.e., in freely moving animals. In this chapter, I will describe the details of these two main research fields, with a particular attention to the freely moving case, which is the case of interest for this thesis.

I.2.1 Deep brain functional imaging

Apart from small transparent animal models to study neurons (e.g., zebrafish), the application of conventional optical microscopy is limited to brain regions located at shallow depths by light scattering in tissue, in mice for instance. To date, 2P imaging gives access to 1 mm depth from the brain surface. The imaging performances are limited and high-resolution in depth becomes impossible for traditional fluorescence microscopy (Ji *et al.* **Nature Methods** 2010; Wang *et al.* **Nature Methods** 2014; Helmchen and Denk **Nature Methods** 2005). One strategy, employed in optical microscopy to alleviate the scattering effects, is the use of near-infrared light and hence multiphoton (2P or 3P) microscopy. Indeed, the free path of photons in scattering samples increases with the wavelength (longer attenuation length; Oheim *et al.,* 2001; Helmchen and Denk, 2005). The recent application of three-photon microscopy for imaging (Horton *et al.* **Nature Photon.** 2013; Ouzounov *et al.* **Nature Methods** 2017; Wang *et al.* **Nature Methods** 2018; Wang and Xu **Optica** 2020; Hontani *et al.* **Sc. Adv.** 2021) using 1300-1700 nm wavelength allowed to achieve imaging up to 2 mm depth in the mouse brain.

Relying on 2P approach, a more invasive solution to reach deeper structures could be removing a part of the cortex to image the hippocampus (Mizhari *et al.* **J. Neuro.** 2004; Dombeck *et al.* **Nature Neuro.** 2010; Marshel *et al.* **Neuron** 2012). However, keeping intact brain to study behaviour is essential. Indeed, several important structures are located even deeper. For example, to cite some depth example references in the mice, the neocortex is about 1mm thick, the thalamus located at 3mm in depth, the lateral hypothalamus as the food intake regulator is at 5mm depth (*Allen Institute Atlas website* **Fig.I.20**.). Thereby, the removal of large volumes of tissue for imaging the region of interest may impact on the integrity of the entire neural circuit, causing eventually some abnormal animal behaviour, unusual neuronal activity, or inflammatory reactions, which may last for several weeks, affecting the *in vivo* imaging (Bocarsly *et al.* **BioMed. Optics Express** 2015).

To gain access to deeper regions, a possible solution is the use of a small diameter endoscope that can be minimally invasively impanted at the desired depth (Baretto *et al.* **Nature Methods** 2009; Helmchen *et al.* **Neuron** 2001; Sawinski *et al.* **Proc.Natl. Acad. Sci USA** 2009; Gu *et al.* **J. Micro.** 2014; Zong *et al.* **Nature Methods** 2017).

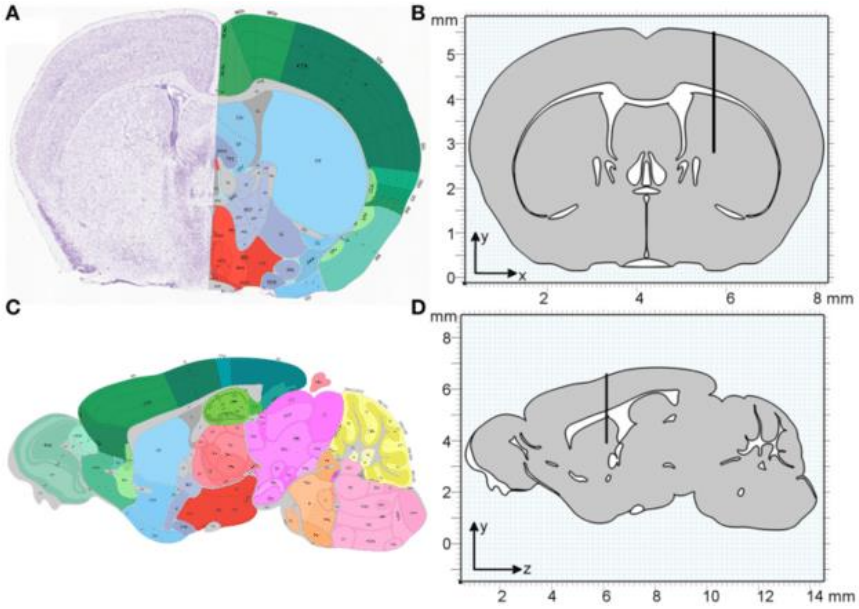

Fig.I.20. Brain mouse atlas (*Allen Institute*)

Microendoscopy employs implantable relay lenses, such as gradient refractive index (GRIN) lenses. **GRIN lenses** (**Fig.I.21.**) are miniature rod-like lenses with a radial refractive index profile of near parabolic shape (Gomez-Reino *et al.* **Springer-Verlag** 2002), commercialized by *GrinTech* (Germany) and *Thorlabs* (USA) among others. Its small size enables it to be directly implantable into the mouse brain (Baretto *et al.* **Nature Methods** 2009) or to be slid in an implanted guide cannula. This latter solution allows not only the re-use of the same GRIN lens but also to move the focus in the z direction (Bocarsly *et al.* **BioMed. Optics Express** 2015). Important parameters of GRIN lenses are: (1) the size, i.e., diameter and length; (2) the working distance, in the air for the image side, and in the water for the object side; (3) the numerical aperture; (4) the magnification.

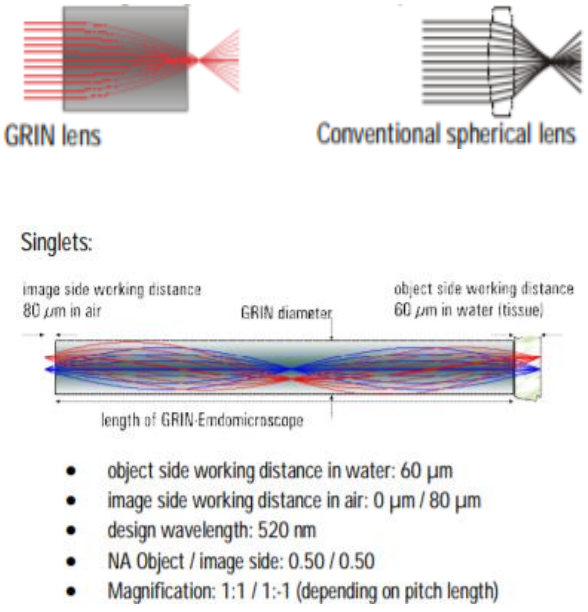

Fig.I.21. GRIN lenses characteristics (from *GrinTech* company website)

Here, I will quote some research labs using GRIN lens, their advantages and applications. Starting with mice animal model, the challenges are multiple: to image small neuronal structures such as spines, to image deeper structure by resolving scattering issues, to improve optical system for gaining lateral resolution and axial resolution.

The first brain structure studied with an implanted GRIN lens endoscope was the hippocampus, a brain station, involved in learning and memory functions. By 2PFM with a directly implanted GRIN lens, spines from GFP expressing CA1 hippocampal pyramidal neurons at 1.2mm depth were imaged in live mice (Baretto *et al.* **Nature Methods** 2009). They achieved 1.6µm lateral and 12µm axial resolution with 0.8NA. For shaping research on long-term memory, Schnitzer's Lab (Stanford, USA) used a sealed glass guide tube implanted dorsally to CA1, which allowed time-lapse *in vivo* imaging in behaving Thy1-**GFP** mice to image about 5000 spines over a month (Attardo *et al.* **Nature** 2015).

GRIN lenses have been used not only to image fluorescent reporters but also **GECI** *in vitro* and *in vivo*. In Fellin's Lab (Genova, Italy), the GCaMP6s fluorescence signals of CA1 neurons, located at ~1.2mm depth within the mouse brain, were recorded with a 40-125 Hz acquisition rate (n=10 cells in a FOV of 250µm^2; Moretti *et al.* **Biomed. Optic Express** 2016). The optical system used was 2P scanning with a customized holder for the GRIN lens. **Behavioural** studies in head-fixed animals have also been carried out, for instance, about memory (Allegra *et al.* **Neuron** 2020, Schmidt-Hieber's Lab) or locomotion process (Schwenkgrub *et al.* **Science Adv.** 2020, Bathelier's Lab) or social interactions (Jennings *et al.* **Nature** 2019, Deisseroth's Lab).

Aiming to perform deep brain manipulation with light, Emiliani's lab demonstrated the use of 3D holography and temporal focusing through a GRIN lens (Accanto *et al.* **Scientific Reports**, 2019) as the first demonstration of 2P stimulation through this microendoscope type. With a GRIN lens with NA of 0.5, a pattern of 30 spots was generated in a volume of 100*150*300µm^3. The FWHM was under 30µm, limited by NA and aberrations. This method allowed to perform *in vivo* imaging of GCaMP6s expressing neurons in L2/3 of primary visual cortex V1, applying 2P scanning imaging at 12Hz and patterned photostimulation in a large volume.

GRIN lenses enable the investigation of previously inaccessible in-depth brain areas to confirm or refute neuronal mechanisms with repetitive imaging sessions lasting months. Nevertheless, a GRIN lens alone lacks flexibility for behaviour-related studies. Thereby, we proposed a complementary approach to do freely-moving experiments based on fiber bundle and GRIN lens assembly.

I.2.2 Freely-moving system

The importance of a flexible optical system

Studying animals' behaviour in free exploration without restriction is important to probe the involvement of specific brain circuits in the accomplishment of specific tasks. Some imaging techniques require working in anaesthetized or restrained animals and this could be a major limitation when studying neural dynamics and animal's perception. Moreover, neuronal activity changes significantly while the animal is asleep, anaesthetized or awake. Therefore, to establish reliable theory about circuits involved in a particular behaviour, working with awake behaving animals is the best choice. For example, probing the neural basis of crucial cognitive and vital functions, such as spatial memory or active decision-making, food intake or anxiety, social interaction, alertness or locomotion, implies performing freely-moving experiments.

An optical system hosting a GRIN lens coupled with a fiber should meet some requirements: first, the smallest and minimally invasive device to study intact brain circuits; second a high-resolution imaging and photostimulation system for monitoring single- or multiple-cells in a large FOV of 200 μm^2 or more; third the microendoscopy would rather be compatible with advanced optics and avoid heavy devices mounted on the head of the animal (<2g).

For these reasons, in this work, we have decided to focus on the development of a flexible fiber-based endoscope that could be used for studies in freely-moving animals. If several solutions exist already for imaging in behaving animals, as we will see in a moment, none of them is really compatible with single cell precise photostimulation. In this thesis, we therefore aim to develop the first 2P flexible endoscope for simultaneous imaging and photostimulation of neuronal circuits in freely-moving animals. I will now describe the previously available technologies to image neurons in freely-moving animals.

The miniscopes

The miniaturized 1P fluorescence microscopes, so-called "miniscope" with wire-free recordings have met open-source development the past 5 years (Aharoni and Hoogland, **Frontiers in Cell. Neuro** 2019; **Fig.I.22**). It consists in a miniaturized microscope of about 2g mounted on top of the mouse head to image neurons in freely-behaving animals. A miniaturized 1P excitation microscope uses LED as light source, CMOS imaging sensors, off-the-shelf optical components and single or set of GRIN lenses. There are currently 4 main open-source miniscopes: UCLA miniscope, FinchScope, miniScope and CHEndoscope. First, 3g UCLA miniscope (Ghosh *et al.* **Nature Methods** 2011) is widely used in 400 labs around the world. It offers 60Hz maximum imaging rate in FOV of 700 by 450µm. In 2016, it permitted to show that memories formed close in time show a greater overlap of CA1 neural ensembles (Cai *et al.* **Nature** 2016). Secondly, 2g FinchScope initiated at Boston University (Liberti *et al.* **J. Neural Eng.** 2017) enabled 30Hz imaging in FOV of 800 by 600µm for neural dynamics in bird vocalization studies. It used high-resolution 3D printed parts, allowing rapid prototyping and lighter designs at a reduced cost. Third, 2.4g miniScope from National Institute on Drug Abuse (Barbera *et al.* **Neuron** 2016) achieved larger FOV of 1.1 by 1mm at 10Hz rate to record activity patterns in the medial prefrontal cortex with ongoing locomotory behaviour. Fourth, 4.5g CHEndoscope (Jacob *et al.* **Current Protocols in Neuro.** 2018) from Toronto University achieved 20Hz imaging in FOV of 500µm. In short, miniscopes can perform

large FOV functional imaging (~1mm^2) at high acquisition frame rate (20-100Hz) with awake freely-behaving animals. As most of GECI have slow kinetics, typical frame rate of 30Hz is generally sufficient. Unfortunately, optical sectioning with good axial resolution cannot be reached with 1P WF. Despite a large FOV, 1P imaging cannot reach an efficient out-of-focus background rejection to target multiple neuronal sites in a small volume (e.g., 200µm). In short, miniscopes are using single-photon (1P) illumination only and widefield technique. Hence, they are limited by scattering and light absorption into tissue. Most importantly, cell precise photostimulation is today incompatible with the miniscope technology.

Fig.I.22. Miniscope scopes (from Aharoni and Hoogland, **Frontiers in Cell. Neuro** 2019)

Fiber-based microscopes

An alternative to the miniscope, which is also compatible with 2P excitation, is the optical fibers. There exist two main class of fiberscopes which one either based on individual fiber with a miniaturized scanning unit attached to the animal head; or on a fiber bundle, made of ~10 000 different cores.

i. Single-core fiber

In the case of **single-core** optical fiber, the core is unique and small (~5µm diameter), and a compact scanning device is used (Helmchen *et al.* **Cold Spring Harb. Protoc.** 2013). The single-core optical fiber guides the light from a point to another one and is surrounded by a clad and a jacket protection. The jacket determines the mechanical robustness of the cable (e.g., plastic, PVC). The more flexible (rather than rigid), the better it is for freely-moving experiments. The core is a cylinder of very small diameter (~5µm) made of glass (silica) or plastic in which the light propagates and that runs along the fiber's length.

There are two different ways to perform scanning illumination through single-core fiberscope (line, spiral or raster scanning, **Fig.I.23.**). The fist way is to move the tip of the fiber with lateral movement (line scan, Giniunas *et al.* 1991) thanks to a piezoelectric device to which the fiber is glued. This is called a resonant mechanical vibration. Its frequency is ranged from 20 to 100Hz.

The Lissajous scanning uses also piezo but with a rigid fiber end leading to have two distinct resonance frequencies (5-10 Hz) enabling to move in different directions (x and y) instead of one (Helmchen *et al.* 2001, Flusberg *et al.* 2005). Spiral scanning approach (Seibel and Schmithwick 2002) is performed thanks to a piezoelectric tube in which the fiber is inserted. All those scanning approaches would involve fluorescence detection via PMT (photomultiplier tube). A piezo tube with quadrant electrodes induces spiral scanning by driving x and y directions at the same resonance frequency but with a 90° phase shift. The second way is to use a micromirror device on top of the animal head to move the laser beam coming out of the fiber (Kiloutchnikov *et al.* **Nature Methods** 2020, Zong *et al.* **Nature Methods** 2017, Zong *et al.* **bioXriv** 2021*).* Fast high resolution miniaturized 2P microscope, can perform imaging at a 40 Hz frame rate, but on a smaller FOV of 130x130 µm^2, and at about 60 µm depth (Zong *et al.* **Nature Methods** 2017). It permits to obtain a better axial resolution (~10µm) and to reach single-cell resolution. As a latest reference, the laboratory of Jason Kerr recently performed 3P head-mounted microscope for imaging deep cortical layers (Klioutchnikov *et al.* **Nature Methods** 2020). The fiber used has a 25µm core diameter. It enabled imaging at 27 Hz with maximum square FOV of side length 140µm in freely-moving rats at 1320nm of layer 5 of GCaMP6s expressing neurons (up to 1120µm below the cortical surface).

Single core 2P system provide a very powerful tool to image neuronal activity in freely-moving animals. However, at least for the moment, they are not easily compatible with 2P photostimulation of multiple cells.

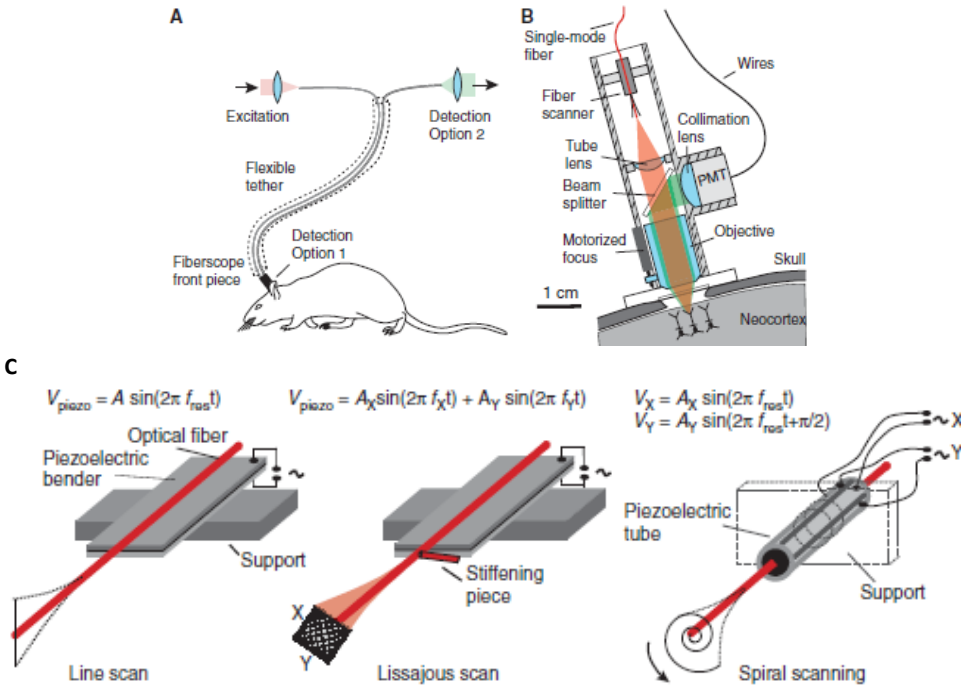

Fig.I.23. 2P Fiberscope scopes (Helmchen *et al.* **Cold Spring Harb. Protoc.** 2013)

A. Two-photon fiberscope setup. Excitation light is delivered through fiber optics to a miniaturized microscope front piece that is attached to the head of a freely behaving animal.

B. Original design used by Helmchen *et al.* (2001). Excitation light is guided through a single-mode fiber. Scanning is achieved using resonant mechanical vibration of the fiber tip. Near infrared excitation light (red) is passed through a long-pass dichroic beam splitter and fluorescent light (green) is detected by a small photomultiplier tube (PMT) at the front piece.

C. ***Left:*** Resonant fiber scanning. ***Middle:*** Two-dimensional Lissajous scanning. ***Right:*** Spiral scanning.

ii. Fiber-bundle

The **fiber-optic bundle** is composed of about 10,000 individual cores of ~5µm diameter each in a closely packed arrangement (Flusberg *et al.* **Nature Methods** 2005, 2008; Goto *et al.* **J. Light. Tech.** 2015). To achieve single-cell resolution in-depth, 2P scanning imaging through a coupled fiber-GRIN microendoscopy has been performed in some labs (Helmchen, 2004; Ozbay *et al.* **Scientific Reports** 2018). A great advantage of fiber bundle approaches is the possibility of transmitting holographic patterns through it, thanks to the multiple core geometry. The multiple cores of the fiber-bundle permit to scan each core from the proximal end of the fiber and transmit a specific pattern to the distal end based on the Computer-Generated-Holography technique (Szabo *et al.* **Neuron** 2014; **Fig.I.24**.)

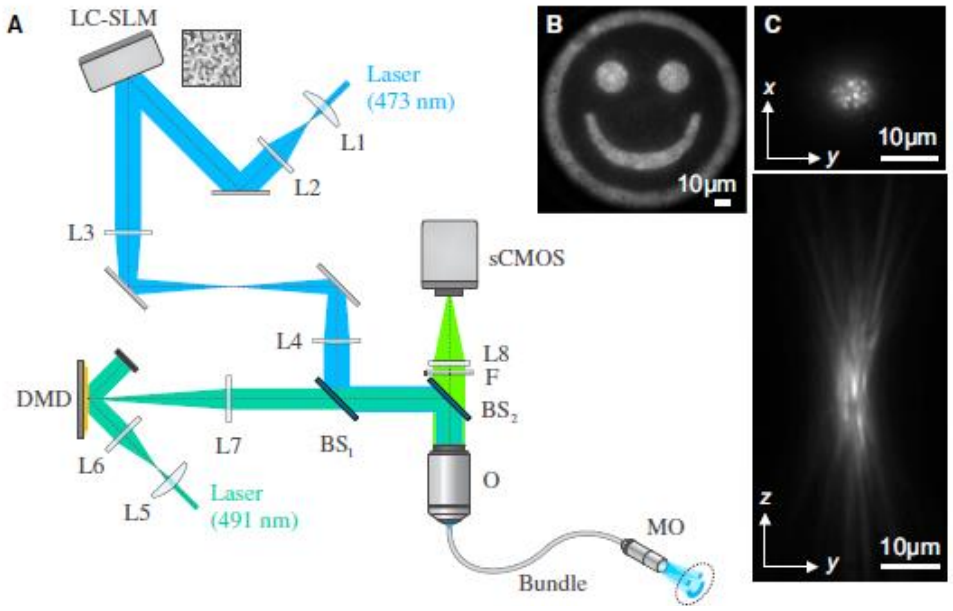

Fig.I.24. Optical Setup of the Fiberscope and Characterization of CGH (Szabo *et al.* **Neuron** 2014)

A. The fiberscope is composed of two illumination paths: one for photoactivation with CGH (blue path), including an LC-SLM, and a second for fluorescence imaging (dark green path), including a DMD. Backward fluorescence (light green path) was detected on a sCMOS camera. The paths were coupled to the sample using a fiber bundle attached to amicro-objective (MO). L, lens; BS, beamsplitter; O, microscope objective; F, emission filter.

B. ''Happy face'' illumination pattern generated with CGH and recorded with the fiberscope from the layer of (fluorescent) rhodamine, showing the full field of view (diameter, 240 mm) that was accessible for photoactivation.

C. Sections of photoactivation beam along the x-y plane (top) and y-z plane (bottom) for a 5-mm-diameter spot.

Our new system is based on previous fiberscope developed in the lab (**Fig.I.24.**) but is upgraded with simultaneous 2P imaging and 2P stimulation techniques. Owing to complex optical features of both fiber-bundle and GRIN lens, many optic developments are to set for reaching suitable resolutions for in-depth neuronal investigation with freely-moving animals. The main differences or current systems are summarized in **Fig.I.25.** with the frame acquisition rate and the field of view size (FOV) size. To date, there are not available microendoscope enabling simultaneous fast imaging (> 40 Hz) and precise 2P holographic photostimulation.

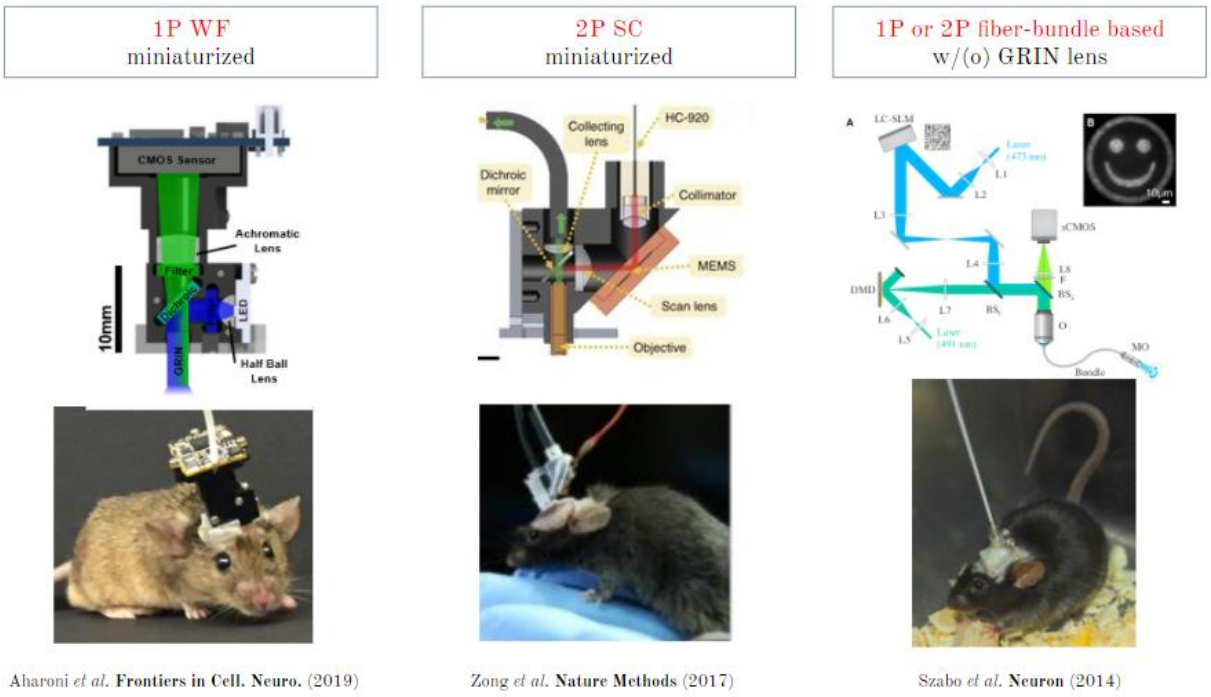

	Miniscope	**3P head-mounted microscope**	**MINI-2P**	**Fiberscope**	**2P-FCM**
Fiber type	Miniscope	Single core	Single core	Fiber bundle	Fiber bundle + GRIN lens
Ref.	Aharoni *et al.* **Frontiers in Cell Neuro.** (2019)	Klioutchnikov *et al.* **Nature Methods** (2020) Kerr's Lab	Zong *et al.* **bioXriv** (2021) Moser's Lab	Szabo *et al.* **Neuron** (2014) Emiliani's Lab	Ozbay *et al.* **Sc. Reports** (2018) Gibson's Lab
Imaging	1P	3P	2P	1P	2P
Imaging rate (Hz)	30-100	27	40	20	3
FOV size (µm³)	700*600*360	140*140 (z=1120)	420*420*180	120*120*60	220*220*180
2P photostimulation	NO	NO	NO	1P	NO

Fig.I.25. State of the art of flexible microendoscopy systems
(from Aharaoni *et al.* **Frontiers in Cell Neuro**. 2019, Zong *et al.* **Nature Methods** 2017, **bioXriv** 2021, Szabo *et al.* **Neuron** 2014, Ozbay *et al.* **Sc. Reports** 2018)

I.2.3 Challenges for micro-endoscopy and perspectives

Coupling a microendoscope system with GRIN lens and fiber bundle permits to manipulate neurons in freely-moving animals with high precision. The multiple cores of the bundle, in contrary of single core fiber, enables to apply several optical techniques, such as scanning imaging and holographic stimulation. Indeed, our final goal is to propose a new 2P system to simultaneous image and stimulate neurons, which does not exist yet.

Based on the literature, current microendoscopy system present some limitations in imaging rate, size of FOV and absence of precise neural stimulation. Indeed, a high acquisition rate is necessary for capturing fast events correlating with neuronal activity, such as intracellular calcium or membrane voltage changes (Rad *et al.* **Biophys**. 2017). Moreover, recording from large FOV is crucial to decipher biological functions over statistically significant cell populations or investigate neural network properties within the integrative function (e.g., visual function, memory mechanism, olfaction properties etc.).

To put it in a nutshell, we aim to reach *in vivo* (1) fastest frame rate, (2) bigger FOV, (3) photostimulation at the same time (4) with flexible 2P micro-endoscope for freely-moving animals (**Fig.I.26.**) All together in a robust animal preparation expressing the best combination of genetically encoded calcium indicator and optogenetic actuator for achieving all-optical *in vivo* manipulation of neurons in-depth but most importantly in freely moving small animals to meet the growing challenge of linking neural circuits with behaviour mechanisms.

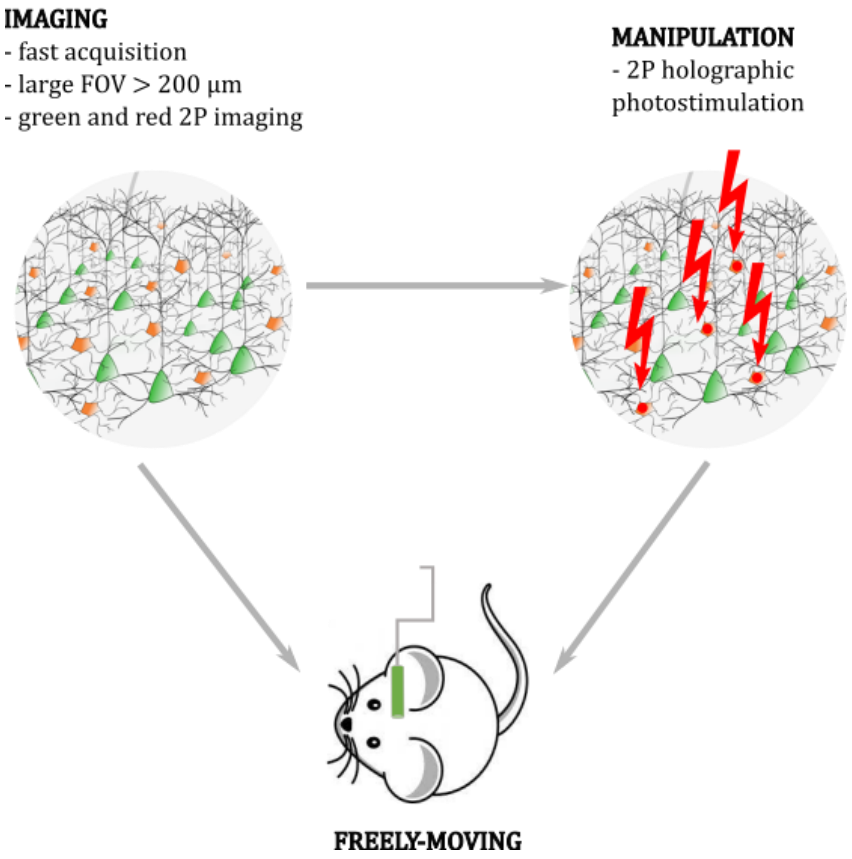

Fig.I.26. Challenge map of a new 2P microendoscope development for all-optical investigation

II. METHODS

Contents

II.1 Optical system of the new microendoscope “2P-FENDO”

II.1.1 Description of the optical setup

In this chapter, I will describe the technical details of our newly developed 2P fiber-based microendoscope as well as the biological preparations we used to test the endoscope. As already mentioned above, our goal is the development of a microendoscope that could fill the gaps of the current state of the art, particularly regarding two main aspects: 1) our endoscope should be the first one capable of simultaneous and precise 2P imaging and 2P photostimulation; 2) it should provide high imaging sensitivity, which could result in faster acquisition frame rates.

Prior to detail the new two-photon microendoscope setup, I will describe the basic principle of a conventional two-photon microscope that we will use as a reference to compare the imaging and photostimulation capabilities of 2P-FENDO.

Schema of standard two-photon microscopy setup

Excitation light is provided by a near-infrared mode-locked laser with ultrashort pulses (100fs) and high repetition rate (>80MHz). The light focused on the sample through a water immersive objective with a sub-micrometre diffraction limited spot while scanning. Indeed, the light is deflected by a scanning mirror and a dichroic beam splitter that separates the laser light from the emitted fluorescence (e.g., red and green). The emission wavelength is detected with a photomultiplier tube (PMT) (**Fig.II.1.**)

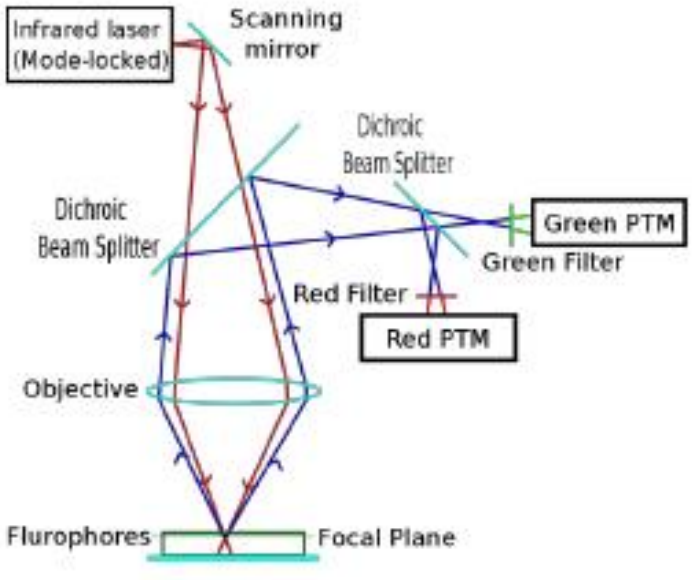

Fig.II.1. Schema of a conventional 2P microscopy setup

Schema of TWO-Photon Flexible microENDOscopy setup ("2P-FENDO")

Our new two-photon flexible microendoscope is called 2P-FENDO. It aims to be used for freely-moving experiments thanks to the combination of a 2m long fiber bundle and GRIN lens of 1.4 mm diameter. It presents two main novelties. First, a new 2P illumination approach is used for imaging through the fiber bundle, and second, the system is capable of simultaneously perform 2P photostimulation.

i. 2P Imaging

It is not trivial to propagate an ultrashort laser pulse, such as the ones needed for efficient 2P excitation, through an optical fiber, for two main reasons: first, the chromatic dispersion inside the fiber, and second, the self-phase modulation effect (Helmchen *et al.* **Appl. Opt.** 2002).

The chromatic dispersion induces a larger pulse because each wavelength propagates with a different speed along with the fiber. To compensate for this effect, the laser pulses are compressed before their propagations in the fiber. In our case, both the imaging and the photostimulation lasers are equipped with internal compressors that can counteract the fiber dispersion. The self-phase modulation (SPM) is a nonlinear effect appearing for sufficiently high-power densities (> 10 mW per fiber, Helmchen *et al.* **Appl. Opt.** 2002), whose consequence is also a longer pulse, and therefore a less efficient 2P excitation at the fiber output. However, it cannot be easily compensated by an optical device. SPM in practice limits the maximum power that can be delivered through each core of the fiber bundle, which in turns limits the total 2P fluorescence that can be generated. This is why, in previous works (Ozbay *et al.* **Sc. Reports** (2018), Emily Gibson's Lab), 2P calcium imaging through a fiber bundle, which was performed by scanning core by core the laser light at the fiber entrance, could only be demonstrated at an imaging speed inferior to 10 Hz.

To overcome this scanning speed limitation, we chose to illuminate several cores at a time with a larger excitation spot of about 20 µm diameter, by using the maximum allowed power before the onset of SPM, that is, around 10 mW per core. In this way, the total power at the sample plane could be increased to N_{cores}*10 mW, thus increasing the total 2P signal, without increasing the power density. The large imaging spot was then scanned by a galvo-resonant scanner at the fiber entrance. A motorized iris on the path to the fiber bundle is used to change the imaging spot size and thus the total amount of power at the focal plane. The emitted fluorescence is collected through the same GRIN objective with fiber bundle system, separated from the laser light using a dichroic mirror, and detected by a high yield EM-CCD camera (Andor IXon Ultra).

ii. 2P Photostimulation

Because the fiber bundle is composed of cores, we can apply 2P holographic approach for stimulating neurons (protocol in **Fig.II.2.**). In previous references, only one system did perform photostimulation but with 1P approach (Szabo *et al.* **Neuron** 2014). To reach precise manipulation of neurons at the single level, 2P illumination is more suitable. We used a spot of 5 to 15 µm diameter to match the size of a neuron via in-house *Wavefront* software, with a total power of 20-60 mW. In this way, the SPM effect is kept under control for the photostimulation laser as well.

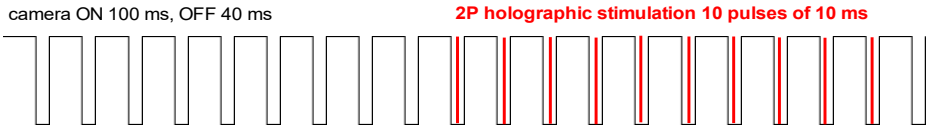

Fig.II.2. Protocol of 2P holographic stimulation

iii. Choice of fiber bundle, GRIN lens and lasers

The imaging and photo-stimulation lasers are focused by a 0.3 NA objective at the entrance of the endoscope. We have tested several fiber bundles and GRIN lenses and found the best combination for our system, which the results are described in the next chapter. In short, the fiber bundle used is FUJIKURA model with small core bodies where the distance between them is less than 2 µm to gain better lateral resolution than other fiber bundle candidates. It is a 2-m long fiber bundle (Fujikura model FIGH-15-600N). Concerning the GRIN lens attached to the animal head, we used GT-MO-080-032-ACR-VISNIR-08CG-00 model from *GRINTech*, allowing to image a big field of view (FOV) of 250 µm.

Since our new microendoscope aims to perform both 2P imaging and photostimulation for freely-behaving animals, there are two paths in the optical setup: one for imaging and one for photostimulation. For imaging, the light source for 2P we used is Spark Alcor laser, for which the central wavelength is 920 nm, pulse duration of 150 fs, total power of 4 W, repetition rate of 80 MHz. This ultrafast imaging laser is scanned by a galvo-resonant scanner at the entrance of the fiber bundle. And for stimulating, the photostimulation laser is a low repetition rate laser: Amplitude Goji, central wavelength of 1040 nm, pulse duration of 150 fs, total power of 5 W, repetition rate of 10 MHz. This photostimulation laser is spatially shaped by a SLM (Hamamatsu) using computer-generated holography (CGH) to excite simultaneously multiple neuronal somas at the imaging plane. The optical setup of 2P-FENDO is schemed in **Fig.II.3.**

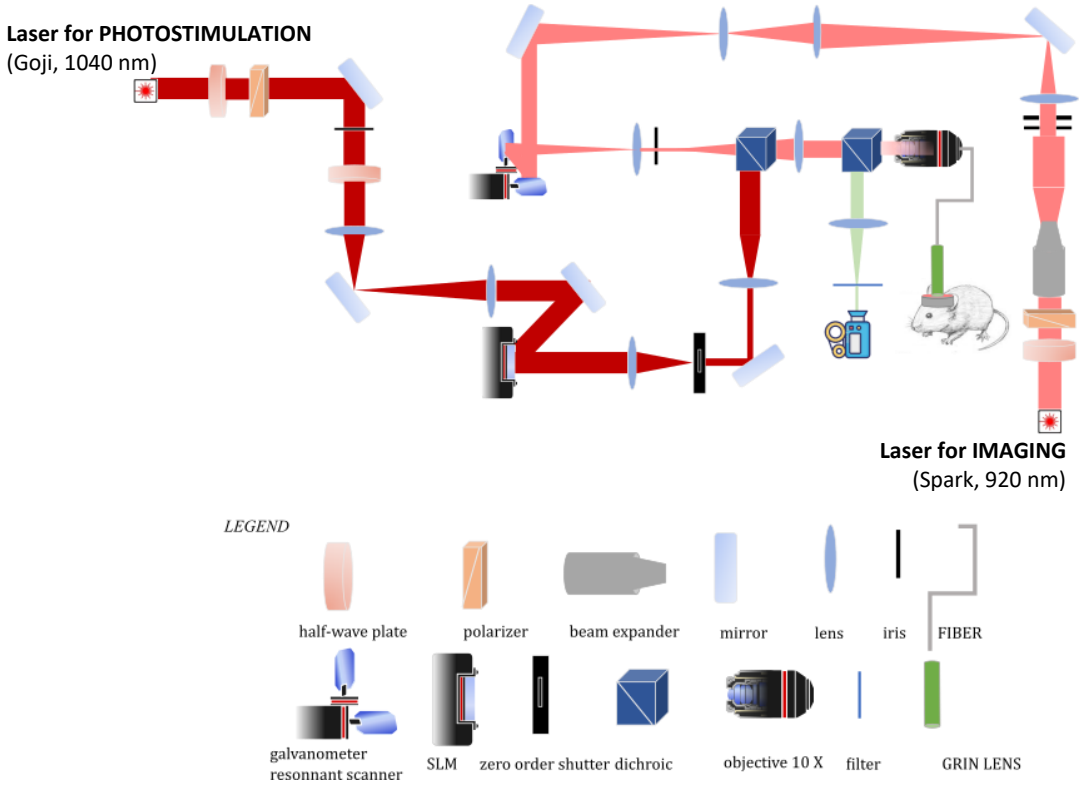

Fig.II.3. Schema of 2P-FENDO optical setup

II.1.2 Fiber and GRIN lens characterization on rhodamine

2P-FENDO uses large excitation spots for both imaging (10-30 µm in diameter) and photo-stimulation (5-15 µm in diameter). In a classical optical setup however, this would result in a dramatic loss in axial resolution, which could undermine the advantages of using 2P excitation. As demonstrated in the next figure, 2P-FENDO circumvents this problem by taking advantage of the intrinsic temporal properties of the fiber bundle, in particular of its the inter-core delay dispersion.

Fig.II.4. illustrates this phenomenon. In practice, the fiber bundle separates the pulses from each core in time. This is due to imperfections in the fabrication process of the bundle, which result in slight geometrical differences among each core, and therefore in slightly different propagation times. When the GRIN lens is placed at the fiber output, it re-images the cores at the sample plane. Because the pulses from each core are separated in time, they do not interact with each other, which effectively decreases the out of focus exitation and maintains good axial resolution even for large excitation spots, as demonstrated in **Fig.III.5.**

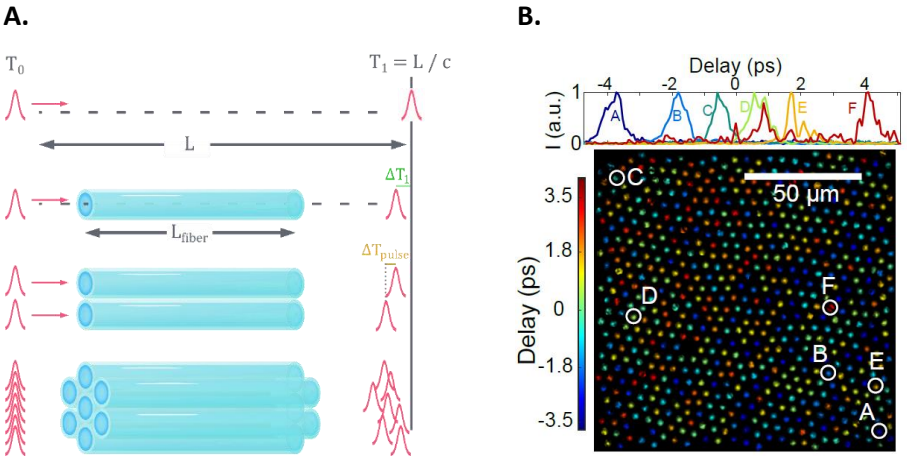

Fig.IIL.4. Inter-core delay dispersion through the fiber bundle

A. Schema of the phenomenon
B. Measurements

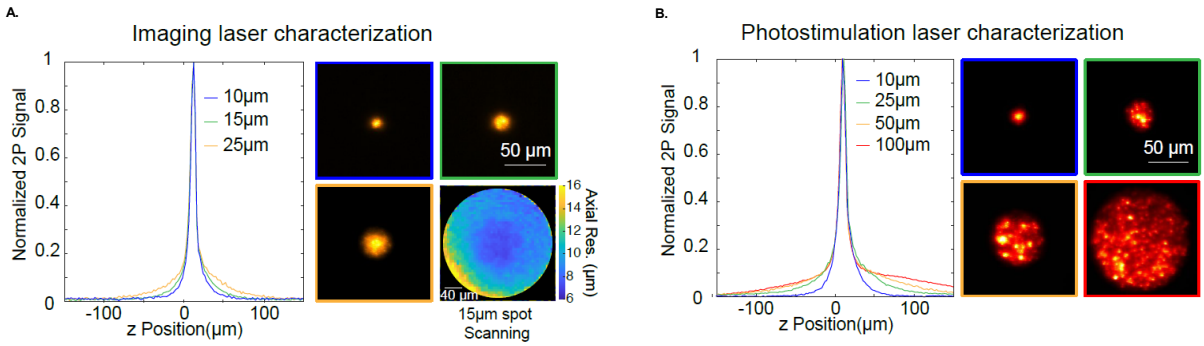

Fig.II.5. Axial resolution of extended spots of different sizes for the imaging and photostimulation on rhodamine

A. Imaging laser characterization
B. Photostimulation laser characterization

In **Fig.II.5.**, the different sizes correspond to different aperture diameter of the motorized iris in the case of the imaging laser and to holographic spots of different sizes produced by the SLM for the photostimulatiuon laser. The axial resolutions are measured by moving the distal end of the fiber plus the GRIN lens system together in z using a vertical step motor while recording the emitted 2P fluorescence from a thin (~ 1 µm) rhodamine layer on the camera detector. The axial full width at half maximum of the central Lorentzian peaks is as narrow as 7 µm for the imaging laser and 8 µm for the photostimulation one. The red curve was acquired by raster scanning a 25 µm spot across the sample and measuring the axial profile. All the measurements were acquired using the GT-MO-080-032-ACR-VISNIR-08CG-20 GRIN lens. The spot sizes correspond to sizes at the sample plane, i.e., after the GRIN lens. To know the size at the entrance of the fiber one should multiply the spot diameter by the GRIN lens magnification (M=2.2).

The axial profiles, even for 30 µm imaging spots or for 100 µm holographic spots are dominated by a full width at half maximum (FWHM) of 7-8 µm. As the 2P spots are made larger, a broader pedestal appears, resulting in some out of focus excitation, especially for spots of diameter superior to 50µm. However, we always kept the imaging spot at a diameter inferior to 30 µm, whereas the photostimulation spots were always of diameter comprised between 5 and 15 µm, to match the size of a neuron.

In the future, the GRIN lens could be implanted inside the brain tissue for going in deeper brain region, which we did not do in this proof-of-principle. In perspective, it may provide access to unreachable brain regions involved in perception, cognition and behaviour (e.g., amygdala, hippocampus, thalamus).

To establish the proof-of-principle of this new microendoscopy, it is obviously essential to have proper biological preparation to image and photostimulate. In the next section, I will outline the biological preparations used *in vitro* and *in vivo*.

II.2 Biological preparations

In order to test the imaging and photostimulation capabilities of our newly developed 2P flexible microendoscope for all-optical manipulation of neurons in freely-behaving animals, several preliminary sets should have been tested. Imaging resolution along with viral expression were first checked on fixed brain slices, then *in vitro* on organotypic slices from hippocampal mouse pups before going *in vivo* with anaesthetized head-restrained mice. After validating all those essential steps, the final all-optical manipulation including 2P photostimulation was then able to be *in vivo* with awake freely-behaving mice. In this chapter, I will outline all biological preparations to get to the best condition for imaging and photostimulation of single to multiple neurons with 2P-FENDO.

II.2.1 AAV viral injection

Animals

All animal experiments were performed in accordance with Directive 2010/63/EU of the European Parliament and of the Council of 22 September 2010. The protocols were approved by the Ethical Committee and by the French Ministery for Research (#201803261541580). I did all necessary trainings and obtained mandatory certifications for animal experimentations and surgeries for mice in UK and France. Adult male C57BL/6J mice (*Janvier Labs*) were anesthetized with intraperitoneal injection of a ketamine–xylazine mixture (0.1 mg of ketamine and 0.01 mg of xylazine/g body weight) prior to stereotaxic surgery. Adult mice of both sexes from the transgenic line GP4.3 (*The Jackson Laboratory*), which express the calcium indicator GCaMP6s (Dana *et al.*, 2014) were used as first attempts of imaging. Then we rather chose viral injection in WT mice with jGCaMP7s (Dana *et al.* 2019) as GECI, without or with the combination of opsin virus which were at the base of ready-to-use animal for all-optical manipulation of neurons. Cortical neurons of 4-week-old mice were infected with viral vectors of opsins using stereotaxic injection. Imaging and photostimulation experiments were performed 3 weeks to 4 months after injection.

Virus injection procedures and viral strategy

The following viral constructs were used: AAV9.CMV.GFP.WPRE.bghpA ($3{,}21 \times 10^{14}$ GC/mL) for expressing green fluorophore GFP and image at 920nm Tsunami laser and AAV1-CAG-tdTomato (*Addgene,* 6×10^{12} GC/mL) for expressing red fluorophore tdTomato and image at 1030nm with Satsuma or Spark lasers. To perform live imaging, we expressed green calcium indicators: AAV9.hSyn.GCaMP6s.WPRE.SV40 (*Addgene* 1×10^{13} GC/mL) and for expressing GCaMP6 for the very first attempts of imaging and then the more efficient indicator newly developed AAV9-syn-jGCaMP7s-WPRE (*Addgene,* 6×10^{12} GC/mL / 2.3×10^{13} GC/mL) expressing jGCaMP7s or red ones such as AAV9.Syn.NES.jRCaMP1a. WPRE.SV40 (*Addgene* 2.1×10^{13} GC/mL).

To manipulate single cell activity, soma-targeted actuator was added. For the first trials of photostimulation (unshown in the Chapter Result), we used the opsin virus AAV9.hSyn.DIO.ChroME.ST.P2A.H2B.mRuby3.WPRE.SV40 (from Hillel Adesnik Laboratory, USA; 5.86×10^{13} GC/mL) with AAV-EF1a-Cre-p2A-WPRE at 1/50) for expressing fast red-tag opsin and

image with Satsuma 1030nm; AAV1-EF1a-ReaChR-p2A-tdTomato (ratio 1:1), AAV9.hSyn. fastChrimson.tdTomato.WPRE.bGH (Chrimson Y261F-S267M from Tobias Moser Laboratory, Germany; 9.9x10^{12} GC/mL) (ratio 1:2). Finally, we rather chose to inject AAV1-hSyn-ChRmine-mScarlet-Kv2.1-WPRE (*Max Planck Florida*, 7,63x10^12 GC/mL) along with AAV(1or 9).hSyn.jGCaMP7s (See Chapter Result) at different ratios (viral vectors for GCaMP7s and opsin expression were used at 1:1; 2:1; 1:0.1 ratios), imaging with Spark laser (920nm) and photostimulation with Goji laser (1040nm). At the end, the best ratio of GCaMP:opsin to enable all-optical manipulation was 2:1.

As a red calcium indicator, we also used the virus AAV9.Syn.NES.jRCaMP1a. WPRE.SV40 (*Addgene*, 2,1x10^{13} GC/mL) associated with the opsin AAV2/1-hSyn-CoChR-GFP (from UNC Core Vector, USA; 1.49x10^{12} GC/mL) (ratio 1:1) for simultaneous calcium imaging with Satsuma laser at 1030nm and photostimulation with Tsunami laser at 920nm (unshown data).

All viruses are mixed with a pipette in small aliquot and centrifuge just before loading it for injection. To avoid brain oedema, anti-inflammatory was injected dexazone subcutaneous 0.01mL before intraperitoneal injection of the anaesthetic ketamine/xylazine. In order to reduce pain due to bone surgery, subcutaneous injection of buprecare 0.05mL and lidocaine 0.02mL were carried out. To hydrate mouse eyes, a gel of lubrithal were applied. The surgery including craniotomy, viral injection and skin suture would last about 45 minutes (including 10-20 min for injection infusion). During the surgery procedure, the animal was placed in a stereotaxic table (*Phymep-KOPF instruments*) and on a heating pad with a rectal probe set at 37°C (*Stoelting*), a survival blanket because of the air flux of the hood, making the ambient temperature dropped. To help the animal waking up, we injected subcutaneously antisedan 0.05mL and the animal was kept in a separate box to avoid animal fighting with each other, and hot thermal mat would help its recovery until it wakes up.

Through a craniotomy over the right primary visual cortex V1 (3.5 mm caudal from bregma, 2.5 mm lateral from the midline) or the somatosensory barrel cortex S1 (-1.5mm from bregma, 2.5 mm from the midline), 500 nL to 1 uL of viral vectors were delivered via a silicate cannula in L1 and L2/3 (50-200 µm deep) at a speed of 75-100 nL/min. Since we do not implant the GRIN lens inside the brain but imaging outside the brain on top of a 3 mm round coverglass (80-130 µm thick #0, *Warner Instruments*), more superficial depth was targeted during injection: two step-depth: 150 µm from the pial surface with half volume and at 50 µm for the half rest, waiting 5 minutes when the infusion ends before slowly retracting the silicate injection needle to avoid loss of virus going out.

The choice of the best opsin also relies on its kinetics and action spectrum. We based our gold-choice of opsin on the following characteristics: first, on fast on- and off-kinetics, to avoid excessive imaging cross-talk and to enable imaging without leading to a high level of unwanted opsin photoactivation; second, on a red-shifted 2P activation spectrum to avoid an overlap of the optogenetic actuator and activity indicator spectra (Chen *et al.* **Current Opinion Neuro.** 2018). As a matter of fact, the kinetics properties of opsins (related to the opening and closing time of the channels) determine the ultimate temporal resolution and precision achievable with photostimulation: fast opening time will enable reaching efficient current integration with short illumination pulses, while fast off-time will enable fast cell repolarization thus enabling generation of high frequency spiking trains when consecutives photostimulation pulses are delivered (Ronzitti *et al.* **J. Neuro** 2017).

For this project, the chosen opsin is ChRmine. The gold-choices for primary visual cortex of mice, are the serotypes AAV1 and AAV9 (Srivastava *et al.* **Current Opinion in Virology** 2016). A high expression level of opsin in neurons can be achieved with the reduced human synapsin promoter (hSyn). As a detailed reminder, herewith I outline some characteristics of the viral construct: **AAV9** (Adeno-associated viruses of 25 nm, single-stranded DNA genome and a capsid comprised of three structural Cap proteins (VP1, -2 and -3) is the serotype for CNS (central nervous system, i.e. brain); **Syn** (synapsin) is a promotor for neuronal specificity; **WPRE** (Woodchuck Hepatitis Virus (WHP) Posttranscriptional Regulatory Element) is a DNA sequence that, when transcribed creates a tertiary structure enhancing expression. Commonly used in molecular biology to increase expression of genes delivered by viral vectors; **SV40** (simian virus 40) refers to polyomavirus (mammals) as a model eukaryotic virus. The fast kinetics opsin ChRmine is a high potential candidate (Marshel *et al.* **Science** 2019). It is combined with the red fluorescent tag *mScarlet* in order to be easily imaged with a GECI, such as jGCaMP7s. Indeed, this combination would allow to image the calcium indicator in green (lambda 920nm). ChRmine was excited at 1040nm. This construct also includes the soma-targeting domain Kv2.1 (Baker *et al.* **eLife** 2016 Bolton's Lab). In this configuration, the calcium indicator has a cytosolic expression, and the opsin has a membrane expression.

Slicing mouse brain

In order to check the viral expression and facilitate imaging, thin fixed brain slices were used. The animal is euthanized, the brain was extracted and the whole brain was kept 24h in paraformaldehyde (PFA 4%) to fix the tissue before slicing it. The day after, the brain was washed with PBS 1X and sliced of 250 µm thick with a vibratome (slicer Leica VT1000). The fluorescent expression of virus (green or red) was checked with a special lamp (*DFP-1 dual fluorescent protein flashlight, Nightsea company*). Mounted with fluoromount-G on the lamella, the sample dried at room temperature in the dark overnight. The coverslip used was about 0.13-0.16 mm thick (No.1, i.e., *Knittel glass*). Before imaging, fluorescent expression (green GFP or red TdTomato) was first tested with Nanozoomer, i.e., a slice scanner working at high speed to obtain high quality images and then screened with a confocal microscope (Olympus) to confirm that individual neurons could be distinguished.

Organotypic slices preparation

To fasten the viral expression checks, we used organotypic preparations to observe within days opsin expression whereas a mouse viral injection takes at least a month. The hippocampus was extracted from C57BL/6J mice pups (Janvier Labs) between P6-P9 anaesthetized by ice under L2 hood and cut 300 µm thickness slices with a chopper (McIlwain Tissue Chopper, Model MTC/2). After half an hour at 4°C in medium, the best slices were selected and placed on a rectangle PTFE membranes (Millipore FHLC04700) on a well of 6-well-plate with 1.1 mL of Opti-MEM medium with the inserts (Sigma PICM03050) and incubated at 37°C, 5% CO2 and medium from Opti-MEM to Neurobasal changed every 2-3 days. The slices were infected with virus after 3 DIV and imaged after 10 DIV.

II.2.2 Surgery for *in vivo* recordings

For the first attempts of *in vivo* imaging, the animal received acute cranial surgery and imaging session was performed within a day in anaesthetized head-restrained condition. As the surgery would last about an hour and the imaging session about 4h, the intraperitoneal injection of anaesthetic (ketamine/xylazine) was repeated every hour or as soon as sign of awakening was detected by pinching its feet (with half initial dose or about 1µL).

A circular craniotomy of 3-4 mm diameter was made over V1 or S1 and the dura mater was removed. A coverglass (No. 0, ie 0.085 to 0.13 mm thick) with agar 4% at the edges were applied on top of the craniotomy to dampen tissue movement. The mouse was anaesthetized with intraperitoneal injection of a ketamine–xylazine mixture (0.1 mg of ketamine and 0.01 mg of xylazine/g body weight) during stereotaxic injection. For reducing pain, local subcutaneous lidocaine is injected (0.02mL), along with the anti-inflammatory dexazone (0.01mL SC) to avoid oedema of brain that would cause movement of the tissue and inflammation reaction of the brain and finally diluted buprenorphine (0.05 mL SC for 25g animal). During functional imaging, the anaesthetized mouse was head-fixed with a home custom-made system with an additional oxygen supply through a nose mask whilst oxygen was monitored with a leg probe (mouseOx, *Harvard Apparitus*) and body temperature was controlled whilst the animal was placed on a heated pad at 37°C (homeothermic monitor with a rectal probe, Harvard Apparatus).

After removing the membrane covering the skull, we removed the dura to reduce the distance between the GRIN lens and the neurons. This crucial step demands preciseness because it may damage the brain surface and leads to blood vessel bleeding, making the immediate imaging impossible. A continuous hydration with NaCl 0.9% helps to dura removal. Then the thin coverglass (80-130 µm thick #0, *Warner Instruments*) is maintained by z axis and custom-needle tip, before pouring agar solution 3% for maintaining the coverglass in place. The flatness of the coverglass in regards with the GRIN lens is checked with a xyz monitor and by moving the stage angles where the animal will be head-restrained. For the chronic preparation, Vetbond glue is used instead of agar and for freely-moving preparation, kwik sil is privileged. Once the coverglass is considered stable, the headplate is cemented with dental ciment (*C&B Superbound kit*). For chronic preparation, aiming to reduce the number of injected animals (3R rule for ethics), I followed the same protocol as in Russell *et al.* **bioRxiv** 2019.

II.2.3 In vivo setup

Before being able to perform freely-behaving experiments with the new microendoscopy system, the anaesthetized animal is head-fixed in a custom-made system (**Fig.II.6.**). We did optimize the head-restrained system from a transparent tube restrainer and big thermal mat to a more stable support where the stage is able to be moved in xyz in order to get a flat coverglass plane (**Fig.II.6.C.**) for stable imaging on unimplanted animals. The self-design headplate (**Fig.II.6.A.**) is screwed after acute craniotomy on the holder system (**Fig.II.6.D**.). A nose mask provides oxygen for the well-being of the animal and a thermal mat with a rectal probe for body temperature control is used to stabilize the anaesthetized animal. Since the right side of the brain is injected (either visual or barrel cortex), the visual stimuli is presented to the left eye. To make sure the recording does not have artefact with surrounding light environment, we designed and 3D-printed cone (**Fig.II.6.B**.) in which a screen monitor displays the visual stimuli. For barrel imaging, the whiskers on the left side are stimulated.

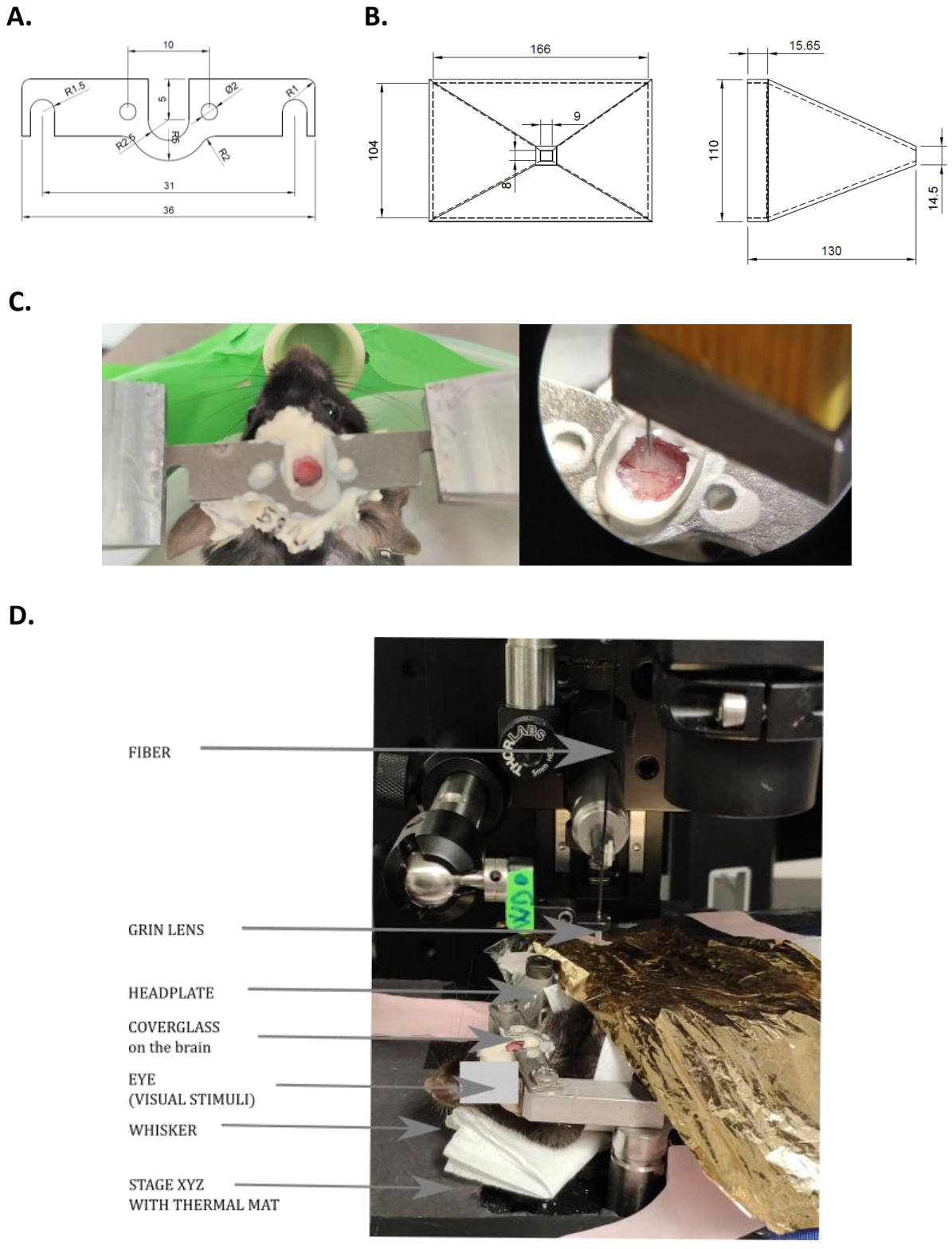

Fig.II.6. Custom-made materials for in vivo imaging of head-restrained mice (*by Christophe Tourain and Florence Bui)*

A. Headplate for maintaining the mouse in head-restrainer for stable imaging.

B. Triangle tube to avoid surrounding light artefact around the eye mouse during visual stimuli.

C. Picture of the head-fixed animal for *in vivo* brain imaging

D. Picture of the 2P-FENDO set up for head-fixed mouse

To evoke neuronal response with sensory stimuli, either visual stimulation or whisker stimulation were carried out.

Visual stimulation

For visual stimulation, a visual monitor with a custom tube is placed in front of the left eye since the injection was done in the right hemisphere brain. The visual stimuli protocol in those experiments is the same as what our lab is commonly using. The drifting gratings are coded via psychophysics toolbox from *Matlab*.

The visual setup is based on three main references in the field: (1) Ko *et al.* **Nature** 2011, (2) Chen *et al.* **Nature** 2013, (3) Dana *et al.* **Nature** 2019. We compare our in-house visual protocol with the references and confirm it is equivalent (see **Annexe 1**).

The protocol is the following:

- White screen « welcome » when launching the visual stimuli protocol
- 4 seconds of grey screen
- 4 seconds of a grating (deg*) (**Fig.II.7.**)
- 4 seconds of grey screen
- 4 seconds of the next grating (deg*)
- Iteration number: from 1 to 5 time for one minute acquisition

*deg: oriented white and grey bars for which the edges are blurred with sinusoidal type, moving from left to right with an angle 0 à 360°, each different drifting grating are different from 45° for a total of 8 different drifting gratings.

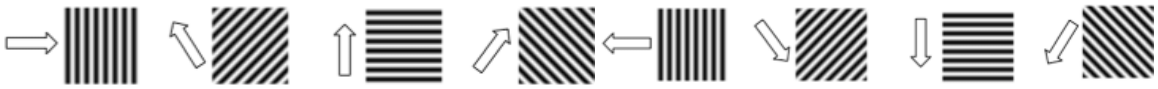

Fig.II.7. Visual stimuli: 8 drifting gratings

Whisker stimulation

For whisker stimulation, the system used is published in Serge Charpak's Lab (Zuend *et al.* **Nature Metab.** 2020). The whiskers were stimulated with a metal rod attached to a mechanical shutter/chopper which deflected the whisker at a rate of 5 Hz.

To put in a nutshell, many preliminary samples were prepared to make the biology consistent for *in vivo* imaging and photostimulation. Going *in vitro, ex vitro* before *in vivo* helped to sketch the perfect conditions for the neurons to express the right combination of calcium indicator and opsin actuators. Moreover, numerous trials were performed, and new equipment were installed to make the stereotaxic surgical procedure robust and custom-made devices were designed and printed inside the lab facility to fit our new microendoscopy system and gain in stability for imaging with fiber and GRIN lens on small animal brains.

II.2.4 Freely-moving setup

Since our final goal is to perform imaging and photostimulation in freely-behaving animal, we need to think in advance about the more stable system to be fix on top of the mouse head.

A.

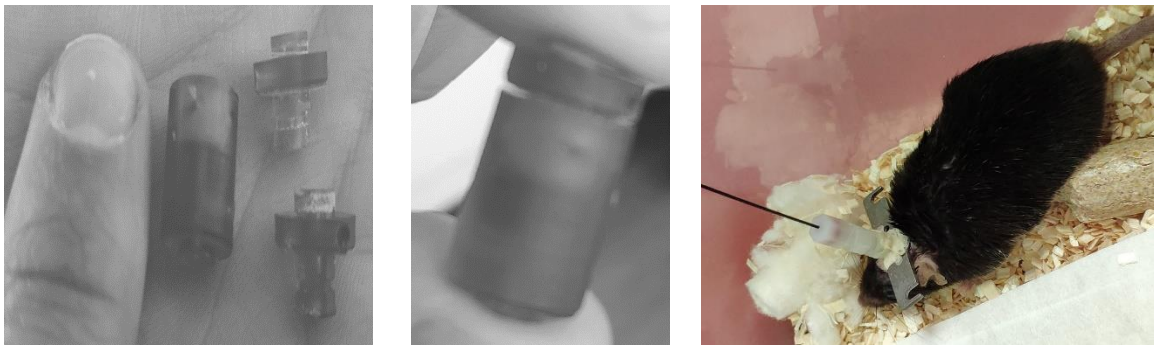

B.

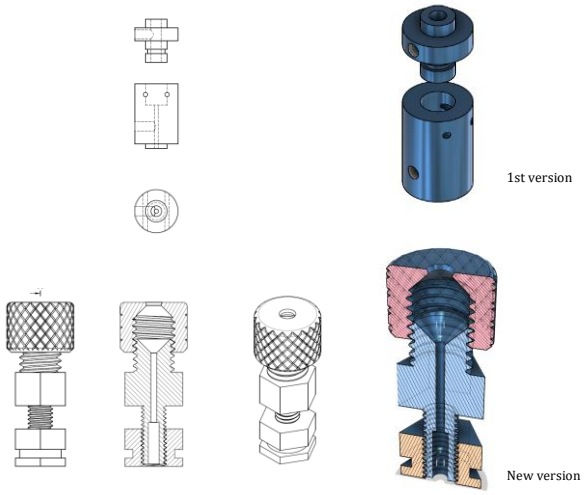

Fig.II.8. Custom-made implant for fiber and GRIN lens to hold on mouse headplate for freely-moving recording under 2P-FENDO

A. Picture of the first (in grey) 3D-printed custom-made material to hold fiber bundle with GRIN lens for freely-behaving mice and the latest (in color) version of the implant.

B. Schema of the implants designed by C. Tourain, F. Bui and F. Blot.

Since our microendoscope combines fiber bundle and GRIN lens for performing all-optical manipulation of neurons in freely-moving mice, we self-designed and printed the holder implant to fit the size of our materials (**Fig.II.8.**). After a few trials with the first version (*left* A, *upper* B), we noticed the rotation movement of the fiber inside the holder. Hence, the holder was optimized to get a more robust holder (*right* A, *down* B). Moreover, the screw of the final implant is M5 type, so the total turn achievable in z axis is about 0.75 µm with 12 steps. By this mean, we can manually move the focal plane of 0.063 mm in z. We reported the latest recording in Chapter Result.

II.2.5 Data analysis

Image analysis was performed by using *Image J*, *MATLAB* (*Mathworks*), *OriginLab* and *GraphPadPrism* softwares. First, ROIs of cell soma were manually screened in ImageJ. Z projection of images were made by summing the stack images, where the background was subtracted of about 50 pixels (depending on the maximum size of a cell), the contrast was enhanced of 0.1% normalized to the entire recording, and gaussian filter was applied of 0.5 to 2 pixels to get rid of cores. The 3D view was made via *Imaris* software. For visualizing the fluorescence contrast, we chose LUT green, red, mpl-viridis or mpl-inferno. The calcium traces were extracted via a *MATLAB* in-house code based on green (jGCaMP7s) fluorescence images. ROI with custom shape and neuropil were manually selected. For each ROI, the relative percentage change of fluorescence was computed as DF/Fo=(F-Fo)/Fo, where Fo was the average baseline fluorescence signal. Fo is calculated based on a published method (Romano *et al.* Nature 2017). The baseline Fo reflects slow fluctuations unrelated to the calcium transients associated with neuronal activations, using a running-window average increasing with the acquisition speed and averaging the 100 to 300 minimum values. The timelapse fluorescence signal of jGCaMP7s from all ROIs was exported in *MATLAB* or *OriginLab*. The peak value of DF/Fo was analysed in *OriginLab* at the local maximum between two positive points for a smoothing window. The statistical analysis was done in *GraphPadPrism,* mostly based on paired parametric t test with 95% confidence interval.

III. RESULTS

Contents

In this chapter, I will outline the main results towards all-optical brain manipulation microscopy showing the development of our brand-new optical system along with the biological preparations from the early stage to the last optimization state to determine (1) the imaging resolution, functional imaging capabilities during (2) spontaneous and (3) evoked activity and to finish (4) the photostimulation performance on single and multiple neurons for freely-behaving experimentations.

The development of the new microendoscopy setup - we named 2P-FENDO - described in the previous chapter, was progressively tested on several biological samples: in fixed brain slices, *in vitro* in organotypic slices, *in vivo* in head-restrained anaesthetized mice and finally, in freely-moving awake mice.

III.1 Single cell resolution on fixed neurons underlying neural morphology

III.1.1 Imaging with two different GRIN lens-fiber combinations

We tested three fiber bundles with three GRIN lenses. Promising results were obtained with SCHOTT and FUJIKURA fiber bundles along with two *GRINTech* lenses.

Made of thousands of cores, the flexible SCHOTT fiber is composed of 3.5µm diameter cores with pitch value between cores of 7.4 µm, it can transmit 30% of the incoming light. The more rigid FUJIKURA fiber displayed nearer (4.2 µm) and smaller core bodies of 2.5 µm diameter where higher IR is transmitted up to 60%. In short, they should present different lateral resolutions that we will demonstrate below on fixed fluorescent brain samples. In fact, the lateral resolution depends on the inter-core distance of the fiber and the magnification of the GRIN lens.

We used two different GRIN lenses with high numerical aperture (NA=0.7) on the sample side with both chromatic and field corrections. The main differences between those two candidates are first, the working distance at the sample side: second, the size of the field of view (FOV). The GRIN lens “GL2” (i.e., GT-MO-080-032-ACR-VisNIR-08) can focus on a plane at 80 µm after 170 µm thick coverglass (we finally used 80-130µm thick coverglass) and image large FOV of 250 µm; whereas GL1 (i.e., GT-MO-070-016-ACR-VisNIR-30-20) is enabled to image at 300 µm depth without coverglass but smaller FOV of 125 µm is accessible.

All characteristics from the optical fiber bundle and GRIN lenses are summarized in **Fig.III.1.**

A.

FIBER BUNDLE	Core diameter	Pitch	Light transmission
SCHOTT	3.5 µm	7.4 µm	30%
FUJIKURA	2.5 µm	4.2 µm	60%

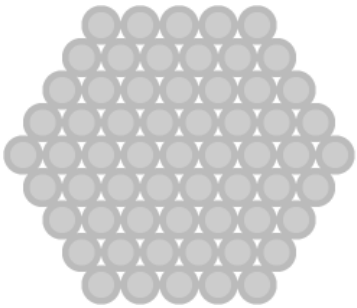

SCHOTT

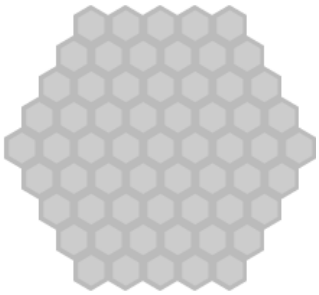

FUJIKURA

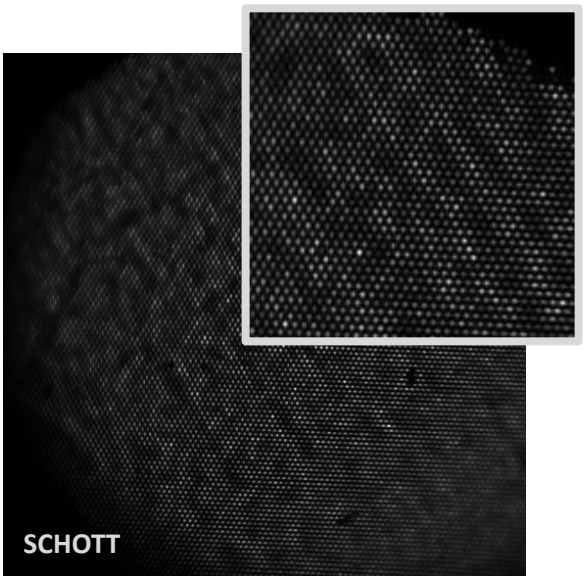

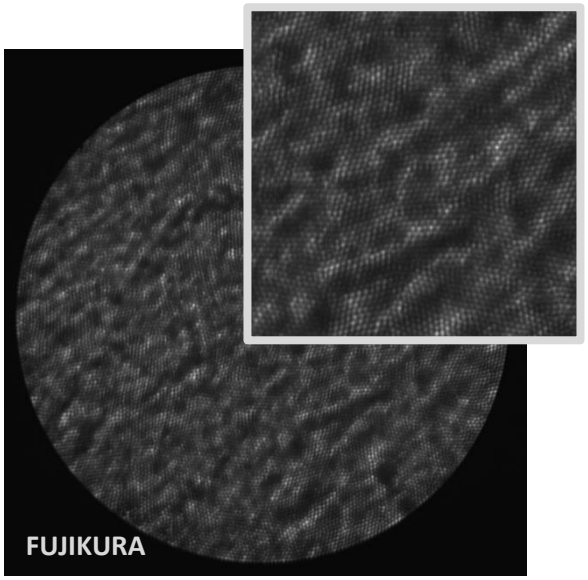

B.

GRIN LENS	Abbreviation	NA: fiber / sample	Magnification	Working distance: fiber / sample (µm)	FOV with current fiber (µm²)	Dimensions: diameter / length (mm)
GT-MO-070-016-ACR-VisNIR-30-20	GL1	0.16 / 0.7	4.5	200/300 no coverglass	125*125	1.4 / 8.36
GT-MO-080-032-ACR-VisNIR-08	GL2	0.32 / 0.7	2.2	200/80 after 170 µm coverglass	250*250	1.4 / 4.84

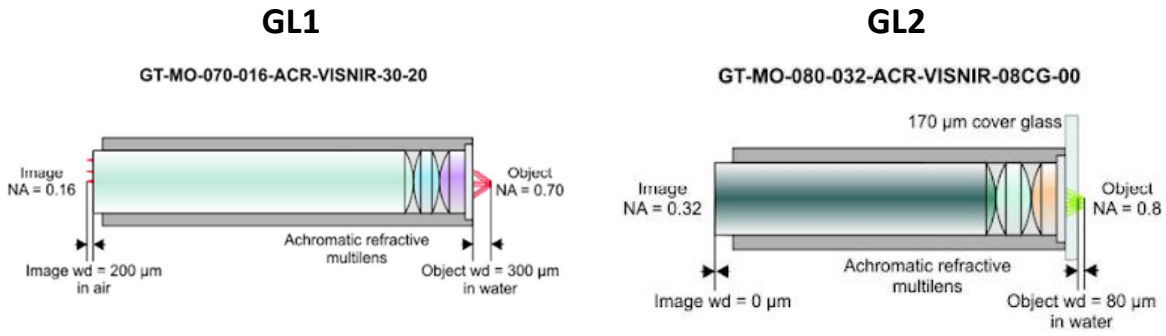

Fig.III.1. Characteristics of optical fiber bundle and GRIN lens candidates.

A. Properties of fiber bundles FUJIKURA and SCHOTT with schema of the cores in theory and in practice (images taken under the microscope).

B. Properties of GRIN lenses with their main optical differences and schematic components.

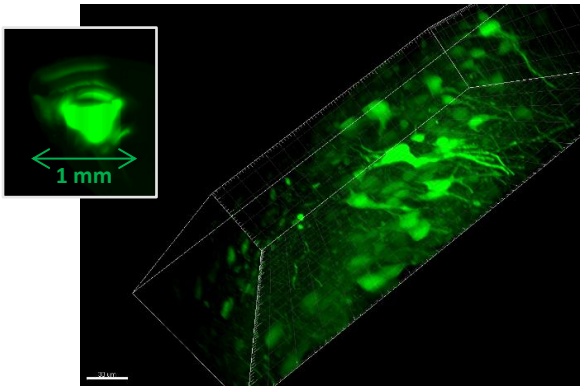

Fig. III.2. Sample of fixed brain slices of mouse subcortical regions expressing GFP.

***Upper*:** Shot from Nanozoomer of the brain slice with the green colour filter, showing the region where neurons express GFP.

Lower: Confocal 3D view of neurons expressing GFP, scale bar = 10 µm.

The samples used here are brain slices (**Fig. III.2.**) with a thickness of 250 µm, fixed and protected by a coverglass. The animal was injected in the thalamus three weeks before PFA fixation with 1µL virus for GFP or TdTomato fluorescent marker expression.

The criteria for selection of the best combination fiber-GRIN lens were based on how precisely we can distinguish a single fluorescent somata in a given field of view. To this purpose, we acquired in-depth (z) stacks of a fixed brain slice under the new 2P microendoscope and extracted the lateral line profile and axial z profile information. The cell body of a neuron in this region ranged from 10 µm to 20 µm diameter size.

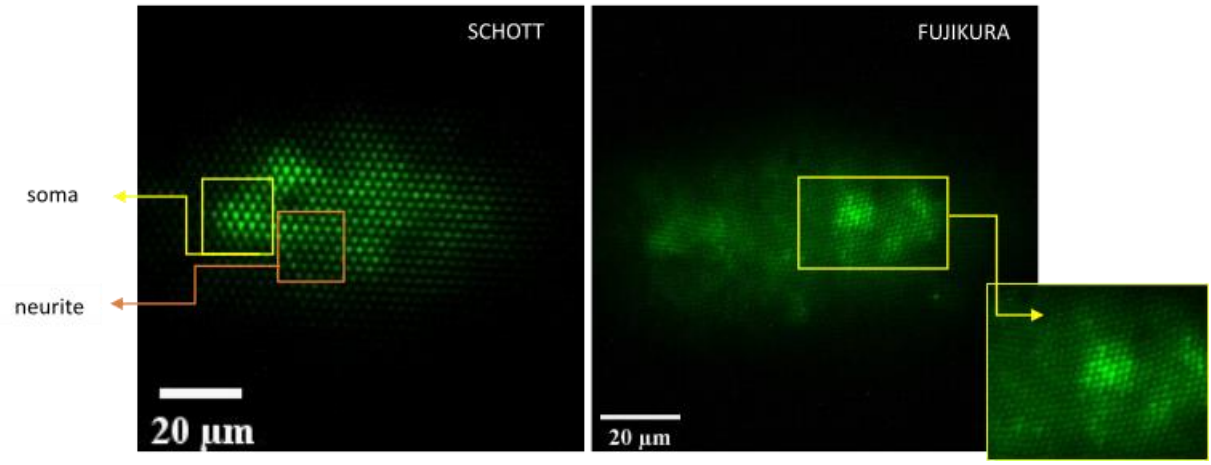

Fig. III.3. 2P-FENDO imaging of fluorescent neurons expressing GFP virus in mouse fixed brain slice

Left: Image through SCHOTT fiber bundle and GRIN lens GL2* at z=11µm depth underlying neurites and somas. Laser Tsunami 920nm; exposure time 500ms, bin 4; Z stack 40µm with dz=1µm.

Right: Max projection image through FUJIKURA fiber bundle and GRIN lens GL2* showing somas with better lateral resolution, Laser Tsunami 920nm, exposure 1000ms, bin 1, Z stack of 40 µm with dz=1µm.

* GL2, i.e., GT-MO-080-032-ACR-VisNIR-08, FOV 250 µm

The **Fig. III.3.** shows images collected with two different fiber bundles: SCHOTT and FUJIKURA, combined with the GRIN lens GL2 that can display a larger field of view (250 µm). In both modalities, fluorescent somata are visible (yellow square) where the size matches the theoretical neuron size. Nevertheless, though FUJIKURA fiber bundle, the smaller core (2.5 µm << 3.5 µm) and a closer inter-core distance (pitch 4.2µm: two-fold than SCHOTT) show a better lateral resolution. Indeed, information can be lost in SCHOTT condition because the inter-core space is gives rise to black region in the image. As a neuronal cell body is about 10-20 µm, there would be about 30% loss of information if the core size and intercore space is of 3.5µm. Thus, lateral resolution is better with nearer and smaller core bodies. The lateral resolution is about ~ 7-10µm (See Chapter Methods): more details are distinguished with FUJIKURA fiber bundle, even without averaging the signal by removing the cores in image treatment. Fluorescence values are normalized to value at position z=0, where the zero position is set at the brightest cell signal. When comparing 2P signal across the depth position, the axial profile of the same cell seen through SCHOTT is bigger than FUJIKURA fiber bundle (See Methods Chapter), it corresponds to a full width at half maximum (FWHM) of ~ 9µm with SCHOTT and ~8µm with FUJIKURA version.

III.1.2 Illumination technique of 2P-FENDO

A.

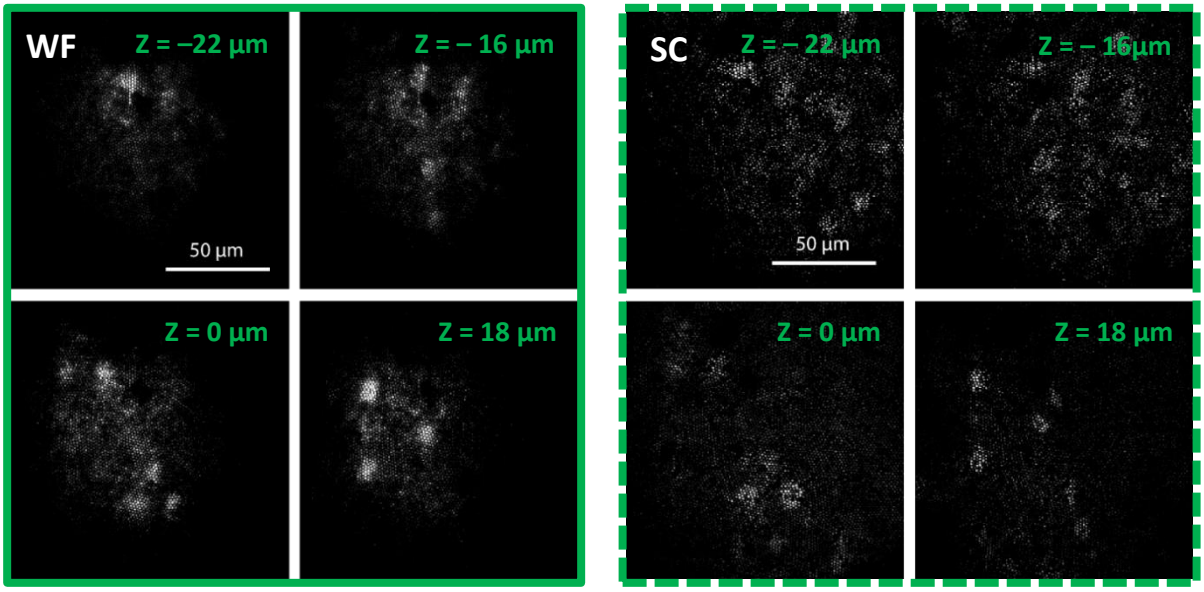

B.

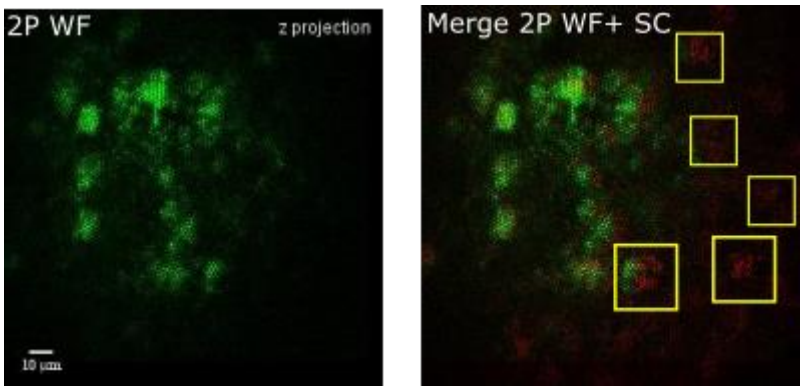

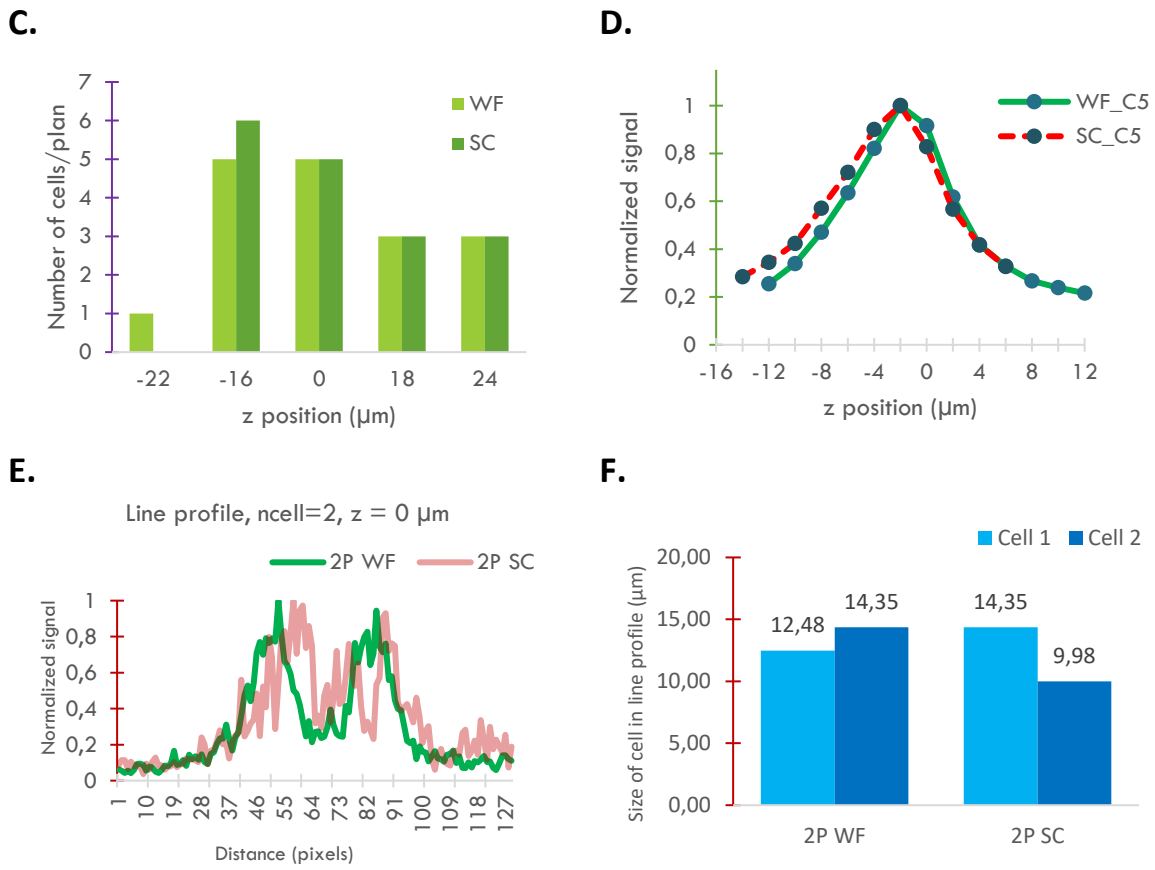

Fig. III.6. Widefield versus Scanning approach

A. *Left*: 2P widefield (2PWF) *Right*: 2P scanning (2PSC) at 30 Hz. GFP expressing neurons imaged with FUJIKURA fiber bundle and GRIN Lens GL1 (FOV 250 µm), Z stack of 70 µm with dz=2µm

B. Z max projection of 60 z images for 2P WF (*left*), merged image of 2P WF and 2P SC Z projection (*right*). Red is the cell enabled to be imaged with 2P Scanning; green is cells imaged with 2P WF and 2P SC.

C. Count of cells for both techniques in 40 µm depth section.

D. 2P widefield and scanning fluorescent signals normalized.

E. Line profiles of fluorescent signals from two neighbouring cells imaged in WF and scanning approaches.

F. Size comparison of two cell soma from both 2P WF and 2P SC techniques.

The figure (**Fig. III.6.**) shows the difference between 2P widefield illumination and 2P point scanning illumination. In both techniques, 4 plans with different cells are visible (**Fig. III.6.A.**). In the merge Z projection of the same cells imaged with 2P widefield (2P WF) technique and 2P point scanning one (2P SC), extra cells are detectable (red somas in yellow square) with this latter approach (see red cells in **Fig.III.6.B.**). Slight differences are quantified (**Fig.III.6.C.**) and 2P fluorescence signal are alike in axial profiles (z=+6µm) and line profiles (soma size +/-2 µm) while imaging the same cells with different imaging approaches (**Fig.III.6.D,E**). In our new microendoscopy, we will use a mixed technique of 2P scanning with a wider illumination spot of 20 µm diameter, to send enough light to the cores keeping the advantages of the fiber bundle properties, as explained in the Chapter Method (**Fig.III.3.**).

III.1.3 *In vivo* imaging in 2 colours

We have started to image in green with GFP fluorophore as being a common reference for fluorescence imaging such as green calcium indicator to track neuronal. Nevertheless, our aim is to develop a system compatible with all-optical manipulation: activity sensor and opsin. As the commonly used calcium sensors have a green fluorescent tag, we need to be able to image the opsin with a red fluorescent tag. Therefore, we have tested the performance of our imaging system with both green (GFP) and red (TdTomato) fluorescent markers *in vivo.* Here, we demonstrated the possibility to image *in vivo* two fluorophore colors through 2P-FENDO.

In **Fig. III.7,** we present two examples of GFP (green) and tdTomato (red) expressing neurons obtained by imaging the cerebral cortex of an anaesthetized head-restrained C56BL6J WT mouse *in vivo*. A viral vector (AAV9-ssCMV-GFP-WPRE-bghpA or AAV1-CAG-tdTomato) was injected 3 to 5 weeks earlier in the primary visual area and the craniotomy was performed the day of the experiment. The animal was anaesthetized with intraperitoneal injection of ketamine/xylazine, oxygen was supplied, and depth of anesthesia was controlled with an oximeter and leg probe, body temperature was kept at 37°C with a thermal mat, monitored with a rectal probe. We recorded several axial stacks with 2µm step where the zero was set at the first plane where cells were detected. Images were obtained with FUJIKURA fiber and GRIN lens GL1 (FOV 125 µm) or GL2 (FOV 250 µm).

First, these results demonstrate that imaging fluorescent neurons through both FUJIKURA fiber and GRIN lens *in vivo* is feasible. Second, we showed the possibility to image red (**FigIII.7.A.B.**) and green fluorophores (**FigIII.7.C.D.**): single somata and even neurites were imaged at different depths. Our system can detect several planes with distinguished cells, and it can image up to ~140µm depth from the pial surface (**Fig III.8A.B.**) with both GRIN lenses with micrometer axial resolution. Third, the advantage of the bigger FOV is the possibility to detect more cells at once (**FigIII.7.B.D.**), although small details, such as neurites, were only revealed with the small FOV GRIN lens (**Fig.III.7.C.**). To check if the imaging quality is preserved while moving the focal plane during imaging acquisition with 2P-FENDO, we compared the cell size for both GRIN lens and both color fluorophores at different depths (**Fig. III.8.D.**). The mean soma size is about 10 +/- 1 µm for all conditions, which is consistent with the size of a neuron at this depth of the mouse cortex. Since we aim at using the system for multi-target optogenetic stimulation, we kept using the GRIN lens with the bigger FOV for the rest of the experiments.

In conclusion:

- To do imaging on dendrites or small blood vessels for example, the GRIN lens GL1 which gives access to FOV of 125 µm is more appropriate.
- To see the highest number of cells, the GRIN lens GL2 which gives access to bigger FOV of 250 µm is a better option.
- 2P-FENDO have sufficient axial and lateral resolution to study neuronal somatas of mouse brain at ~150µm deep.
- Both green and red fluorophores can be imaged *in vivo* with the same microscopy system.

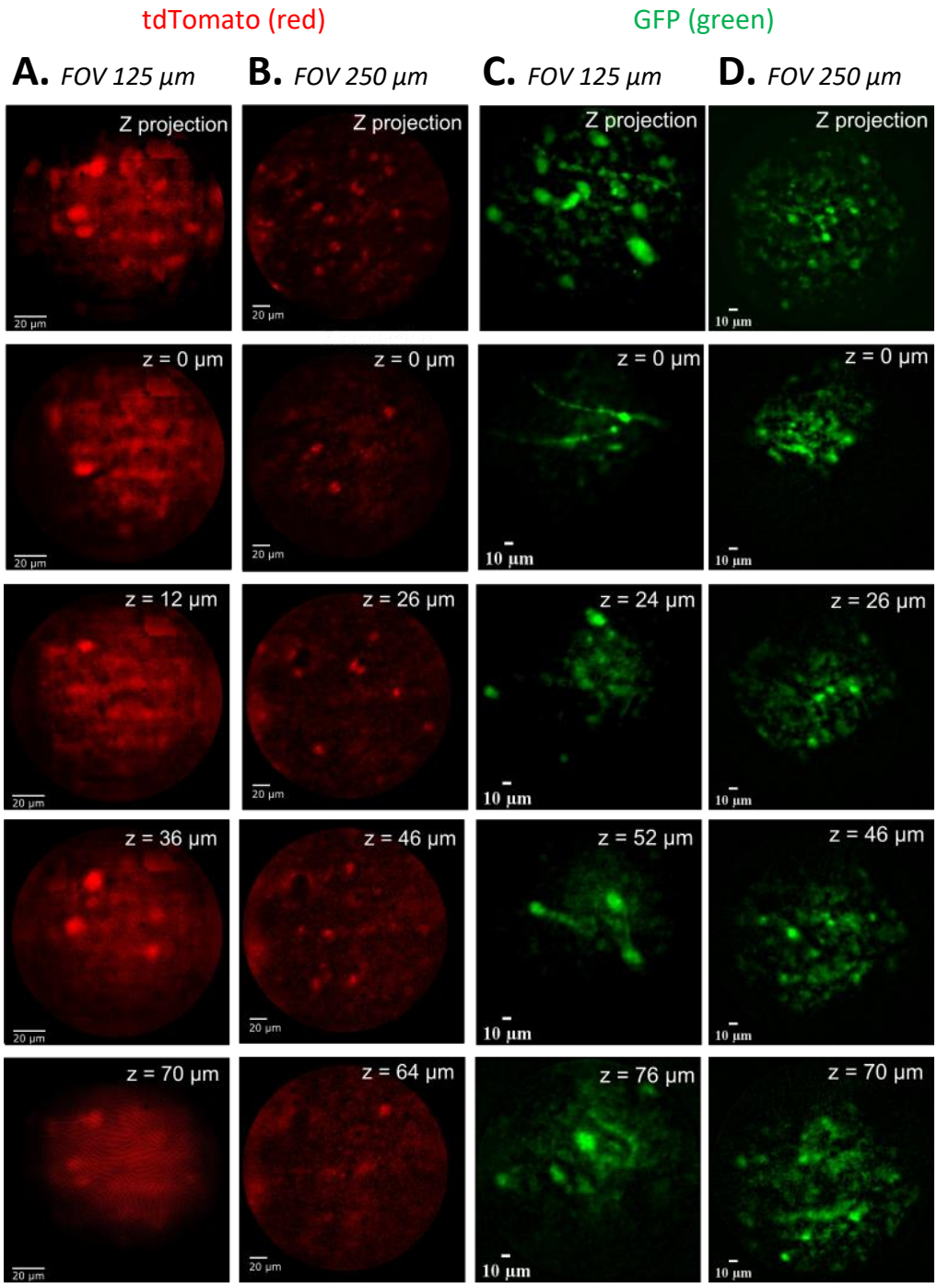

Fig III. 7. Imaging in green and red through 2P-FENDO on C57BL6J mouse visual cortex *in vivo.* Z projections of the axial stack with maximum intensity and individual deep planes of several fluorescent neurons.

A. B. *In vivo* Z stacks of neurons expressing AAV1-CAG- tdTomato, highlighting different plans of cells imaged with single cell resolution through FUJIKURA fiber and GRIN lens: (A) GL1 GT-MO-070-016-ACR, FOV 125 µm; (B) GL2 GT-MO-080-032-ACR-VISNIR-08, FOV 250 µm. Stacks from z=0µm to z=64-70µm (Satsuma laser, 1040 nm).

C. D. *In vivo* Z stacks of neurons expressing AAV9-ssCMV-GFP-WPRE-bghpA, highlighting different plans of cells imaged with single cell resolution through FUJIKURA fiber and GRIN lens: (C) GL1 and (D) GL2. Stacks from z=0µm to z=70-76µm (Tsunami laser, 920nm).

All images were filtered offline with a gaussian blur function to remove the core structure of the fiber bundle; enhanced contrast was normalized for each plane

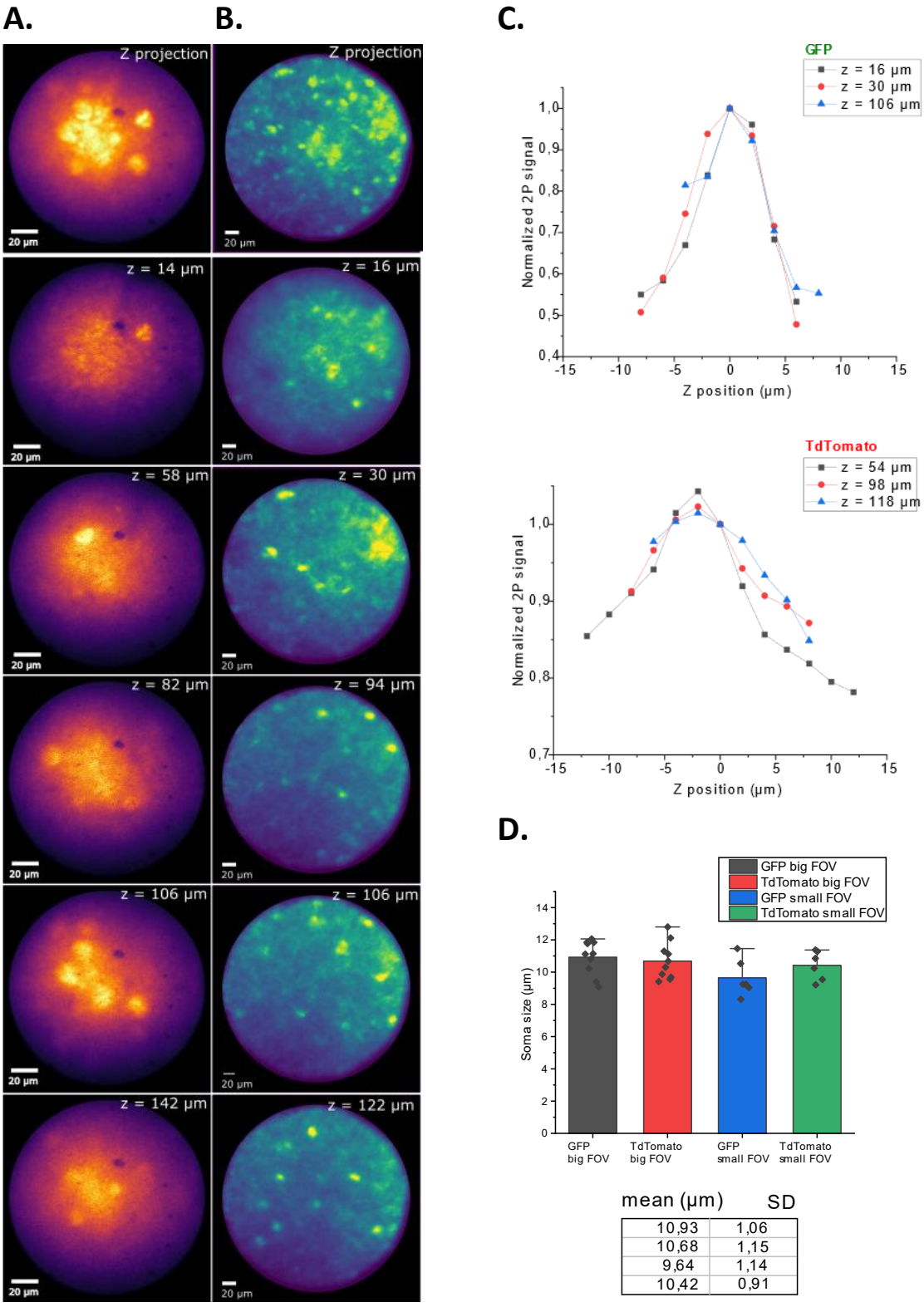

Fig. III. 8. Deeper imaging in green and red through 2P-FENDO *in vivo.*

A.B. Summation of ~60 images with maximal intensity and individual planes of axial stack with dz = 2 µm from: (A) tdTomato expressing neurons imaged through FUJIKURA fiber and GRIN lens GL1, FOV 125 µm, up to z = 142 µm depth; (B) GFP expressing neurons through FUJIKRA fiber and GRIN lens GL2, FOV 250 µm up to z=122 µm depth.

C. Axial profiles of somata from GFP and tdTomato expressing neurons.

D. Soma size from the 4 panels of stacks from Fig.III.7. n=5-10 cells for each Z projection, mean+SD (µm).

III.1.4 Details of cortical blood vessels morphology

Before demonstrating evidence of functional imaging, we show here the level of details this new microendoscope can reach.

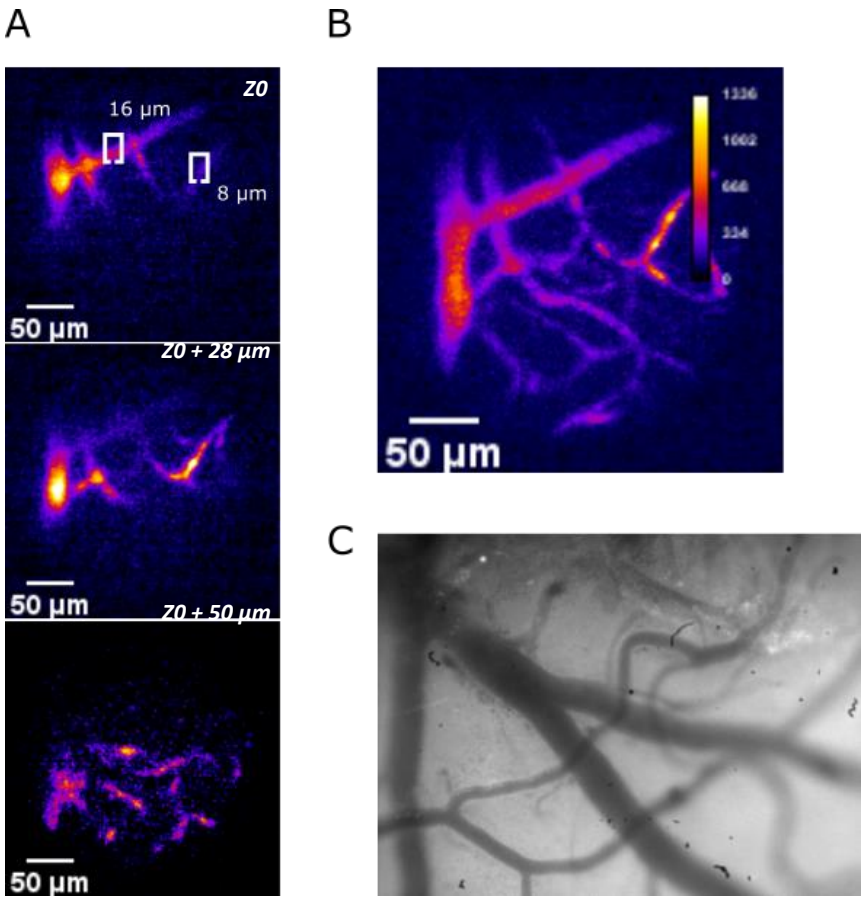

Fig. III. 9. Imaging fluorescein flowing in mouse blood vessels *in vivo*

A. Imaging of fluorescein flowing in blood vessels at 10 Hz at different depths through 2P-FENDO (Tsunami laser 920 nm, 360 mW).

B. Summation of all stack images with maximum intensity.

C. Intact mouse brain before in vivo imaging after performing stereotaxic craniotomy and dura removal under ketamine/xylazine anaesthesia. Transmitted light, objective 10X.

A solution of fluorescein-dextran (10 mg/mL for 70 000 MW, injection of 50 to 100 µL) was injected in one eye (retro-orbital) of the anaesthetized head-restrained mouse. After a few minutes, we could visualize fluorescence in the blood vessels as the fluorescein flows. We obtained a good level of fluorescence and contrast to test the detection limit (**Fig. III.9.B.**) of our system on blood vessels with a diameter ranging from 8µm to 16µm (**Fig III.9.A.**). Not only fixed fluorescent signal can be detected but also the fluorescine signals fluctuations depending on the vessel blood size (**Fig III.9.C.**) through 2P-FENDO can be tracked in small structures. We have set our system with FUJIKURA fiber and GRIN lens allowing access to 250 µm FOV with a mix approach of 2P scanning with a large spot of 20 µm diameter; to image fluorescence in small neurons *in vivo*. In this way, our microscopy system is ready for functional imaging.

III.2 Spontaneous neuronal activity via calcium imaging

Since my thesis goal is to show the proof-of-principle of a new microendoscopy system in the context of all-optical interrogation of visual circuits, the next step to validate is to demonstrate the performance of functional imaging quality in a cortical brain area. The metrics are: (1) the level of calcium indicator expression for which the protocol of viral injection would be progressively optimized; (2) the probability to observe spontaneous neuronal activity across time relative to different frame rate acquisition of imaging; (3) the detection of calcium transients and its variability with the imaging depth; (4) the axial and lateral resolution that the new microendoscopy can reach with respect to expected performances that were modelized.

III.2.1 Organotypic brain slices — *in vitro* functional imaging

In the Methods chapter, I quoted the viral infection of organotypic slices (days) from pup mouse hippocampus as a preparation to minimize the time window expression of a virus in comparison to viral stereotaxic injection in adult mouse brain (weeks). Five days after the viral infection, the sample was ready to be imaged. The organotypic slice, placed in a chamber and perfused with ACSF1X bubbled with O2/CO2, did not always show a sufficient spontaneous activity. To increase neuronal excitation, gabazine was added in the perfused medium (40 µL of 10 Mm Gabazine in 200 mL ACSF1X, i.e., 2 µM). Gabazine is an antagonist of GABAa receptors, acting like a blocker of inhibition of neurons.

Based on the article demonstrating the efficiency of recently developed jGCaMP7s (Dana *et al.* **Nature Methods** 2019), we have chosen to continue functional experiments with this latter GECI version. We can cite the original article "it produces the highest response to small (1-10) action potential trains, presenting a five-fold larger DF/Fo amplitude for one action potential stimuli and faster rise time than GCaMP6s". Its 2P fluorescence absorption and emission spectra are similar to the parent constructs. Here, we present the results from AAV9.hSyn.jGCaMP7s and AAV1.hSyn.jGCaMP7s expressing neurons in organotypic slice, imaged 6 days after transfection through 2P-FENDO after having checked its expression and activity under 2P standard scanning microscope.

Given the 2P scanning as a microscope reference to compare with our new flexible 2P microendoscope, we demonstrated that fluorescent expressing cells can clearly be visualized (**Fig III.10**). However, the cells with low fluorescence or dim cells (donut shape, blue scale **Fig III. 10.C.**) may be not visible with our current system (**Fig.III.10.D.**) where brighter cells are detectable. The surface plot of both imaging (**Fig III.10.E.F.**) shows that the baseline fluorescence and background noise may be involved in detection of low fluorescent cell detection.

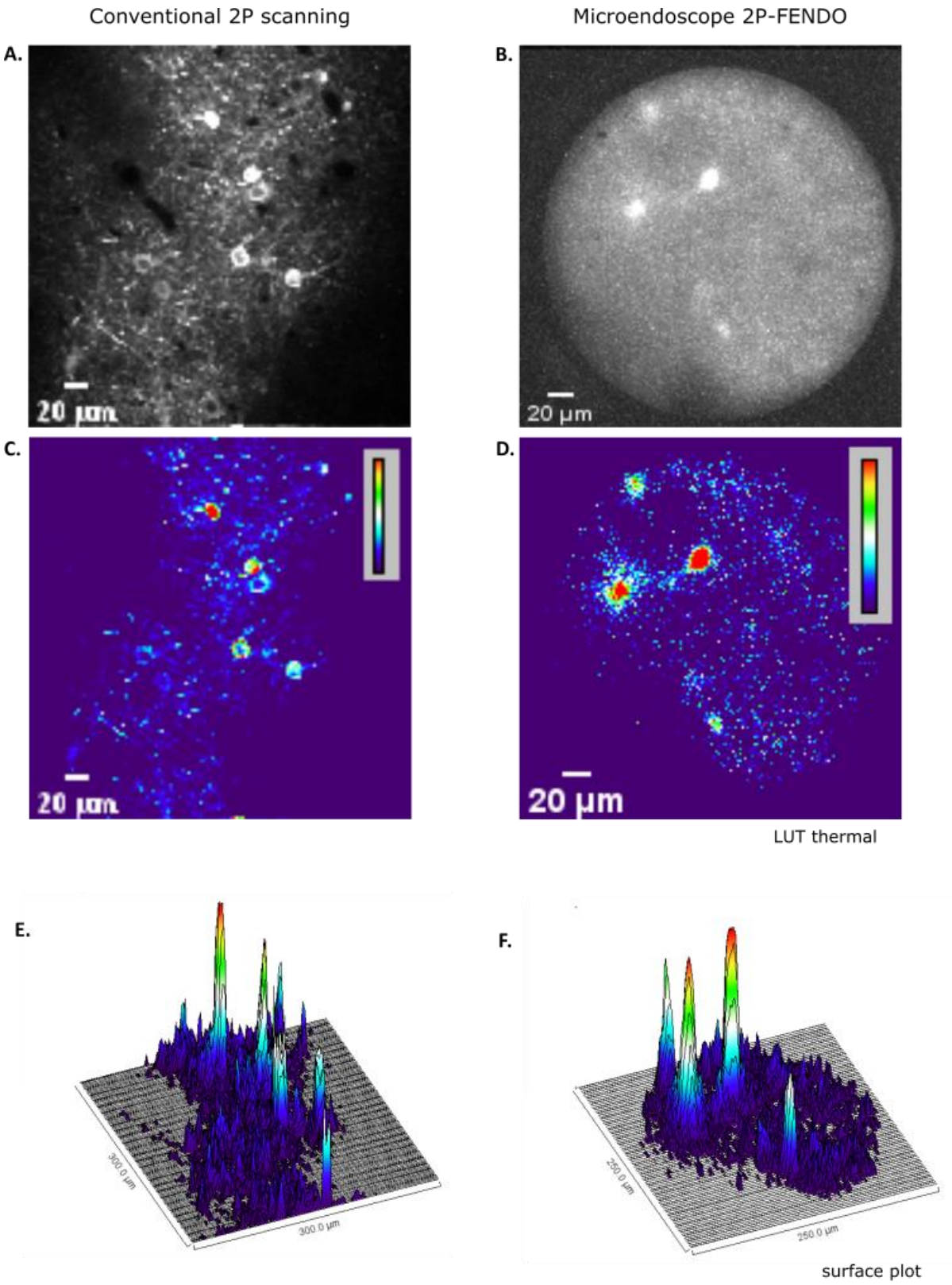

Fig III.10. Comparison of imaging quality between conventional 2P microscope and 2P-FENDO

A. B. Images of neurons expressing calcium sensor jGCaMP7s (Spark 920nm 300mW at z=103µm and 95µm)

C. D. Emphasis of fluorescence level where red is the brighter signal on the calibration bar scale.

E. F. 3D visualization of most fluorescent signals with surface plot.

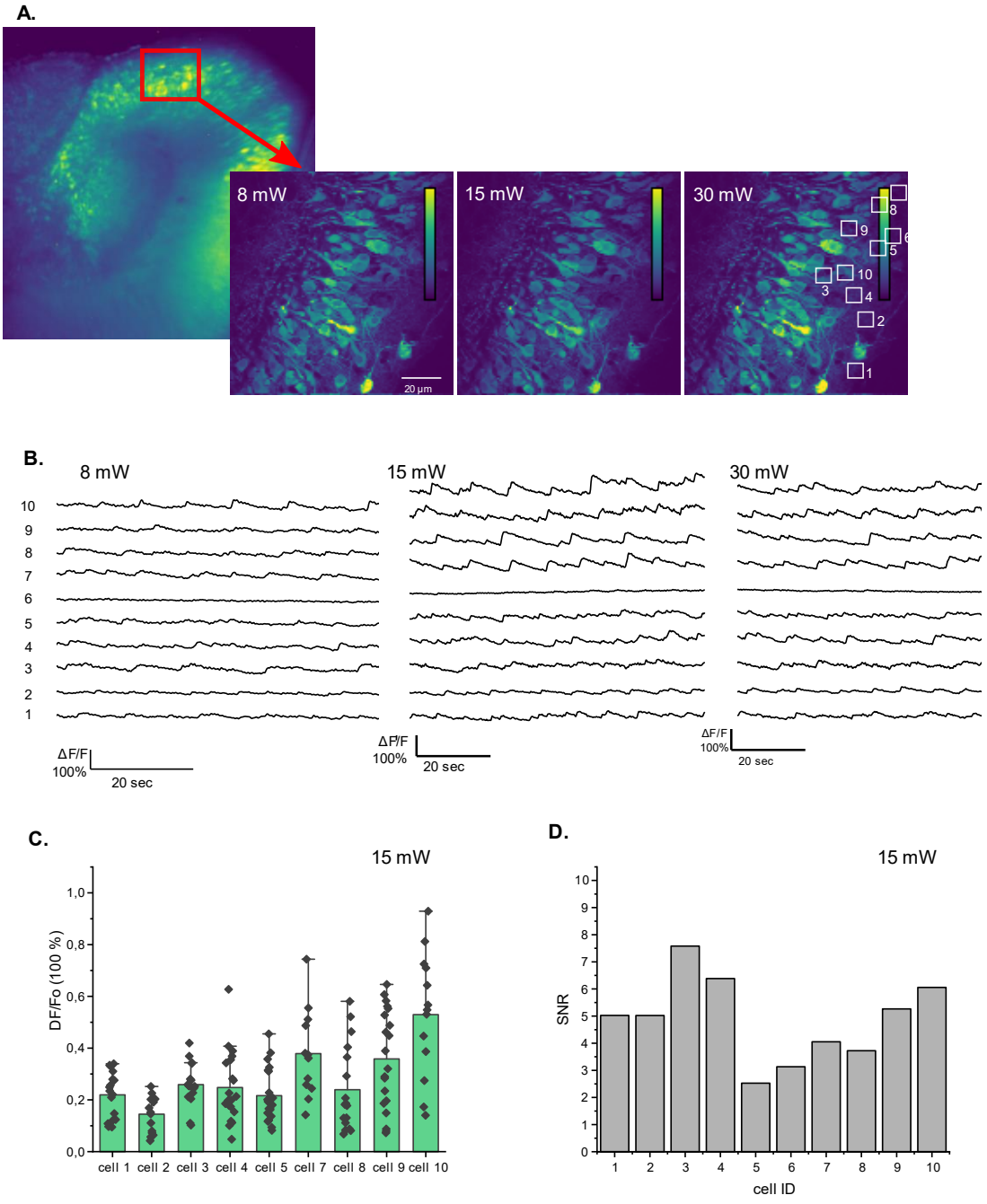

Fig. III.11. Reference activity of GCaMP7s expressing neurons in organotypic slice acquired under 2P scanning microscopy *in vitro.*

A. Summation projection of 500 frames of calcium imaging from hippocampal organotypic brain slice infected with AAV9.hSyn.jGCaMP7s , imaged with 2P scanning technique at 6Hz at 920 nm (laser power 30 mW; 10X objective). Smaller panels show images acquired at different illumination powers under 40X objective.

B. Fluorescent transients DF/Fo of 10 identified cells through standard 2P scanning microscopy at 8mW, 15mW and 30mW laser power.

C. Peak value DF/Fo of 10 cells imaged with 15 mW laser power; histogram: mean, bars: standard deviation, dots: peak events for an identified cell.

D. Signal Noise Ratio (SNR) defined as the peak fluorescence divided by the signal SD of the first 15 frames of acquisition.

To demonstrate 2P-FENDO imaging performance, we compared the imaging of the same *in vitro* sample under 2P scanning microscope as a standard system to refer to. In **Fig. III.11**, we observe the location of jGCaMP7s neurons presenting spontaneous activity with large increases of signal during 1-2 minutes of acquisition. The recognizable form of the hippocampus slice would facilitate the recall of the same region of interest (**Fig.III.11.A.**) when the sample will be moved to the new setup. As the laser and imaging approach are not the same for the two setups, we tested different illumination powers under the 2P scanning microscope, ranging from 8 to 30mW at the sample plane. More peak events could be detected when the sample is illuminated with 15mW (**Fig.III.11.B.**). Therefore, we performed our fluorescent transient analysis on the recording acquired in this experimental condition. The peak DF/Fo ranged from 20% DF/Fo to 92% (**Fig.III.11.C.**). The signal to noise ratio (SNR) will also be a point of comparison to quantify the imaging quality of our new microendoscope. SNR is about 4.87 +/- 1.56 (mean +/- SD) (**Fig.III.11.D.**). This was the only organotypic sample that was both imaged under conventional 2P scanning microscope and our new 2P-FENDO system (**Fig. III.12.**).

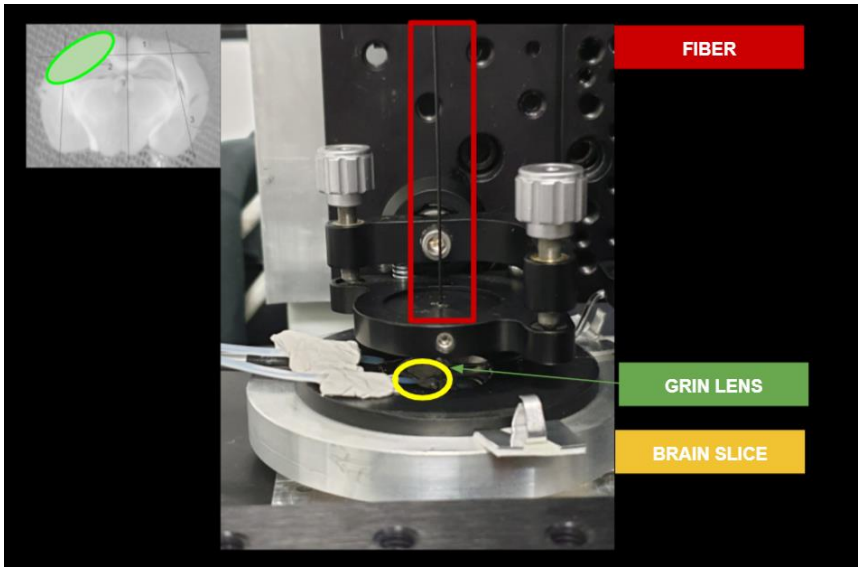

Fig. III.12. Picture of the setup while imaging organotypic slice

The same *in vitro* sample was imaged under our new microendoscopy system. To ensure brain slice quality, we perfused the slice with ACSF1X bubbled with O2/CO2 as shown in the picture above (**Fig. III.12.**). Through 2P-FENDO, as well as conventional 2P scanning microscopy, we can clearly distinguish cell somata and dendrites (**Fig. III.13.A.**). In FOV2 (Fig.III.13A right) of 125 µm depth, the spontaneous activity of five neurons was detectable both at 5 Hz and 10 Hz (**Fig.III.13. B-E**). The signal noise ratio of the acquisitions at 5 and 10 Hz showed no significant difference based on paired t test (p=0.4817 with 95% interval of confidence) (**Fig.III.13.G.**) among the same identified neurons. The range of peak dF/F0 values observed under 2P-FENDO are comparable to those recorded with a conventional 2P scanning microscope (**Fig.III.13.F.**); as the same for SNR on both microscopes. Hence, our optical system presents promising functional imaging capabilities *in vitro*.

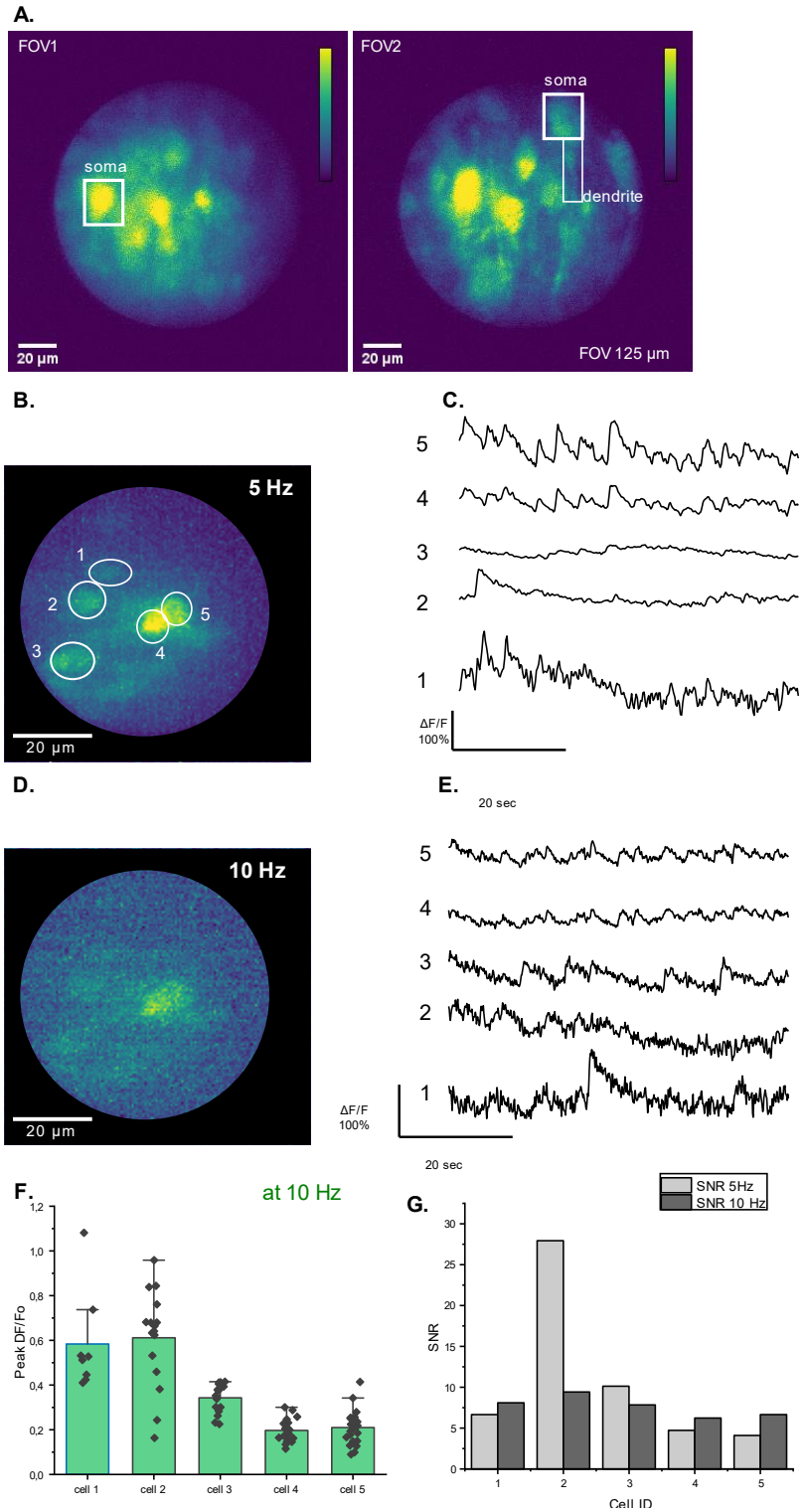

Fig. III.13. Neuronal activity of GCaMP7s neurons in organotypic slice in 2P-FENDO *in vitro*

A. Image of neurons expressing jGCaMP7s in organotypic slice at the best focal plan acquired with 2000ms integration through 2P-FENDO (Tsunami laser, 920 nm, 210 mW). The 2 FOVs show somata and dendrites. FUJIKURA fiber, GRIN lens GL1, FOV 125µm.

B. Summation of 600 timelapse frames acquired at 5Hz at z=50 µm depth.

C. Fluorescent transients recorded at 5Hz (panel B).

D. Same FOV as in B. imaged at 10 Hz. Laser power=210 mW

E. Fluorescent transients recorded at 10 Hz (panel D).

F. Peak DF/Fo values of 5 cells at 10 Hz acquisition rate (histogram: mean, bar: SD, dots: each peak events).

G. Signal Noise Ratio (SNR) defined as the peak fluorescence divided by the signal SD of the first 15 frames acquired at 5Hz & 10 Hz

III.2.2 Mouse primary visual cortex — *in vivo* functional imaging

Understanding how the brain really works, involves investigation at conditions close to the physiological state. To prove the calcium imaging performance of 2P-FENDO, *in vivo* imaging is required to test the system's temporal resolution and signal to noise ratio (peak event relative to baseline fluorescence). The latest developed calcium sensor jGCaMP7s was expressed in neurons with viral injection of AAV1/9.hSyn.jGCaMP7s either in mouse primary visual cortex (V1) or somatosensory barrel cortex (S1) 4-8 weeks before experiments. The animal was anaesthetized under ketamine/xylazine for cranial surgery and during the experiments. To test the viability of our imaging system, we first imaged head-restrained animals before performing experiments in freely-moving animals.

Knowing the nominal working distance of GRIN lens is about 120 µm (in our condition with 130µm thick coverglass and 200 µm distance between the fiber and GRIN lens), I injected at shallower depth in 2 to 3 zones: 150, 100 and 50 µm from the pial surface. In fact, imaging L1 and L2 neurons at 40-200 µm depth was critical to distinguish cells with our current system since we imaged outside the brain through a coverglass (thickness#0, i.e., 80-130µm). For this reason, the protocol of viral injection was changed to fit our imaging goal. The animal was imaged 3-8 weeks after injection to give it enough rest to the animal and time for the virus to express. Acute craniotomy was performed the day of experiments (See Method Chapter). Anaesthetized with ketamine/xylazine in addition of O2 supply, the head-restrained animal was first imaged without visual stimuli to observe spontaneous neuronal activity.

As a reference result, we imaged the anaesthetized mouse under 2P scanning microscope that we recall as conventional microscope, before moving the animal under our new 2P flexible microendoscope, named 2P-FENDO. This helps to check the level of fluorescence that a 2P system can detect, to verify if the cells do present spontaneous activity and at which depth we can expect to see GCaMP expressing somata.

In **Fig.III.14**, we showed an example of recording under the conventional 2P scanning microscope. Cells are starting to be visible at ~65 µm from the pial surface (setting it as the first plane where blood vessel are detected). Based on the calcium traces (DF/Fo), spontaneous neuronal activity were recorded at 5 Hz from 65 µm to 122 µm depth. Although, there is no large increase of activity, we suppose this low activity is due to deep anaesthesia. In the next figure (**Fig.III.15**), we question the level of fluorescence signal at different depth (**Fig.III.15.A.**) in n=4 mice. The average peak DF/Fo is about 50% and seem to be consistent across the tissue depth. To check if we would face a difference of cell density in depth, we counted the number of fluorescent cells within the tissue (**Fig.III.15.B.**). There is no such difference from 65 to 122 µm. As all neurons do express in different way, the baseline fluorescence of each cell may vary and we show this contrast in **Fig.III.15.C**.

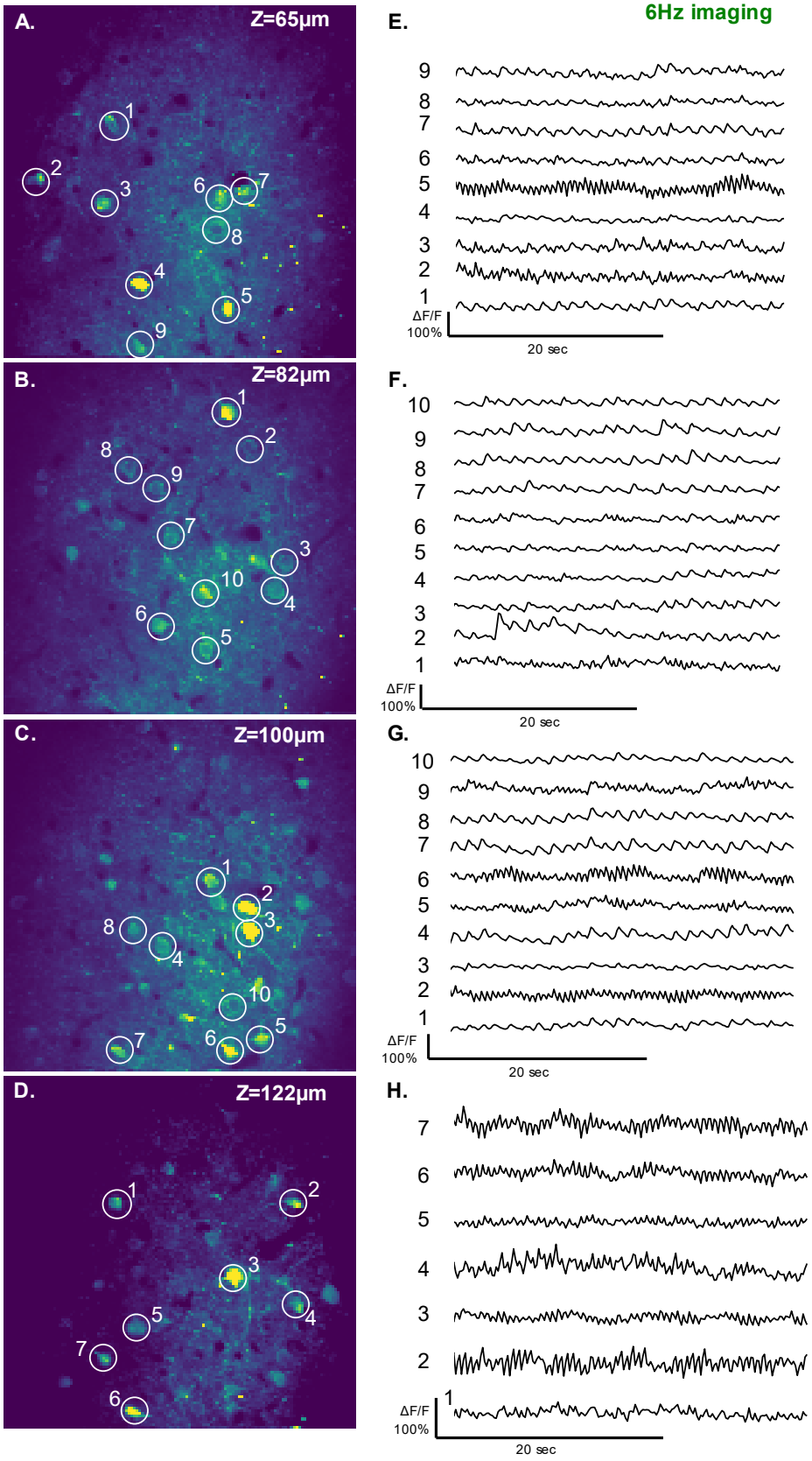

Fig.III.14. Imaging GCaMP7s neurons through conventional 2P scanning microscope

A. B. C. D. *in vivo* images of neurons expressing AAV9.hSyn.jGCaMP7s in the mouse visual cortex at different depth (z=65; 82. 100 and 122 µm from the pial surface) at 6Hz acquisition speed, laser Satsuma 30mW)

E. F. G. H. Calcium traces (DF/Fo) corresponding to images A.B.C.D. respectively.

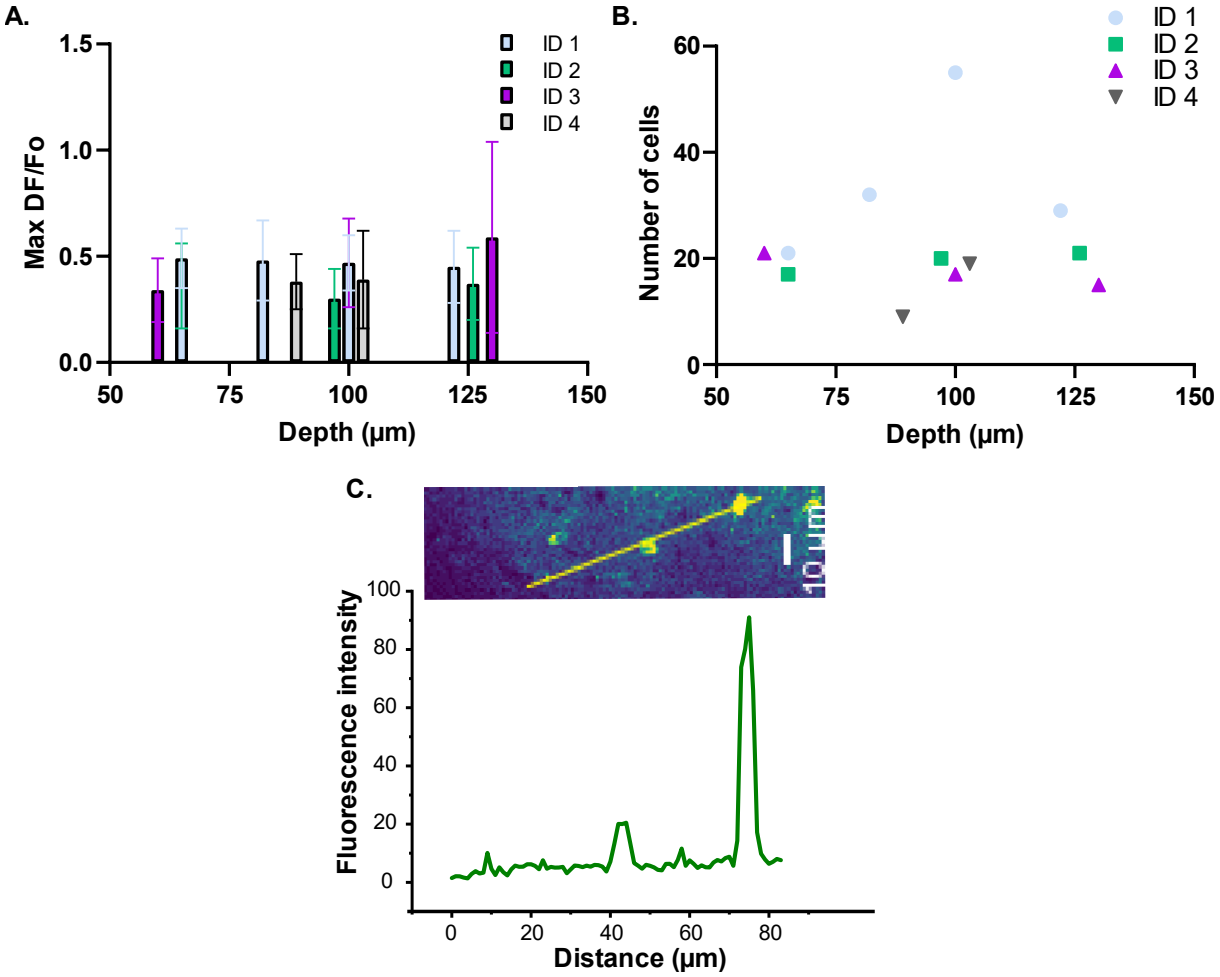

Fig.III.15. Quantification of 2P imaging of GCaMP7s neurons with conventional 2P microscope

A. Quantification of average max value of DF/Fo at different depths from 60 to 130 µm imaged *in vivo* under 2P scanning microscope, n=5 to 10 cells per plane for n=4 mice (legend ID)

B. Number of cells per FOV at different depths detected under 2P scanning microscope

C. Fluorescence intensity of a line profile through n=3 cells at z=60µm normalized with highest value

In the next figure (**Fig.III.16.**), the imaging of neurons in 2P-FENDO *in vivo* showed promising imaging quality. Ten cells are clearly visible in the FOV 250 µm (**Fig.III.16.A.**). We managed to detect neuronal activity amplitude (> 100% DF/Fo) *in vivo* through 2P-FENDO (**Fig.III.16.B**). To test the limit of our imaging system, we recorded spontaneous calcium activity at different frame acquisition rates, ranging from 5Hz to 50 Hz (**Fig.III.16.C-F**). In this specific example at 5Hz, some cells did not show a large increase of intrinsic activity (C1, C2) whereas 2 cells among 10 presented 80-140% DF/Fo transients during a minute of acquisition. The same identified cells were recorded at faster frequencies: 10 Hz, 20 Hz, 50 Hz.

Our 2P-FENDO system can detect fast calcium transients at different acquisition speeds from 5Hz up to 50 Hz. Although, it is still sufficient to image at 5Hz as the decay time of GCaMP7s is slow, however we aimed to test the limitations of our optical system at faster acquisition frame rates (n=6 mice) in regards of further applications of the microendoscopy, for instance with voltage imaging where 100Hz acquisition rates could be required.

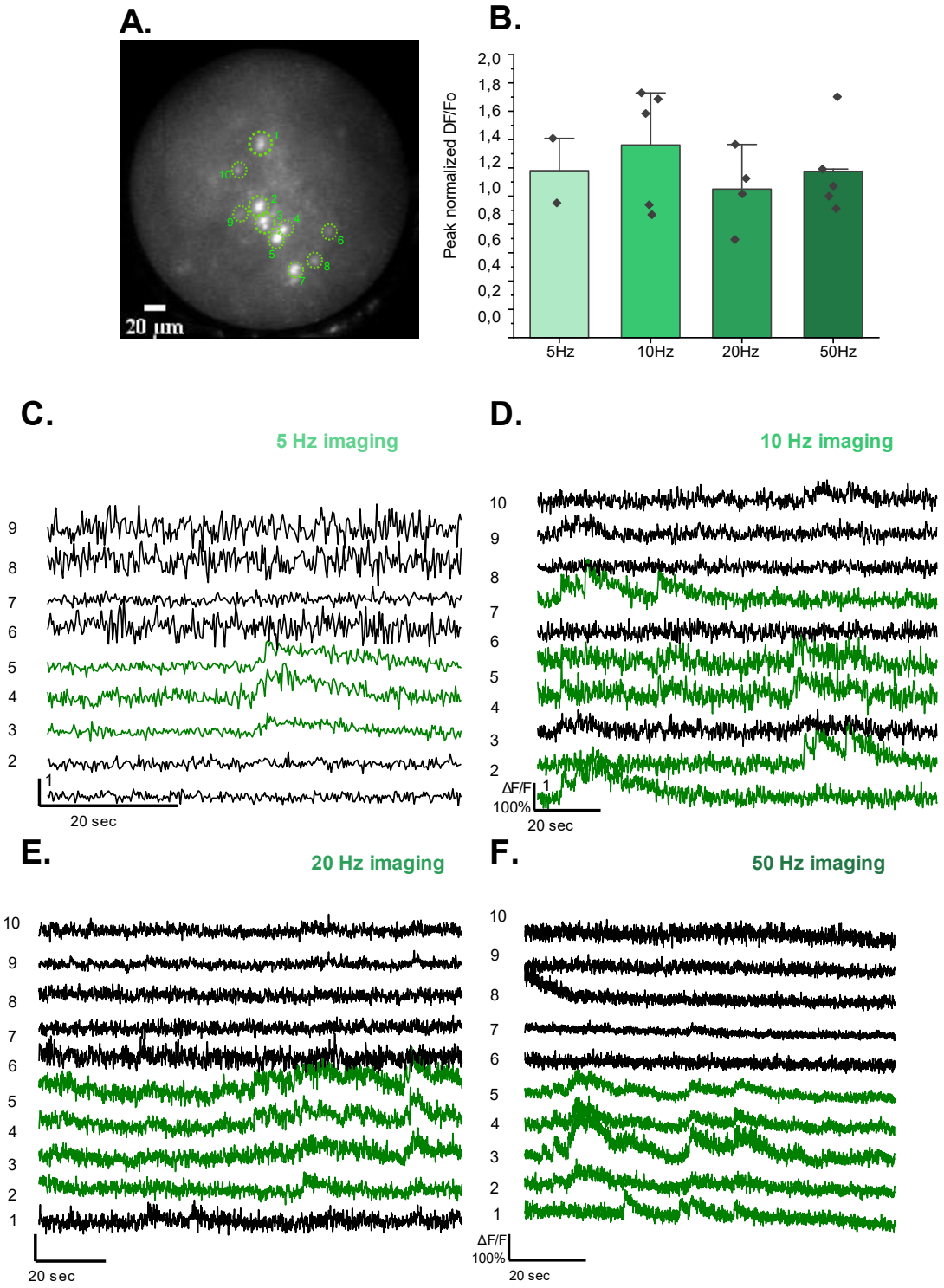

Fig. III. 16. Spontaneous calcium activity of neurons imaged through 2P-FENDO at different frame rates from 5 to 50 Hz.

A. Summation of the timelapse stack with maximum intensity of fluorescent neurons expressing AAV9.hSyn.jGCaMP7s in the mouse visual cortex at z=15 µm, 2 months after injection (circle: regions of interest, cells expressing)

B. Average peak of DF/Fo (mean + SD) of neurons presenting increase of intrinsic activity at different imaging speed

C-F. Corresponding Calcium traces: DF/Fo at different frame rates of 10 cells selected in the FOV at 5 Hz, 10 Hz, 20 Hz with laser power at 220 mW and at 50 Hz with 360 mW at the sample plane with FUJIKURA fiber and GRIN lens GL2. (*Green:* large increase of spontaneous activity)

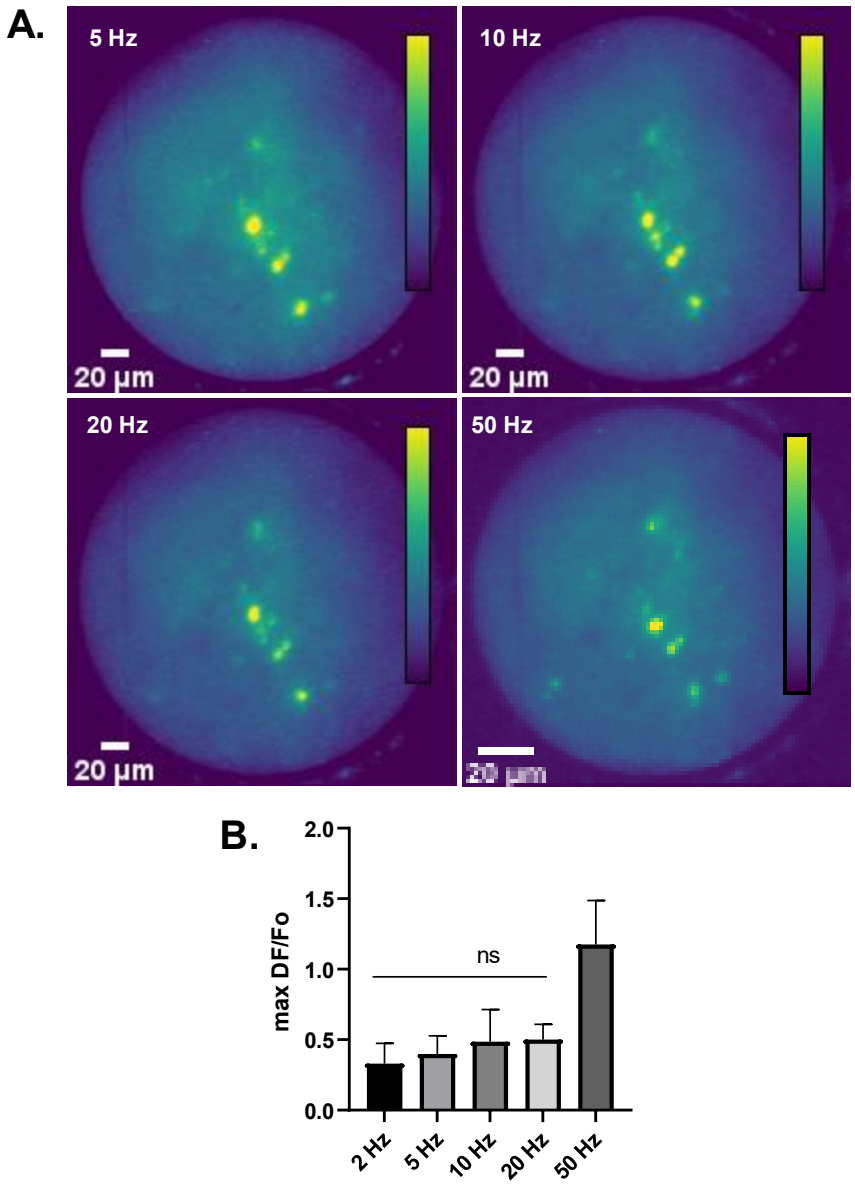

Fig.III.17. Fluorescence detection with 2P-FENDO at different acquisition rates

A. Imaging neurons at 64 µm depth, acquired through 2P-FENDO at 5, 10, 20, 50 Hz

B. Quantification of maximum DF/Fo at different imaging rate for n=6 mice, one-way ANOVA test showed no significant difference (p=0.2815).

As an example of imaging quality at different acquisition speeds, we show in **Fig.17.A.**, the same FOV where multiple cells are visible at different rate from 5 Hz to 50 Hz. Same number of cells are counted at 50 Hz, so no loss of information was observed here. To quantify the level of fluorescence signal, we compared the peak DF/Fo of n=6 mice at those rates (**Fig.17.B.**). Based on one-way ANOVA test, there is no significant difference and the average value of maximum DF/Fo is about 50%. However, for 50 Hz acquisition, we did increase the laser power and detected a higher signal. Our aim is also to test the limitation of our system with the fastest rate. In **Fig.III.18.**, we reported the latest achievement of our system: we were able to image at 100 Hz speed (**Fig.18.B.D.**) where the same identified cells were visible, compared to 10 Hz acquisition (**Fig.18.A.C.**). Moreover, the deepest access we could reach is at 180 µm (**Fig.18.E.**).

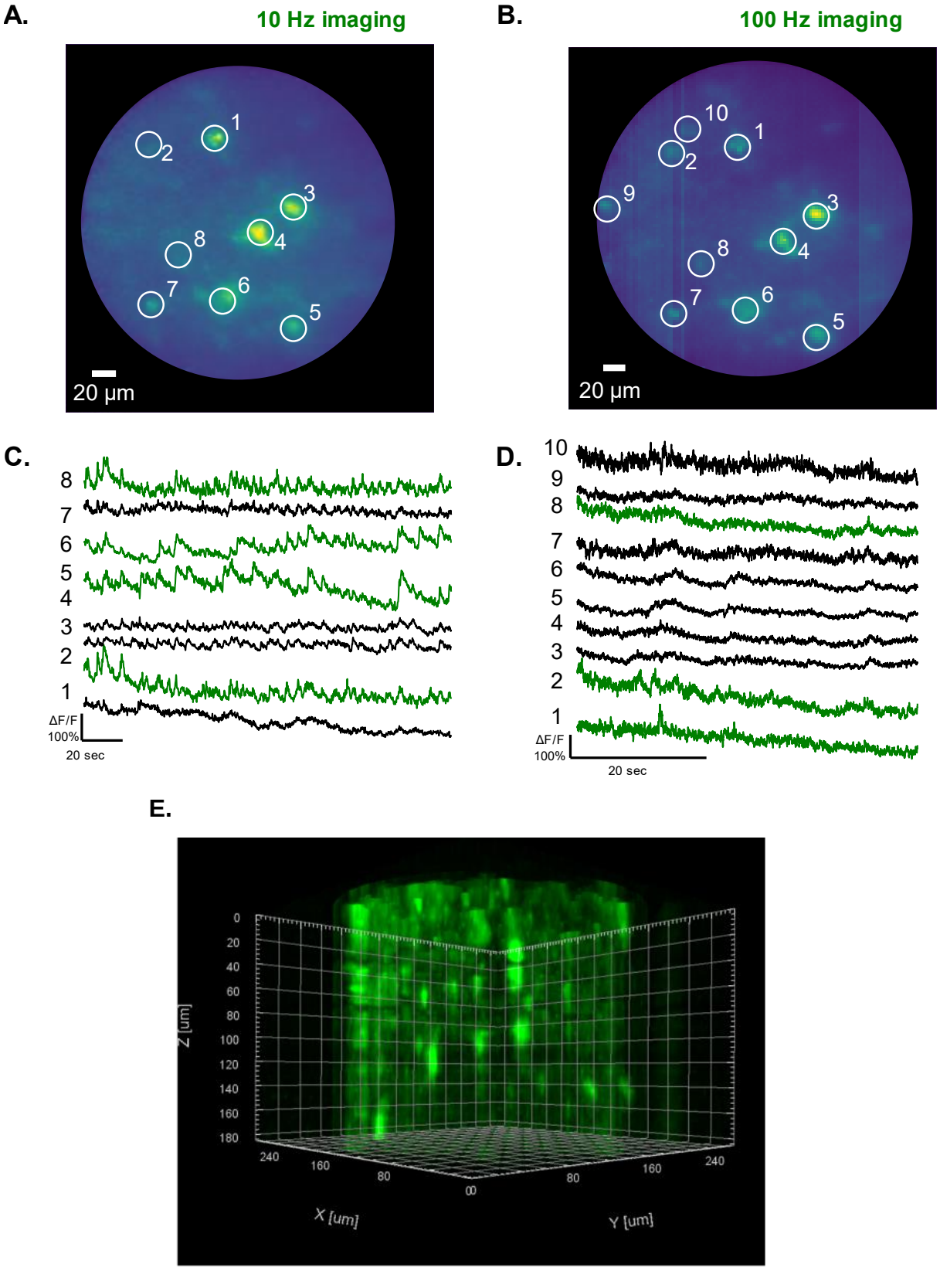

Fig.III.18. Imaging capacity in speed and depth of 2P-FENDO

A. B. Imaging neurons at 10 Hz (A) and 100 Hz (B) in FOV 250 µm.

C. D. Corresponding calcium traces DF/Fo (green: larger increase of fluorescence).

E. 3D view of GCaMP7s neurons stack of 180 µm depth.

III.3 Evoked neuronal activity *in vivo* via visual stimulation

Since the majority of neurons located in the primary visual cortex can be driven to fire action potentials in response to drifting grating visual stimuli (Chen *et al.* **Nature** 2013, Mrsic-Flogel *et al.* **Neuron** 2007, Niell *et al.* **JNeuro**. 2008). Subpopulations of neurons in V1 have preference for oriented stimuli (L2/3 pyramidal neurons) even when the animal is anaesthetized (Ko *et al.* **Nature** 2011). The neurons were imaged 4 to 6 weeks after viral injection of AAV1/9.hSyn.jGCaMP7s as the latest most efficient calcium sensor. We showed the possibility to image neurons during visual stimuli with 2P-FENDO and determined if the system was capable of detecting evoked response to these sensorial stimuli *in vivo* in anaesthetized head-fixed mice. For all the following recordings, 2P-FENDO is composed of FUJIKURA fiber and GRIN LENS GL2 with which the field of view is about 250 µm. The brain was illuminated with Spark laser (920 nm, 150 fs pulse duration, 80 MHz repetition rate) and images were detected with different cameras (EMCCD, ANDOR, NUVU) for which the light gain varies. Finally, we used the higher yield ANDOR which could detect even low fluorescent signal.

As the viral injection was performed in the right side of the brain, we presented the visual stimuli known as grating drifting to the contralateral eye. The visual stimuli protocol on which we based our evoked activity experiments was previously validated in our lab under a conventional 2P scanning microscope (Chen *et al.* **Current Opinion Neuro.** 2018). Projected on LED monitor screen, 8 different directions of grating drifting, coded on *Matlab* Psychotoolbox, were presented for 4 seconds, separated with 4 seconds of blank period (grey screen) (See Methods Chapter). We imaged the evoked neuronal response, known as fluorescence transients, at different rate speed: 5Hz, 10Hz, 20Hz and 50Hz where the visual stimuli started 10 seconds after the onset of imaging acquisition. To ensure the light from the visual display does not interfere with the brain imaging, we designed with a 3D printer a cone around the mouse eye up to the screen (**Fig.III.19;**).

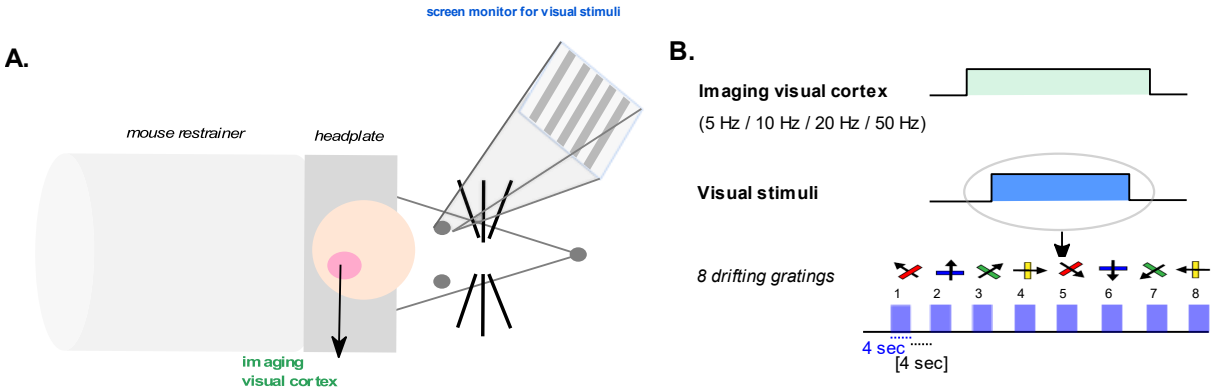

Fig.III.19. Visual stimulation procedure

A. Set up with anaesthetized head-restrained mouse for *in vivo* imaging during visual stimuli

B. Visual stimulation protocol.

Although spontaneous activity may occur before simtuli in responsive cells in the visual cortex, cells displayed increase in neuronal activity during sensorial stimuli (**Fig.III.20.**). Those functional responses were detected in FOV of 250 µm from 5 Hz to 20 Hz imaging speed through 2P-FENDO.

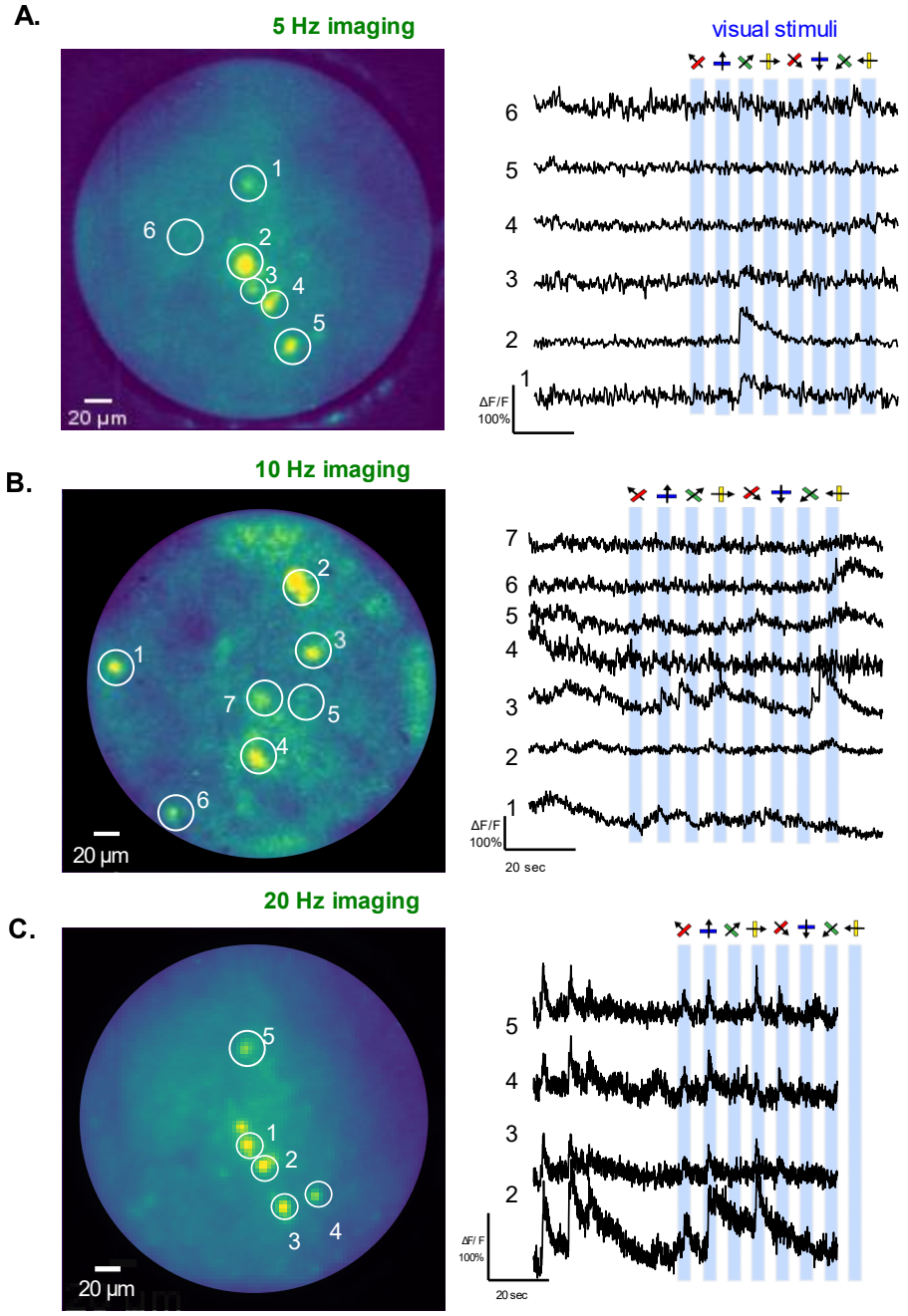

Fig III.20. Neuronal response to visual stimuli from calcium imaging under 2P-FENDO.

A.B.C. Z projection of 1000 frame images at 5 Hz (A), 10 Hz (B), 20 Hz (C), White circle: region of interest, i.e., neurons expression jGCaMP7s calcium indicator (*left*). Corresponding fluorescent transients (*right*) of 3 different mice to show the consistency of image quality over days and animals.

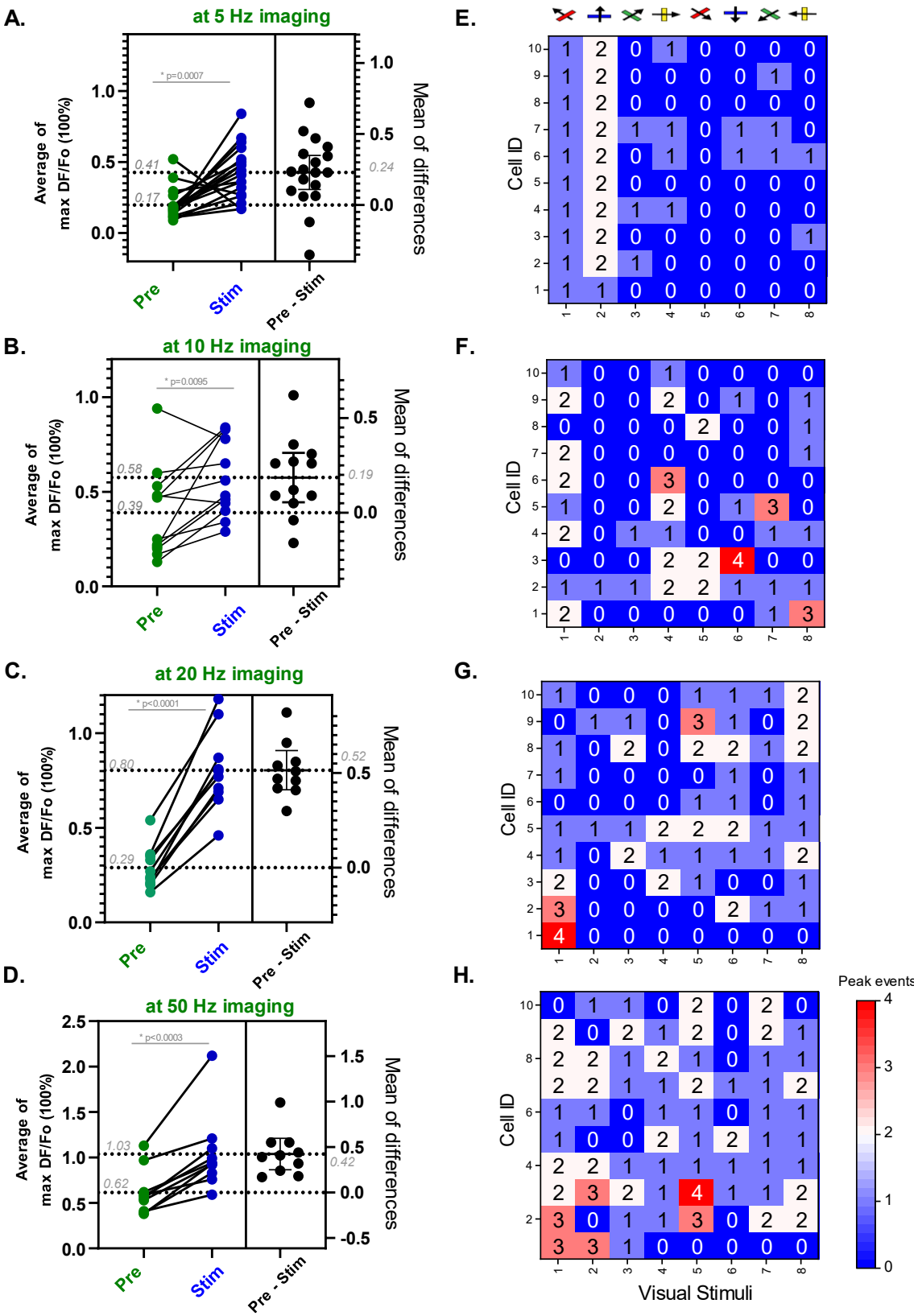

Fig.III.21. Quantification of evoked response of neurons to visual stimuli through 2P-FENDO

A. Neuronal activity before (pre) and during visual stimuli (stim) as average of max values of DF/Fo and mean differences, statistical paired t-test, considered as parametric distribution with 95% confidence interval. n=4 mice.

B. Count of peak events for 10 cells at each visual stimulation period (heatmap: blue to red gradients from none to many events) at different acquisition frequencies from 5 Hz to 50 Hz.

To confirm the hypothesis of neural response to visual stimuli, we quantified the neural response via functional calcium imaging (**Fig.III.21.A-D**) and compare DF/Fo before sensory stimuli at different imaging speed. Based on statistical test (paired t-test with 95% interval of confidence), the visual stimuli do induce neuronal activity increase in the mouse visual cortex. We did compare the average DF/Fo before stimuli (pre) and peak value during stimuli (stim) of ~10 cells per FOV from n=4 mice. The fluorescence increase is present for all imaging speeds from 5 Hz to 50 Hz. The evoked response is of 20% to 60% DF/Fo rise when the stimuli is on compared to pre-stimuli.

We also question if there is difference in the evoked response relative to 8 different drifting gratings of visual stimuli (**Fig.III.21. E-H**). For this purpose, we counted the peak events for each visual grating for 10 cells for the same FOV, imaged at different imaging rate. So far, the number of peaks does not seem to happen at the same grating orientations (**Fig.III.21. E-H**).

We repeated those *in vivo* experiments for n=4 mice and summarize it in **Fig.III.22**. We compared the evoked response to visual stimuli relative to imaging speed through 2P-FENDO (**Fig.III.22.A-B**). The 2P fluorescence signal is ranging from 50% to 200% DF/Fo which is consistent with the literature (Dana *et al.* **Nature Methods** 2019).

Then, the fluorescence of cells does light up during visual stimuli, although those cells are not direction selective, or the signal may be very dim. Indeed, the probability to get direction selective cells is very low.

Therefore, our new 2P flexible microendoscopy system is able to image neurons at different rates and can detect fine fluorescent signal in response to visual stimuli. To extend this observation to other brain region, we tested the imaging capacity to the barrel cortex during whisker stimulation.

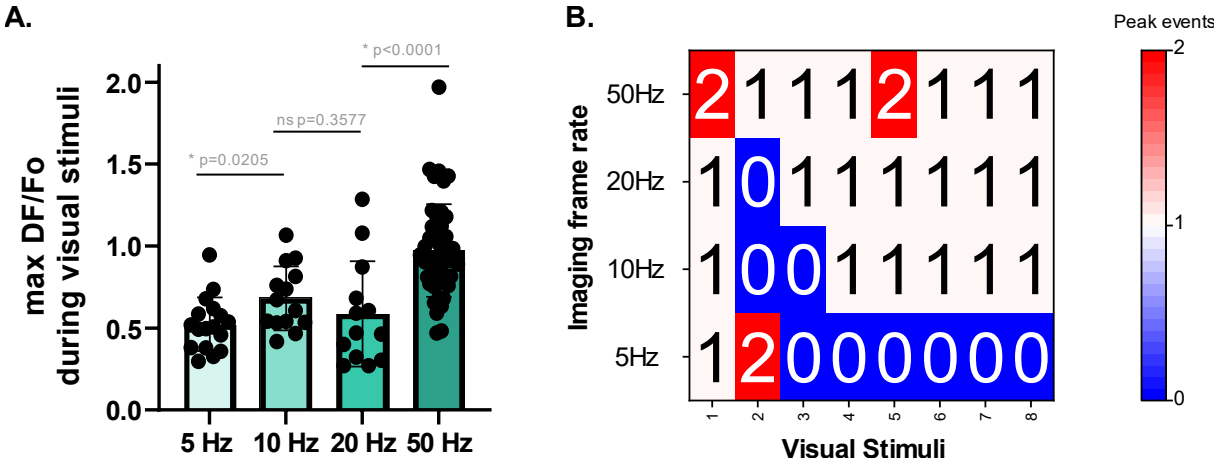

Fig.III.22. Summary of evoked response to visual stimuli through 2P-FENDO

A. Average max DF/Fo during visual stimuli for n=4 mice at 5/10/20/50 Hz imaging acquisition.

B. Average count of peak events for 10 cells at each visual stimuli periods for all imaging rates.

III.4 Evoked neuronal activity *in vivo* via whisker stimulation

Rodents use vision as well as auditory and olfactory cues to explore the world. Nevertheless, mice are far-sighted and must use their whiskers to scope out the space around their head, the same way humans would scan the space with hands. To map out their surroundings, mice move their whiskers. The sensory nerves (N=100-200) at the base of each whisker (n=24; 30mm length) connect to well-defined structures in the barrel cortex (2.5-3 mm). Such as the visual cortex, the barrel cortex can be schemed as layers of cells where layer 1 is about 100-150 µm thick. L2/3 receive input from several barrel cells at once and process this information to other brain areas. The role of whiskers and barrel cortex are about fine object localization and identification needed for behaviours such as prey capture, predator avoidance and navigation. Based on the expertise on this field from Serge Charpak's Lab (Rungta *et al.* **Com. Biol.** 2021), we performed whisker stimulation and observed evoked neuronal response in the barrel cortex where I injected virus encoding for calcium sensor. We reproduced the same protocol as described in Zuend *et al.* **Nature Metab.** 2020. The animal was anaesthetized with ketamine/domitor and the whiskers were stimulated with a metal rod attached to a mechanical shutter/chopper which deflected the whisker at a rate of 5 Hz.

The **Fig.III.23**. outlined the first attempts of imaging in the barrel cortex through 2P-FENDO during 5Hz whisker stimulation in *in vivo* anaesthetized head-restrained mice (**Fig.III.23.A**.). The neurons are imaged at 2 Hz, 5 Hz and 10 Hz and whisker stimulation of 5 Hz lasted 2 seconds (**Fig.III.23.B**.). As the optical setup was progressively optimized, we show the difference between camera performance (Hamamatsu vs EM-CCD Andor iXon Ultra) to detect fluorescence signal from neurons expressing AAV1/9.hSyn.jGCaMP7s and the fluorescence calcium transients at different imaging rates. Compared to previous camera detection (**Fig.III.23.C**.), the new camera (**Fig.III.23.E**.) seems to permit detection of more neurons as it can detect lower signal of fluorescence with lower background signal even with lower laser power (260mW instead of 300mW at the focal plane). The shape of cell soma are more visible. Even though calcium transients were visible both at 2 Hz and 5 Hz (**Fig.III.23.D.)** with the previous configuration, it is even clearer with the new one (**Fig.III.23.F**) where the neurons look to be responsive to whisker stimulation while imaging at 5 Hz or 10 Hz. Responses of neurons in an extended area of the barrel cortex could be because the whisker stimulation was not single whisker selective. Furthermore, we repeated this same experiment with Andor camera to detect fluorescence and we tested different imaging rates during whisker stimulation (n=2 mice for each camera type).

2P-FENDO can detect evoked neuronal activity responding to whisker stimulation in the somatosensory barrel cortex at different acquisition rates (**Fig III. 24.A.**). Calcium fluorescence transients ranging from 20% to 120% DF/Fo are detected when imaging at 5 Hz or 10 Hz (**Fig.III.24.A-B**). On average, the detectable calcium transients were of 55% DF/Fo at 5Hz imaging and 72% DF/Fo at 10 Hz imaging. Nevertheless, considering the average fluorescence before the whisker stimuli (18% and 28% DF/Fo respectively), there is no difference relative to imaging speed. The neurons do respond to whisker stimuli based on paired-t test (**Fig.III.24.C**.).

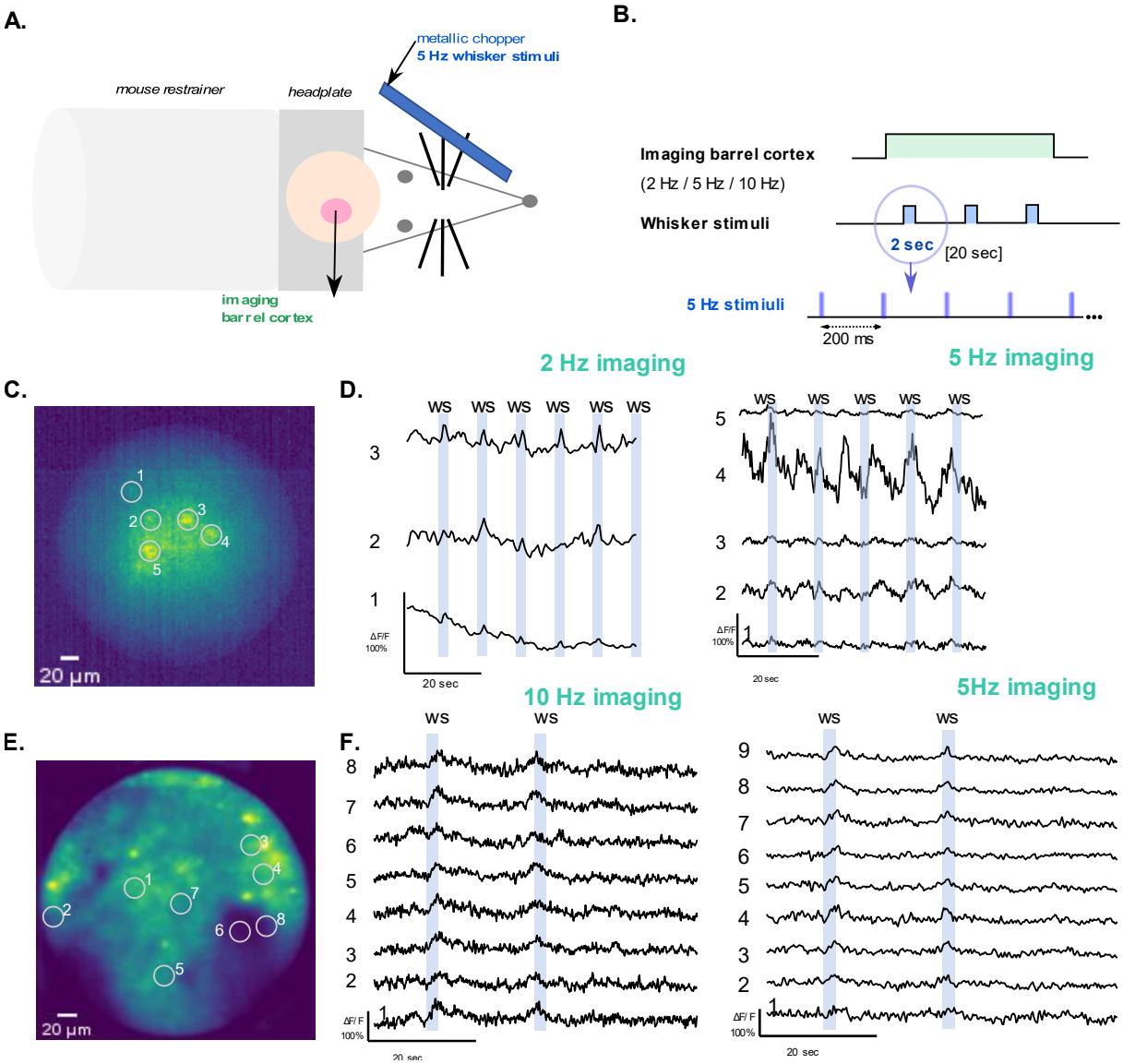

Fig. III. 23. Evoked neural response in the barrel cortex during whisker stimulation

A. Set up for the in vivo anaesthetized head-restrained mouse during barrel cortex imaging through 2P-FENDO and whisker stimulation with metallic chopper, placing on top of a bunch of contralateral whiskers, moving in z at 5 Hz.

B. Example of protocol of whisker stimulation of 5 Hz during 2 seconds.

C. Image of neurons of which fluorescence is detected with camera Hamamatsu at 5 Hz, through 2P-FENDO composed of fiber FUJIKURA, GRIN lens GL2, FOV 250 µm. Red square: regions of interest expressing AAV1.hSyn.jGCaMP7s, 4 weeks after viral injection in the barrel cortex at 70 µm depth from the pial surface, Spark laser (920 nm 150 fs pulse duration, 80 MHz repetition rate) with power 300 mW at the focal plan.

D. Fluorescent transients at 2Hz (*left*) and 5Hz (*right*) during whisker stimuli (blue bar).

E. Image of neurons of which fluorescence is detected with camera Andor at 10 Hz through 2P-FENDO composed of fiber FUJIKURA and GRIN lens GL2, FOV 250 µm. Red square: regions of interest expressing AAV9.hSyn.jGCaMP7s, 4 weeks after viral injection in the barrel cortex at 45 µm depth from the pial surface, Spark laser (920 nm 150 fs pulse duration, 80 MHz repetition rate) with power 260 mW at the focal plan.

F. Fluorescent transients at 10Hz (*left*) and 5 Hz (*right*) during whisker stimuli (blue bar).

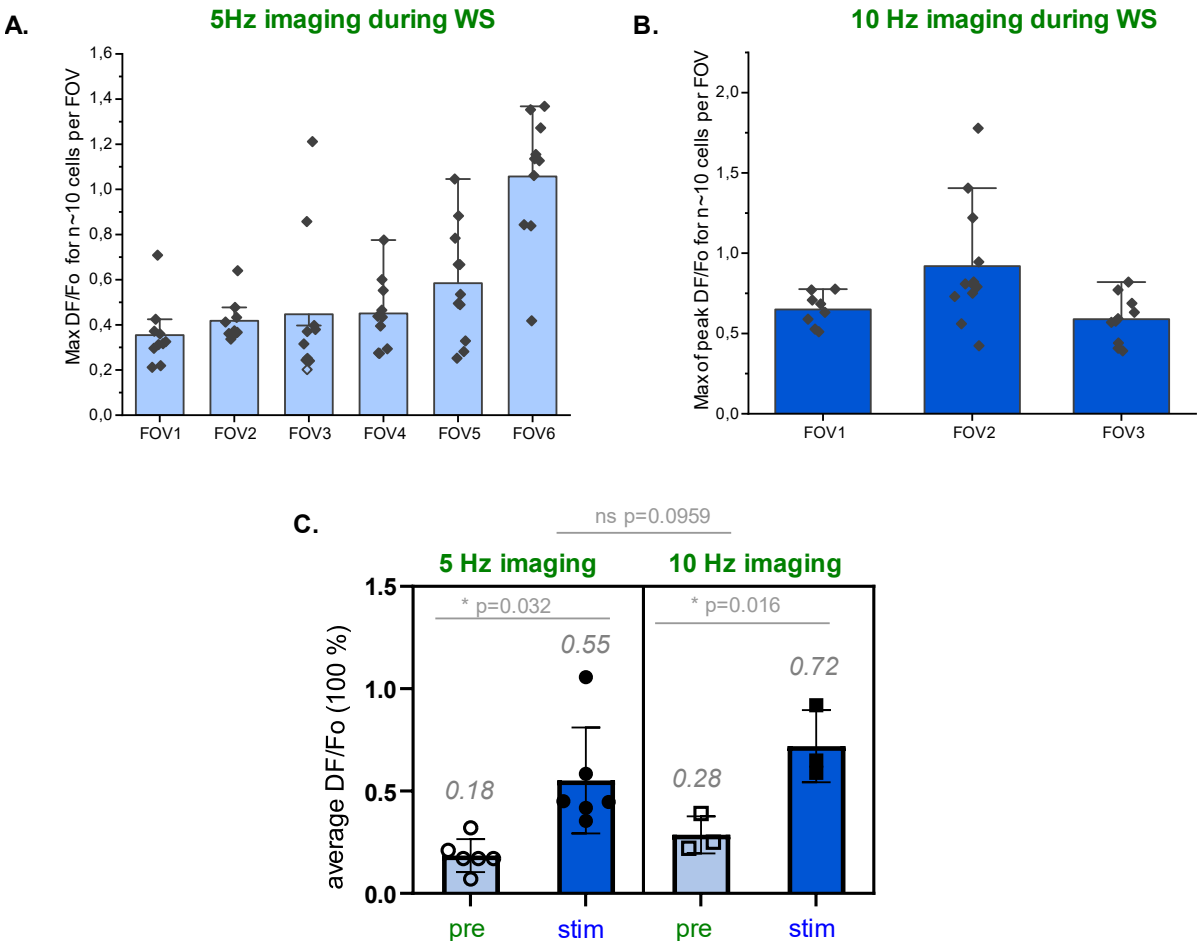

Fig. III. 24. Quantification of neuronal activity during whisker stimulation under 2P-FENDO.

A. Quantification of peak values DF/Fo for 5 Hz imaging acquisition during whisker stimulation (n=10 cells per FOV, n=6 FOV).

B. Quantification of peak values DF/Fo for 10 Hz imaging acquisition during whisker stimulation (n=10 cells per FOV, n=3 FOV).

C. Average of maximum peak value of DF/Fo during whisker stimulation for 5 Hz and 10 Hz imaging during whisker stimuli acquisition (5 Hz during 2 seconds) (n=3 mice, n=6 FOV, n=60 cells).

III.5 2P photostimulation

III.5.1 Co-expression of calcium sensor and opsin actuator

All-optical strategy relies on simultaneous recording and manipulation of the activity of multiple neurons with cellular resolution and millisecond precision in vivo with patterned light. To get a reliable optogenetic toolkit, the co-expression of genetically encoded calcium indicator and opsin actuator must be in a good balance.

To combine the ultrasensitive green fluorescent genetically calcium indicator with an opsin, this latter should be red-shifted and avoid cross-talk during 2P excitation. While imaging the neurons, one must be able to distinguish cells expressing both sensor and actuator and cells expressing only sensors as well. Moreover, for multi-targeted excitation, we should have sufficient expression to use low photostimulation power.

We chose the opsin virus AAV1.hSyn.ChRmine.Kv2.1.WPRE.mScarlet (Marshel *et al.* **Science** 2019) because mScarlet enables to distinguish positive cells from GCaMP expressing neurons, and ChRmine is a red-shifted, high efficient opsin.

Preliminary, we tested the co-expression of the viruses on fixed brain slices under confocal microscope (**Fig.III.25.**) to visualize the colocalization of calcium sensor and opsin actuator expression. The functionality of the opsin was tested: induced responses were observed under conventional 2P imaging with holographic stimulation (unshown data).

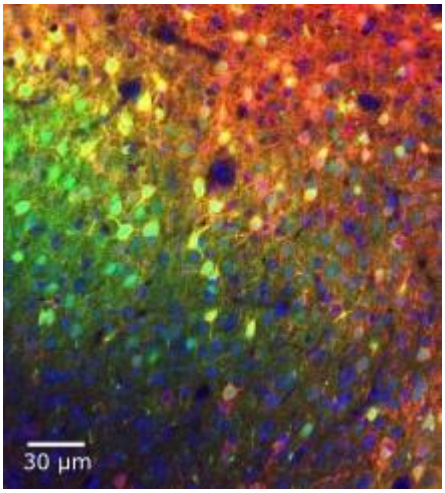

Fig; III. 25. Co-expression of calcium indicator jGCaMP7s and opsin ChRmine-mScarlet.
Confocal imaging of fixed slice, sagittal cut of 200 µm thickness,
4 weeks after viral injection in V1 mouse brain.

Blue: DAPI to label neuronal nucleus.

Green: Cells expressing only the calcium sensor.

Red: Cells expressing only the opsin.

Yellow: Co-expression of both calcium indicator and opsin actuator.

III.5.2 2P holographic stimulation under 2P-FENDO

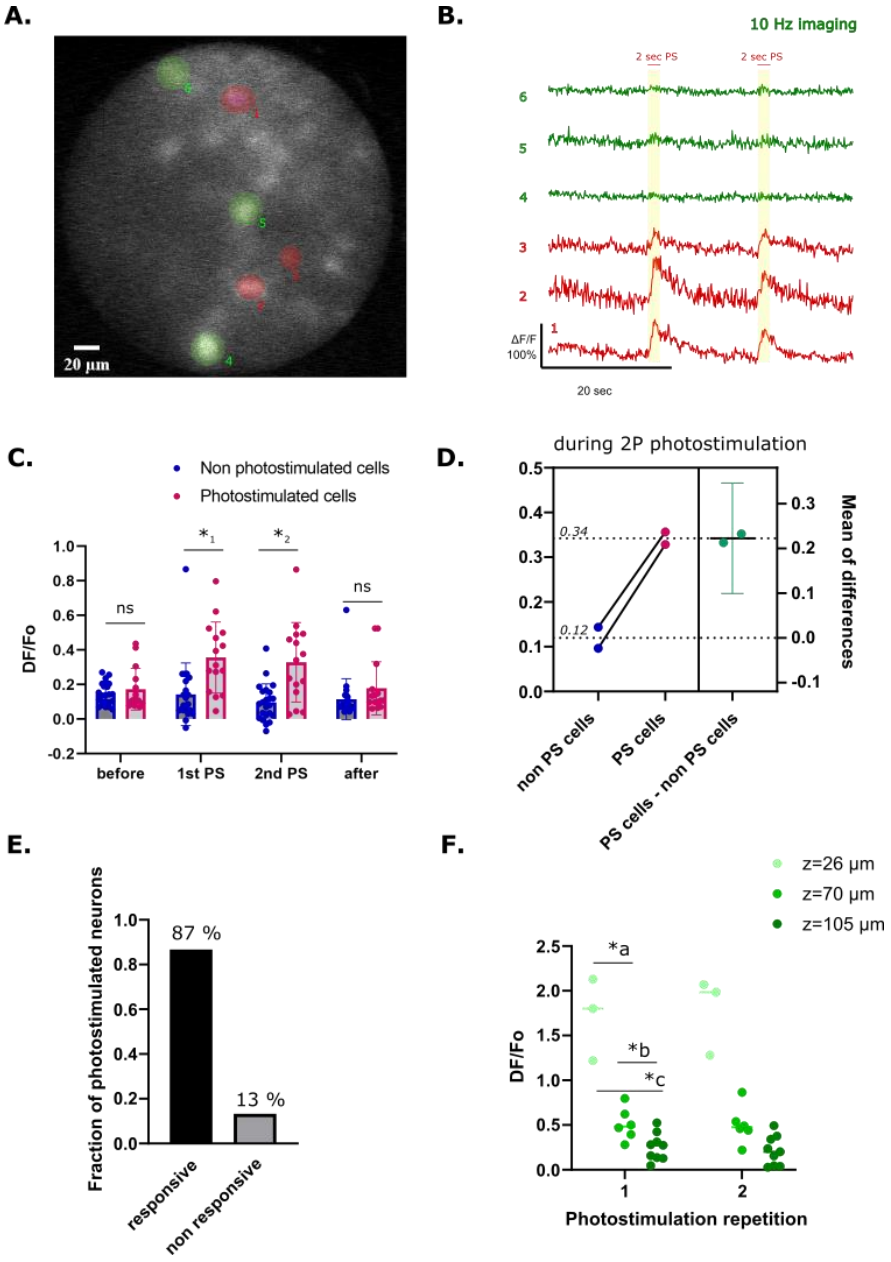

Fig.III.26. 2P holographic photostimulation of neurons under 2P-FENDO

A. Image of neurons expressing calcium sensor AAV9.hSyn.jGCaMP7s and opsin AAV1.hSyn.ChRmine.mScarlet.Kv2.1.WPRE in C57BL6J mouse through 2P-FENDO composed of FUJIKURA fiber and GRIN lens GL2 of FOV 250 µm. Red: holographic spot with 0.6W Goji laser, i.e., 40mW per spot, green: control cells, non photostimulated.

B. Fluorescent 2P signal transients corresponding to (A) regions of interest. Yellow bars: stimulation period; red trace: photostimulated cells; green trace: non photostimulated ones.

C. Average DF/Fo before, during the first and second photostimulation, then after 2P photostimulation; 5 µm holographic spots; blue dots: non photostimulated cells, n=23 cells; red dots: photostimulated neurons, n=15 cells. Paired t-test parametric with p*1~p*2=0.035, alpha=0.05.

D. Average of DF/Fo of non- and photostimulated cells during 2P holographic stimulation through 2P-FENDO for n=15 cells and mean difference calculated as difference of average DF/Fo of non- and -photostimulated cells

E. Fraction of responsive cells among photostimulated neurons, where threshold is set at 12% DF/Fo, n=15 cells.

F. Distribution of DF/Fo values for z=26µm; z=70µm and z=105µm during 2 repetitions of photostimulation; paired t-test parametric with p*a ~p*b~p*c=0.0006 with 95% confidence interval.

In anaesthetized mice, we have performed 2P holographic photostimulation on neurons while imaging calcium fluorescent transients through our new built 2P microendoscope *in vivo*. The protocol of stimulation consists in 10 pulses of 10 ms. During 10 Hz imaging (**Fig.III.26.A.**), three cells expressing both calcium sensor AAV9.hSyn.jGCaMP7s and opsin AAV1.hSyn.ChRmine.mScarlet.Kv2.1.WPRE were illuminated with holographic spot at 40mW per targeted cell. The 2P signal fluorescence transients were detected along one minute of acquisition (**Fig.III.26.B.**). We compared the peak values of DF/Fo of control non photostimulated cells and photostimulated ones during different periods of the imaging acquisition: before (150 first frames), during (averaging peak during 10 frames centered to the maximum value) and after the stimulation (100 last frames). The average fluorescent signal does not seem to vary during the protocol (**Fig.III.26.C.**), however the increase of signal due to photostimulation is significant (paired t-test). To quantify the difference with the neurons that were photostimulated, we averaged the values of DF/Fo during the stimulation for n=15 cells. The average value of DF/Fo is about 34% (**Fig.III.26.D.**). The mean value of DF/Fo of non photostimulated cells is 12% DF/Fo. Therefore, we set the threshold at this value. We consider that targeted cells are responsive to the stimulation if the 2P signal is superior to this threshold (**Fig.III.26.E.**): 87% of targeted cells did respond when averaging data of n=15 cells. To determine if there is a different signal levels at different depths, we observe the distribution of cells located at z=26 µm, 70µm and 105µm depth in the primary visual cortex (**Fig.III.26.F.**). Based on few cells compared with paired t-test, the 2P signal is significatively different and tends to be lower with greater depth in tissue when using the same photostimulation laser power (Goji, 600mW). However, this experiment should be reproduced with different illumination intensity due to the effect of scattering in thicker brain tissue.

In the next figure **Fig.III.27.**, we checked if the level of 2P fluorescence signal induced by stimulation would vary with the laser power at the same brain depth (z=70 µm) in FOV of 250 µm. The induced response is about 40% to 50% DF/Fo. Based on t-test, there is no significant difference (**Fig.III.27.A.**). Furthermore, the mean of differences between the DF/Fo at the two different powers is about 0.1% (**Fig.III.27.B.**). Similar activity at two powers means that in both cases, we did not produce more spikes than pulse stimulation and did choose the correct protocol.

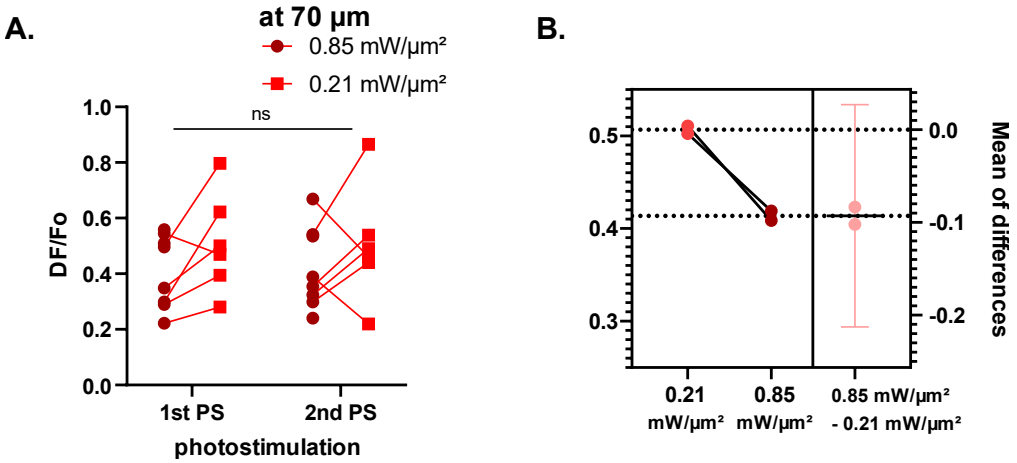

Fig.III.27. Effect of photostimulation intensity on neuronal response through 2P-FENDO

A. Maximum DF/Fo during 2 repetitions of holographic photostimulation at two different powers: 53mW/spot (n=6 cells) and 40 mW/spot (n=6 cells) with Goji laser (1040 nm, pulse duration of 150 fs, repetition rate of 5 MHz). Paired-t test, non-significative with p=0.0645 with 95% confidence interval.

B. Average DF/Fo at two different laser powers during 2P photostimulation.

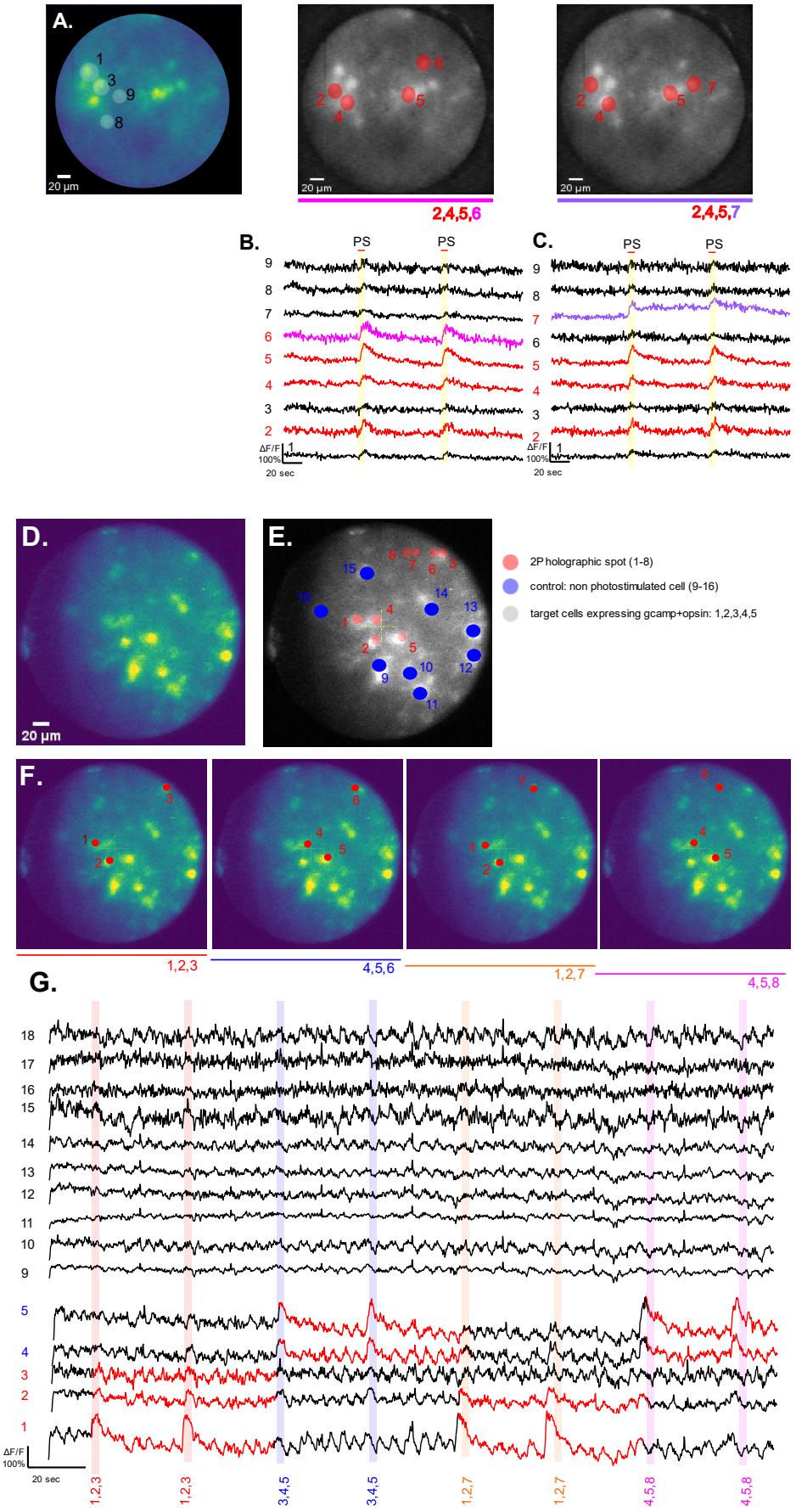

Fig. III. 28. Neurons responding to 2P holographic photostimulation through 2P FENDO

Detailed captions are in the next page.

A. Image of neurons expressing both GCaMP7s and ChRmine-mScarlet in FOV 250µm through Fujikura fiber and GRIN lens 2. Laser Goji (40mW per holographic spot of 5µm diameter). Targeted region of interest, blue region: control neurons, red region: photostimulated neurons. Cells 1,3,9,8 are control cells; cells in red are the photostimulated ones: 2,4,5, and 6 or 7. Holographic spot diameter: 5µm.

B-C. Calcium fluorescence transients for 2 different protocols of photostimulation (repetition: 2 times).

D-E. Image of neurons in C57BL6J mouse expressing both calcium sensor AAV9.hSyn.jGCaMP7s and opsin AAV1.hSyn.ChRmine.mScarlet.Kv2.1.WPRE through 2P-FENDO (FUJIKURA fiber and GRIN lens GL2); FOV 250 µm. Grey spots on left panel: control cells; red spots on middle and right panels: holographic patterns, 53mW/spot. Cells 9 to 18 are control cells; red circles are the position of holographic spot where only 1,2,3,4,5 are cells.

F. Pattern protocol of 2P holographic stimulation in the same FOV.

G. Calcium fluorescent transients corresponding to above pattern stimulation protocol, red: during stimuli.

To confirm that photostimulation is confined to the targeted cell, we moved one spot away from a cell (**Fig.28.A.**) and observed the response of the previous targeted cell becomes silent (**Fig.28.B. vs C.**). To extend this experimentation, we repeated different patterns of photostimulations in one long acquisition of 4 minutes (**Fig.28.D-F**) while looking at the calcium response of the same targeted cells imaged at 10 Hz (**Fig. III.28.F-G**). In more details, we photostimulated three cells at the time, repeating the stimulation 2 times. Then we changed the pattern to other three cells (**Fig. III.28.F.**). Neurons seem to respond when being photostimulated and stay silent in other pattern configurations. Whilst stimulating the cell #1, #2, #3, the cell #1 respond with an increase of about 164% DF/Fo, while the average fluorescence without photostimulation is about 107%. Although the baseline fluorescence is high, the increase of activity is clearly visible on the calcium transient traces. During these 4 minutes acquisition, this cell was photostimulated again and we observed again increase of activity of 181% DF/Fo. All targeted cells do not respond the same way: amplitude vary. The control cells (#9 to #18) present spontaneous calcium activity and some peaks are visible, even though their amplitudes are lower than the photostimulated cells.

In the next figure (**Fig.III.29**.), to confirm and quantify the relationship between the distance of the photostimulation pattern and the cell response, we observe the decreasing of induced activity in a targeted cell, while progressively moving away the excitation spot from the cell soma. By this mean, we demonstrated the performance of the lateral resolution of 2P-FENDO holographic stimulation *in vivo*. The imaging was recorded at 7.14 Hz. On the same FOV, we deliver the 5 µm holographic spot on the cell of interest and moved it progressively 5 to 40 µm away from the cell's soma (**Fig.29.B**). We extracted the fluorescent transients of the cells expressing both calcium sensor and opsin (cell#1/5/6/7/8/9/10) (**Fig.III.29.C**). Although the neurons of interest might present spontaneous activity, it is clearly visible that the cells responded to the photostimulation (**Fig.III.29.D**): the threshold is set at 22.93 DF/Fo based on the maximum average value of DF/Fo of fluorescent transients when there is no photostimulation.. For instance, cell #1 showed DF/Fo of about 117% and cell #2 of 105%. We observed that the peak value of DF/Fo during the photostimulation on the soma varies among the cells and the response of the cell of interest decreases with the distance of the holographic spot. The **Fig.III.29.E**. illustrates the decrease of the peak DF/Fo when the holographic spot is moved far away from the cell. The response of the cell to the photostimulation starts to decrease when the spot is about 5 µm away from the cell and the cell is responding less than 50% when the spot is of about 5 um away from cell's soma (data from 2 cells, 2 FOV; **Fig.III.29.F**). These data suggest that the lateral resolution in *in vivo* experiments is consistent with the optical lateral resolution (7-8 µm).

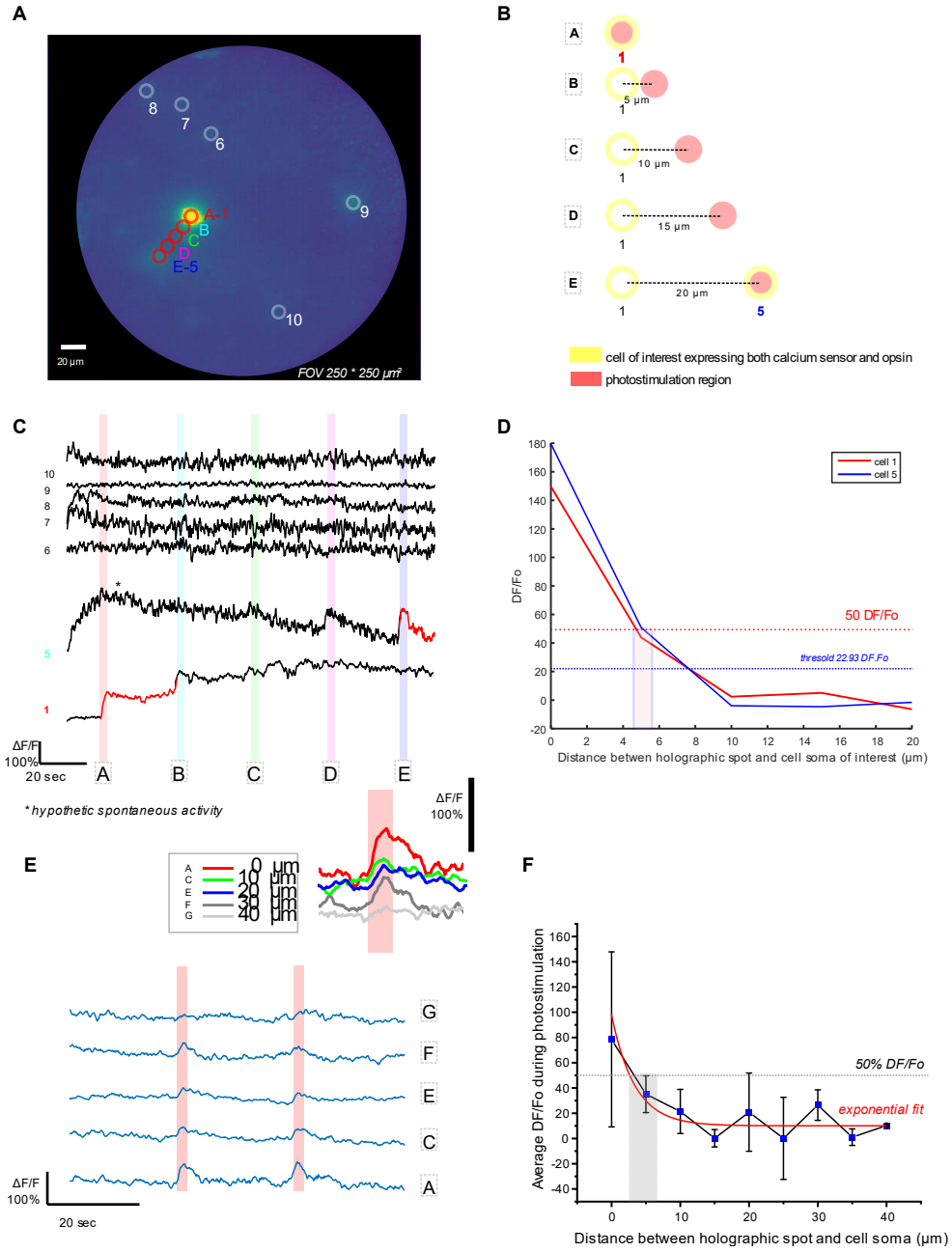

Fig.III.29. Lateral resolution of 2P-FENDO photostimulation performance *in vivo*

A. Z projection of calcium imaging recording of neurons at 7.14 Hz in a FOV of 250 µm, where 2 cells #1 and #5 express both calcium sensor AAV9-hSyn-jGCaMP7s and opsin AAV1-hSyn-ChRmine-mScarlet-Kv2.1-WPRE. Red spots A-E are the 5 µm diameter holographic spots. Cells #6/7/8/9/10 are control neurons expressing jGCaMP7s.

B. Protocol of holographic stimulation to determine lateral resolution of 2P-FENDO photostimulation performance. Stimulation spots A/B/C/D/E were placed 5 µm away from each other. Photostimulation power was 160mW at the focal plane (Goji laser, 1040 nm, 5MHz repetition rate).

C. Fluorescent traces of the targeted cell #1, #5 and control cells #6,7,8,9,10 during 4 minutes acquisition at 7.14 Hz; photostimulation lasted 2 seconds.

D. DF/Fo of the cell of interest #1 (red line) and #5 (blue line) as a function of the distance separating the stimulation spot and the cell soma in µm. Fo was calculated as an average fluorescence in 20 frames, 1 second before peak signal (as the average of fluorescence signal 10 frames centred to the maximum value).

E. Fluorescent transients of one cell at different photostimulation patterns A//C/E/F/G positioned respectively at 0/10/20/30/40 µm away from the cell of interest; red bar is the photostimulation period.

F. DF/Fo peak value during the photostimulation as a function of the distance from cell of interest. DF/Fo when the spot is on the cell of interest. Photostimulation spot were placed 5 µm away from each other. n=2cells, 2 FOV, n=2mice.

III.6 Freely-moving animals

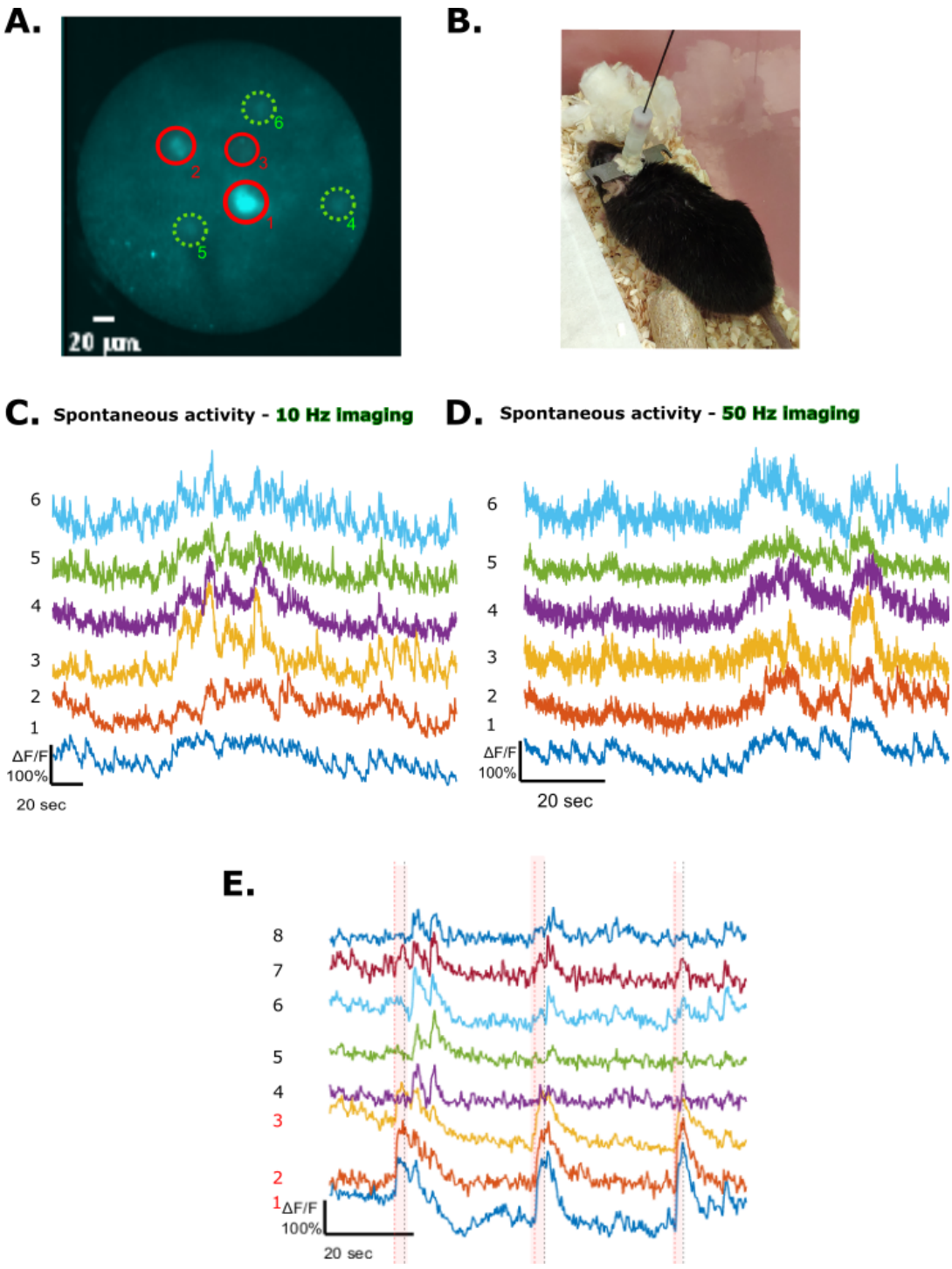

Fig. III. 30. 2P holographic stimulation in freely-moving animals with 2P-FENDO

A. Image of neurons expressing both calcium sensor (jGCaMP7s) and opsin (ChRmine).

B. Picture of the animal with the implant of GRIN lens and fiber, hold on the headplate.

C. Calcium traces DF/Fo of spontaneous neural activity acquired at 10 Hz.

D. Calcium traces DF/Fo of spontaneous neural activity of same cells acquired at 50 Hz.

E. Induced response of neural activity to 2P holographic stimulation (red bar), spots on cell #1/2/3 and observing activity of control cell #4/5/6/7/8.

The first attempt of imaging recording and 2P manipulation in freely-moving animals looks promising (**Fig.III.30.B**.). Although the animal took a long time to wake up, we did the recording of spontaneous neural activity at 10 Hz and 50 Hz (**Fig.III.30.C/D** respectively). The increase of 2P signal started when the animal was walking in the cage, following a pen moving. Some cells showed DF/Fo >200%. We photostimulated 3 cells among 8 visible in FOV of 250 µm (some of them, did appeared during the imaging session day). The imaging was at about 7 Hz. In **Fig.III.30.E**., the photostimulated cells do have an increase of fluorescence signal when the photostimulation is on, whereas the non photostimulated cells signal are at the baseline during that period. Although, they do have intrinsic activity outside those periods of stimulation.

The experiments in freely-moving animals are still ongoing and we hope to establish robust chronic animal preparations, in order to get repetitive all-optical recordings to confirm the performance of 2P-FENDO in freely-behaving animals.

IV. DISCUSSION

Contents

In this thesis project, we have developed a new 2P flexible microendoscope, we named 2P-FENDO, for imaging and photostimulation of cells in in vivo freely moving mice. *In vivo* and *in vitro* samples were employed for the development. Those served to characterize the imaging capabilities, the level of neuronal activity detection during spontaneous and evoked response during sensorial stimuli, and photostimulation performance of the system. Those pilot experiments were carried out in the mouse visual and barrel cortex as first in vivo attempts. We started all-optical investigations with anesthetized head-restrained animals. Then we performed it for freely-behaving mice.

The microendoscope resolution

In this context, we have found the best combination of fiber with GRIN lens to enable both flexible and deep tissue imaging. The combination of a FUJIKURA fiber and GRIN lens GT-MO-080-032-ACR-VisNIR-08 in the microendoscope permits the access of a FOV up to 250 µm with a good axial sectioning and sufficient lateral resolution to image and stimulate, with single-cell precision, neurons with a soma size of about 8 µm diameter. Combined with a GRIN lens GT-MO-070-016-ACR-VisNIR-30-20, the microendoscope give access to neuronal details such as dendrites or small blood vessels in the neurovascular network, with the compromise of a FOV that is twice smaller (125 µm). For the collection of our results, we mainly employed a combination of GRIN lens and fiber that allowed us to stimulate/image several neuronal somata. The more soma we can visualize the better it is. Therefore, the good balance was to adopt the configuration with a bigger FOV. We could achieve ~200 µm depth with dozens of neurons visible per focal plane.

The good axial resolution was achievable thanks to the intrinsic properties of the fiber bundle: its inter-core delay dispersion involves a certain degree of disorder among the cores, then inducing a sufficient decoupling in the time of the excitation among different cores. The result is a temporal focusing effect, which decreases the out of focus 2P interaction. The GRIN lens can be directly implanted in the tissue to access deeper brain regions since its diameter is about 1.4 mm and length of 4.84 mm. In this first proof of concept, the microendoscope was kept outside the tissue. However, we think that this new system is a promising tool for studying deeper brain areas such as the hippocampus, the thalamus, or the amygdala. It has already been demonstrated the feasibility to implant and perform imaging with GRIN lens in brainstem and hippocampus (Schwenkgrub *et al.* **Science Advances** 2020; Allegra *et al.* **Neuron** 2020). However, no flexible optical system with a fiber and 2P all-optical performances such as ours have been demonstrated up to now.

Imaging rate acquisition

To demonstrate fast functional imaging,we employed an AAV9 viral vector for expression of jGCaMP7s under hSyn promoter. We imaged neurons in the neocortex superficial layers at 920 nm at acquisition rates of 5 Hz to 100 Hz in a FOV of 250µm diameter. The imaging technique relies on scanning a large laser spot of 20 µm on the 250 µm FOV with high power density, and on the detection with an EM-CCD camera (Andor). Moreover, the GRIN lens used, characterized by low chromatic aberrations, enables both the fluorescence and laser light to be focused on the same plane.

The unprecedent high imaging speed reachable with the 2P-FENDO (up to 100 Hz) is of particular importance for imaging fast events, like neurovascular dynamics (Fan *et al.* **Nature Com.** 2020), or to perform voltage imaging (Villette *et al.* **Cell** 2019). In principle, to be able to reach imaging performances that could allow imaging of voltage reporters, some additional modifications would be necessary, like a smaller imaged region. In addition, imaging at higher speeds would permit the scanning of more plans in a given time. To get a real picture of the local neuronal dynamics and relate it to behaviour, our optical system may be the key tool. For instance, layer 4 of the primary auditory cortex show high gamma band rhythms of 50-90 Hz with high cell spiking rates (Ainsworth *et al.* **Neuron** 2012), as well as for interneurons in the visual cortex for epileptic human patients (Hermes *et al.* **Current Biol.** 2017). For genetically encoded voltage indicator (GEVI) imaging, real-time measurements require a frame rate of ~1 kHz since action potentials are 100–1000 fold faster than Ca2+ transients, demanding correspondingly faster imaging speeds (Xu *et al.* **Curr Opinion Chem Biol.** 2017).

Anaesthesia and neural activity

During our pilot imaging experiments through 2P-FENDO, we did observe spontaneous activity of neurons in anesthetized animals. Although, amplitude of 2P fluorescent signal would be higher for awake animal when the animal is in motion, running on a treadmill for instance (Russell *et al.* **bioRxiv** 2021). Based on literature on anaesthesia effect on neuronal activity, deep anaesthesia induced by high-dose isoflurane or ketamine/xylazine would not change the peak frequency or peak amplitude of stimulus induced Ca2+ transients in layer 2/3 neurons of the somatosensory cortex, while high anesthesia-dose would significantly increase neuronal synchronicity and decrease responses specificity (Lissek *et al.* **Front Cell Neurosci.** 2016). Similarly, it has been reported that deep isoflurane anaesthesia increased synchronicity also in primary visual cortex, attenuating the direction selectivity of tuned cells to moving visual stimuli (Goltstein *et al.* **PlosOne** 2015), while not significantly changing the orientation tuning. Therefore, direction selectivity and population coding seem to be more efficient in awake animals. Therefore, the observed neuronal evoked responses in somatosensory and visual cortex would differ if the animal was awake and not anaesthetized.

Since our microendoscope is meant to be used on freely-moving animals, we expect to observe more significant 2P fluorescence variations when the animal is in locomotion mode. In addition to our first attempt of freely-behaving imaging in a cage, the imaging sessions with 2P-FENDO could include a maze with controlled sensory stimuli where the animal would be free to move (Thurley and Ayaz, **Curr. Zool.** 2017; Chen *et al.* **eLife** 2018; Havenith *et al.* **Scientific Reports** 2018), allowing to observe and manipulate with photostimulation functional responses during natural behaviour.

Simultaneous 2P imaging and photostimulation with microendoscope

2P-FENDO is the first fiber-based endoscope to simultaneously perform reading and writing neuronal activity with 2P technique with single-neuron precision in freely-moving animals. 2P patterned stimulation consists in projecting 2P holographic excitation spots at the entrance of the fiber bundle with a SLM. With this illumination technique, 2P-FENDO is capable of selectively activating single neurons located at less than 50 µm from one another. The first attempts of 2P photostimulation were performed on one focal plane with a train of 10 pulses of

10 ms every140 ms, repeated every 20-30 seconds (imaging exposure time lasted 100 ms). Since an average of 10 expressing cells are expressing in FOV 250 µm, 2P-FENDO would be capable of stimulating sequentially on 5 different planes (10 cells per plane~50 cells) within 140 ms, before returning to the original plane to send the second photostimulation pulse of the sequence. As a consequence, 50 different cells could be photostimulated almost simultaneously.

In depth access

To date, neurons localized up to 150 µm depth could be detected through 2P-FENDO and both intrinsic activity and responses induced with 2P holographic stimulation could be recorded. This working distance was limited by the coverglass placed on top of the pial surface. Therefore, once the GRIN lens will be directly in contact with the brain tissue or implanted in depth, we expect a greater working distance of ~250 µm and therefore to have access to a bigger volume. This is consistent with the literature. Indeed, in scattering tissue and with a camera detection, fluorescence signals were detected down to 300 µm in the brain (Zhang *et al.* **Nature Methods** 2019).

Surgery and viral expression optimization

To get in vivo proof-of-concept of our new 2P microendoscope, the recordings were conducted on acute animal preparations. The mice had 1h to 2h surgery under deep anaesthesia including bone removal (craniotomy), followed by 30 minutes-4 hours imaging session. Anaesthesia level was kept constant with repetitive intraperitoneal injection of ketamine/xylazine and the full waking up of the animal, for freely-moving experiments, took up to 1 hour. To solve those issues, chronic preparation would facilitate the handling of awake animals. With injection, craniotomy and implants performed on the same day the gain of time and reproducibility of experiments could substantially improve. Nevertheless, since an inflammatory process and fibrosis were observed between the brain and coverglass, I was limited in the use of chronic implants until now, and I foresee a further optimisation of this type of chronic implants. Further efforts will be needed to move on this direction and to improve implants stability, like the changes in the design of the headplate or the implant for grin lens/fiber fixation.

As a final remark, an important development in the optigenetic tool that could substantially improve the rate of success of the all-optical experiments, is the combination of opsin and activity reporter in the same viral vector. To enhance the chance of having high colocalization of calcium sensor and opsin actuator, a unique virus combining somatic targeted sensor (Baker *et al.* **eLife** 2016) and actuator (Sridharan *et al.* **bioXriv** 2021) could be implemented to scale up the success rate to hit a FOV with sufficient neuronal opsin/activity reporter co-expression. We also have to consider that the proportion of neurons expressing opsins and calcium reporter may vary from an area to another depending on the distance from the injection site and the diffusion properties of the viral compound. To overcome the problem of decreased density of expression when moving far away from injection site, we targeted regions, up to 1mm diameter, that were centred on the injection site, which was visible by eye. Some optimization was necessary for our injection strategy too, to guarantee viral expression at shallower cortical depth.

Future perspectives

Voltage 2P-FENDO

Taking advantage of fast imaging capability of 2P-FENDO up to 100 Hz, our system would be suitable for voltage imaging requirements. By this mean, greater understanding about hyperpolarizing (inhibitory) and subthreshold depolarizing (excitatory) signals can be investigated, which is limited with current calcium imaging approach (Knöpfel and Song, **Nature Rev. Neuro.** 2019). For example, we would gain meaningful insights from hypocretin neurons in the lateral hypothalamus, involved in the arousal mechanism (Tyree *et al.* **Int. J. Mol. Sci.** 2017) where freely-moving configuration is surely a benefice.

Visual pathway

Since our lab is now established in the Vision Institute, 2P-FENDO can also be a powerful tool to study the visual pathway, i.e., the mechanisms regulating functional connectivity (Guido. **J.Neuro**. 2018) and signal processing along the visual pathway from the lateral geniculate nucleus (LGN) to the primary visual cortex (V1) in the mouse (Kerschensteiner and Guido **Vis. Neuro.** 2017). The Hubel & Wiesel model (J. Physiol. 1962) about receptive field in dLGN can be deeply investigated with all-optical approach in replacement of electrophysiological invasive recordings. Orientation tuning in dLGN neurons could be measure during visual stimuli as dLGN is known to convey retinotopically to precise visual signals (Roth et al. **Nature Neuro.** 2016), thus identified activated ensembles can be replayed with 2P holographic technique, directly at the targeted regions instead of relying on their projections from the cortical layers (Sun *et al.* **Nature Neuro.** 2016).

Dual brain region connectivity

Besides the direct implantation of the GRIN lens inside the brain to image deeper neural circuits, the advantage of using a microendoscope fiber-based with a GRIN lens of 1.4mm width remains on its small size and light weight of 2g. The system is fairly light and small for the mouse to give room for another GRIN lens implant. Therefore, a double implant of GRIN lenses would permit imaging of 2 brain regions at the same time and at different depths. By this means, direct correlation of neural activity and functional connections can be studied and manipulated with 2P-FENDO. For instance, decoding the visual attention (visual cortex, Speed *et al.* **Nature Com.** 2020) and motion reaction (cerebellum, Muzzu *et al.* **PlosOne** 2018) of the animal. In humans, it was observed a cerebrocerebellar loop between posterior parietal cortex V5 based on fMRI observations (Kellermann *et al.* **Journal of Neuro.** 2012): "Attentional mechanisms appear to emphasize parietocerebellar influences on motion processing in V5". They questioned about how those events act and if other regions are involved in the prediction of perception events. Therefore, local circuit investigation and manipulation of dual brain regions at the single cell resolution may be worth it to decipher this neural mechanism. Since cerebellum not only serves motor control but also support various cognitive function, it would be interesting to take advantage of the GRIN lens to have access to deeper brain regions and observe the functional connection with other areas to decrypt the neuronal circuits of behaviour and perception processes in freely-moving animals.

Deep local circuits

If we focus investigation on a local circuit, 2P-FENDO enables to access deeper brain regions when being directly implanted in the brain tissue (See **Annex 3**) during natural behaviour to validate some recent theories. Recent publications on neural circuit stated that the brain is capable of plastic connectivity and relies on simple pattern completion: if group of neurons, one just need to activate very few cells to make the entire circuit fire, called "recall ensemble" (Carrillo-Reid *et al.* **Science** 2016) or that only controlling 14 to 37 neurons is sufficient to pattern completion in the cortical circuits to drive perception (Dalgleish *et al.* **eLife** 2020). Hence, our new 2P flexible microendoscopy system may permit to recall ensembles of deeper regions involved in behaviour that requires the animal to be freely-moving (memory, anxiety, decision making, etc.).

V. CONCLUSION

My thesis project aimed to prove the performance of a newly built 2P flexible microendoscope for all-optical investigation of neurons in freely-moving animals. Evolving with the optical development, we carried out the pilot experiments from *in vitro* to *in vivo* preparations. It raised the importance of optimising the best settings at different scales: from the virus choice as an efficient optogenetic tool, the strategy for testing the imaging capability in a short time with organotypic slices, the details of the materials used (thinner coverglass, fiber, GRIN lens), the self-design of materials (headplate, restrainer, implant), the meticulous and numerous surgeries with the maintenance of optimal anaesthesia level and optimization of biological preparations *in vivo (*a clean and stable brain window).

Our 2P-FENDO, did outperform previous imaging and photostimulation capabilities of microendoscopic systems. It is the first microendoscope capable of simultaneous 2P imaging and 2P holographic stimulation in freely-behaving animals at a high acquisition speed of 100Hz (>>40 Hz), up to 200 µm depth. We have determined the best combination of fiber and GRIN lens to see cells somata expressing jGCaMP7s in a FOV of 250 µm. The axial and lateral resolutions are both about 7 µm, based on rhodamine imaging. It was possible to perform calcium imaging at different acquisition rates from 2 Hz to 100 Hz. We observed spontaneous activity with fluorescent transients in the order of DF/Fo>100% *in vivo* in a head-restrained mouse. Sensory stimuli highlighted the capability of the system to image neuronal activation in the visual and the barrel cortex with visual stimuli and whisker stimuli in anaesthetized head-fixed animals. Simultaneous stimulation of multiple 2P holographic spots was possible with 2P-FENDO, where 87% of cells were responsive to photostimulation of 30 mW with an increase of DF/Fo of about 20%. The lateral resolution of photostimulation was 5 µm. Hence, our system could perform manipulation of dense neurons. To finish, 2P-FENDO can also achieve robust imaging and stimulation in an awake, freely-behaving animal with implant of the microendoscope maintained with a customized support on the mouse headplate.

We think that our new 2P-FENDO is a promising tool for all-optical investigation of circuits during natural behaviour. It can provide direct insights of neuronal activity during sensorial stimuli by imaging multiple cells somata with sufficient resolution, and by manipulating their activity with an efficient optogenetic tools. The technique will open the way toward experiments in which it will be possible, for example, to replay sequences of neuronal activity, exploring the mechanisms at the origin of animal behaviour in natural environment. To date, the study of neural circuits with a flexible endoscope, was limited to low imaging rates (40Hz) and 1P stimulation, with poor axial sectioning and one-colour imaging. Therefore, 2P-FENDO overcomes those limitations to enable fast calcium imaging (100 Hz) and reliable 2P holographic stimulation in freely-behaving animals. The experiments to test the freely-moving are still ongoing to prove the system's robustness in the long term with chronic animals. By this way, we are confident that 2P-FENDO can be a key microendoscope for all-optical neuronal investigations in freely-moving animals at the single cell precision. It could scale up the deciphering of the links between neuronal circuits involved in perception and behaviour in the most natural environment.

VERSION FRANCAISE *(selon les règles spécifiées par l'Ecole Doctorale)*

DISCUSSION

Dans ce projet de thèse, nous avons développé un nouveau microendoscope flexible 2P, que nous avons nommé 2P-FENDO, pour l'imagerie et la photostimulation de cellules chez des souris se déplaçant librement *in vivo*. Des échantillons *in vivo* et *in vitro* ont été utilisés pour ce développement. Ceux-ci ont servi à caractériser les capacités d'imagerie, le niveau de détection de l'activité neuronale pendant la réponse spontanée et évoquée lors de stimuli sensoriels, et les performances de photostimulation du système. Ces expériences pilotes ont été réalisées dans le cortex visuel et le cortex somatosensoriel de la souris, comme premières tentatives *in vivo*. Nous avons commencé toutes les investigations optiques avec des animaux anesthésiés et attachés à la tête. Ensuite, nous les avons réalisées sur des souris mobiles.

La résolution du microendoscope

Dans ce contexte, nous avons trouvé la meilleure combinaison de fibre et de lentille GRIN pour permettre l'imagerie du cerveau. La combinaison d'une fibre FUJIKURA et d'une lentille GRIN GT-MO-080-032-ACR-VisNIR-08 pour le microendoscope permet l'accès à un champ d'imagerie large allant jusqu'à 250 µm avec une bonne section axiale et une résolution latérale suffisante pour imager et stimuler, avec une précision à l'échelle de la cellule unique, des neurones dont le corps cellulaire (soma) a un diamètre d'environ 8 µm. Combiné à une lentille GRIN GT-MO-070-016-ACR-VisNIR-30-20, le microendoscope donne accès à des détails neuronaux tels que les dendrites ou les petits vaisseaux sanguins du réseau neurovasculaire, avec le compromis d'un champ d'imagerie deux fois plus petit (125 µm). Pour la collecte de nos résultats, nous avons principalement utilisé une combinaison de lentille GRIN et de fibre à corps multiples qui nous a permis de stimuler/imager plusieurs somas neuronaux. Plus on peut visualiser de soma, mieux c'est. Par conséquent, le bon équilibre était d'adopter la configuration avec un champ d'imagerie plus large. Nous avons pu atteindre une profondeur de ~200 µm avec des dizaines de neurones visibles par plan focal.

La bonne résolution axiale a pu être obtenue grâce aux propriétés intrinsèques du faisceau de fibres à corps (noyaux) multiples : la dispersion du délai entre les noyaux implique un certain degré de désordre entre les noyaux, ce qui induit un découplage suffisant dans le temps de l'excitation entre les différents noyaux. Le résultat est un effet de focalisation temporelle, qui réduit l'interaction 2P hors foyer. La lentille GRIN peut être directement implantée dans le tissu pour accéder aux régions plus profondes du cerveau puisque son diamètre est d'environ 1,4 mm et sa longueur de 4,84 mm. Dans cette première preuve de concept, le microendoscope a été maintenu à l'extérieur du cerveau. Cependant, nous pensons que ce nouveau système est un outil prometteur pour l'étude de zones cérébrales plus profondes telles que l'hippocampe, le thalamus ou l'amygdale. Il a déjà été démontré qu'il était possible d'implanter et de réaliser des images avec la lentille GRIN dans des régions profondes, comme le tronc cérébral et l'hippocampe (Schwenkgrub *et al.* Science Advances 2020 ; Allegra *et al.* Neuron 2020). Cependant, aucun système optique flexible avec une fibre et des performances tout-optique 2P avec photostimulation précise comme le nôtre n'a été démontré jusqu'à présent.

Vitesse d'imagerie

Pour démontrer l'imagerie fonctionnelle rapide, nous avons utilisé un vecteur viral AAV9 pour l'expression de jGCaMP7s sous le promoteur hSyn. Nous avons imagé des neurones dans les couches superficielles du néocortex (920 nm) à des vitesses d'acquisition de 5 Hz à 100 Hz dans un champ d'imagerie de 250µm de diamètre. La technique d'imagerie repose sur le balayage d'un large spot de 20 µm sur le champ d'imagerie de 250 µm avec une densité de puissance élevée, et sur la détection avec une caméra EM-CCD (Andor). De plus, l'objectif GRIN utilisé, caractérisé par de faibles aberrations chromatiques, permet de focaliser la fluorescence et la lumière laser sur le même plan.

La vitesse d'imagerie élevée sans précédent que permet d'atteindre le 2P-FENDO (jusqu'à 100 Hz) est particulièrement importante pour l'imagerie d'événements rapides, comme la dynamique neurovasculaire (Fan *et al.* Nature Com. 2020), ou pour l'imagerie du voltage (Villette *et al.* Cell 2019). En principe, pour pouvoir atteindre des performances d'imagerie permettant l'imagerie de rapporteurs de tension, certaines modifications supplémentaires seraient nécessaires, comme une région imagée plus petite. En outre, l'imagerie à des vitesses plus élevées permettrait de balayer un plus grand nombre de plans dans un temps donné. Pour obtenir une image réelle de la dynamique neuronale locale et la relier au comportement, notre système optique peut être l'outil clé. Par exemple, la couche 4 du cortex auditif primaire présente des rythmes élevés de bande gamma de 50 à 90 Hz avec des taux élevés d'activation cellulaire (Ainsworth *et al.* Neuron 2012), ainsi que pour les interneurones dans le cortex visuel pour les patients humains épileptiques (Hermes *et al.* Current Biol. 2017). Pour l'imagerie de l'indicateur de voltage génétiquement encodé (GEVI), les mesures en temps réel nécessitent une fréquence d'images de ~1 kHz, car les potentiels d'action sont 100 à 1000 fois plus rapides que les fluctuations Ca2+, ce qui exige des vitesses d'imagerie plus rapides (Xu *et al.* Curr Opinion Chem Biol. 2017).

Anesthésie et activité neuronale

Au cours de nos expériences pilotes d'imagerie à travers le 2P-FENDO, nous avons observé une activité spontanée des neurones chez les animaux anesthésiés. Bien que l'amplitude du signal fluorescent 2P soit plus élevée chez un animal éveillé lorsque celui-ci est en mouvement, par exemple lorsqu'il court sur un tapis roulant (Russell *et al.* bioRxiv 2021). D'après la littérature sur les effets de l'anesthésie sur l'activité neuronale, l'anesthésie profonde induite par de fortes doses d'isoflurane ou de kétamine/xylazine ne modifierait pas la fréquence ou l'amplitude maximale des fluctuations Ca2+ induits par un stimulus dans les neurones des couches 2/3 du cortex somatosensoriel, alors que de fortes doses d'anesthésie augmenteraient considérablement la synchronisation neuronale et diminueraient la spécificité des réponses (Lissek *et al.* Front Cell Neurosci. 2016). De même, il a été signalé que l'anesthésie profonde à l'isoflurane augmentait la synchronisation également dans le cortex visuel primaire, atténuant la sélectivité directionnelle des cellules accordées aux stimuli visuels en mouvement (Goltstein *et al.* PlosOne 2015), tout en ne modifiant pas significativement la sélectivité d'orientation visuelle. Par conséquent, la sélectivité de direction des stimuli visuels et le codage de ces populations cellulaires semblent être plus efficaces chez les animaux éveillés. Par conséquent, les réponses neuronales évoquées observées dans les cortex somatosensoriel et visuel seraient différentes si l'animal était éveillé et non anesthésié.

Comme notre microendoscope est destiné à être utilisé sur des animaux se déplaçant librement, nous nous attendons à observer des variations de fluorescence 2P plus importantes lorsque l'animal est en locomotion. En plus de notre première tentative d'imagerie lorsque l'animal est mobile dans une cage, les sessions d'imagerie avec 2P-FENDO pourraient inclure un labyrinthe avec des stimuli sensoriels contrôlés où l'animal serait libre de se déplacer (Thurley et Ayaz, Curr. Zool. 2017 ; Chen *et al.* eLife 2018 ; Havenith *et al.* Scientific Reports 2018), permettant d'observer et de manipuler par photostimulation précise les réponses fonctionnelles pendant un comportement naturel.

Imagerie 2P et photostimulation 2P simultanées avec un microendoscope

2P-FENDO est le premier microendoscope à fibres optiques à effectuer simultanément la lecture et l'écriture de l'activité neuronale par la technique 2P avec une précision à l'échelle de la cellule unique chez des animaux se déplaçant librement. La stimulation holographique 2P consiste à projeter des spots d'excitation holographiques 2P à l'entrée du faisceau de fibres avec un SLM. Avec cette technique d'illumination, 2P-FENDO est capable d'activer sélectivement de multiples neurones uniques situés à moins de 50 µm les uns des autres. Les premiers essais de photostimulation 2P ont été réalisés sur un plan focal avec un train de 10 impulsions de 10 ms toutes les 140 ms, répétées toutes les 20-30 secondes (le temps d'exposition de l'imagerie a duré 100 ms). Étant donné qu'en moyenne 10 cellules s'expriment dans un champ d'imagerie de 250 µm, 2P-FENDO serait capable de stimuler séquentiellement sur 5 plans différents (10 cellules par plan~50 cellules) en 140 ms, avant de revenir au plan d'origine pour envoyer la deuxième impulsion de photostimulation de la séquence. Par conséquent, 50 cellules différentes pourraient être photostimulées presque simultanément.

Accès en profondeur

Jusqu'à présent, les neurones localisés jusqu'à 150 µm de profondeur ont pu être détectés par 2P-FENDO et l'activité intrinsèque ainsi que les réponses induites par la stimulation holographique 2P ont pu être enregistrées. Cette distance de travail était limitée par le verre recouvrant le cerveau. Par conséquent, lorsque la lentille GRIN sera directement en contact avec le tissu cérébral ou implantée en profondeur, nous prévoyons une plus grande distance de travail de ~250 µm et donc l'accès à un plus grand volume. Ceci est cohérent avec la littérature. En effet, dans des tissus diffusants et avec une détection par caméra, des signaux de fluorescence ont été détectés jusqu'à 300 µm dans le cerveau (Zhang *et al.* Nature Methods 2019).

Optimisation de la chirurgie et de l'expression virale

Pour obtenir une preuve de concept *in vivo* de notre nouveau microendoscope 2P, les enregistrements ont été réalisés sur des préparations animales aiguës. Les souris ont subi une chirurgie de 1h à 2h sous anesthésie profonde, y compris l'ablation d'os (craniotomie), suivie d'une session d'imagerie de 30 minutes à 4 heures. Le niveau d'anesthésie était maintenu constant par des injections intrapéritonéales répétées de kétamine/xylazine et le réveil complet de l'animal, pour des expériences de mouvement libre, prenait jusqu'à 1 heure. Pour résoudre ces problèmes, une préparation chronique faciliterait la manipulation des animaux éveillés. Avec l'injection, la craniotomie et les implants réalisés le même jour, le gain de temps et la

reproductibilité des expériences pourraient être considérablement améliorés. Néanmoins, étant donné qu'un processus inflammatoire et une fibrose ont été observés entre le cerveau et le verre de recouvrement, j'ai été limité dans l'utilisation des implants chroniques jusqu'à présent, et je prévois une optimisation supplémentaire de ce type d'implants chroniques. D'autres efforts seront nécessaires pour avancer dans cette direction et pour améliorer la stabilité des implants, comme les changements dans la conception de la plaque de tête ou de l'implant pour la fixation de la lentille/fibre.

En guise de conclusion, un développement important de l'outil optogénétique qui pourrait améliorer considérablement le taux de réussite des expériences tout-optique, est la combinaison de l'opsine et du rapporteur d'activité dans le même vecteur viral. Pour augmenter les chances d'obtenir une colocalisation élevée de l'indicateur calcique et de l'opsine, un virus unique avec un indicateur calcique ayant une expression somatique ciblée (Baker *et al.* eLife 2016) et une opsine (Sridharan et al. bioXriv 2021) pourrait être mis en œuvre pour augmenter le taux de réussite et atteindre un champ d'imagerie avec une co-expression suffisante de l'opsine neuronale et du rapporteur d'activité. Nous devons également tenir compte du fait que la proportion de neurones exprimant les opsines et l'indicateur calcique peut varier d'une zone à l'autre en fonction de la distance du site d'injection et des propriétés de diffusion du composé viral. Pour surmonter le problème de la diminution de la densité d'expression lorsqu'on s'éloigne du site d'injection, nous avons ciblé des régions, jusqu'à 1 mm de diamètre, centrées sur le site d'injection, qui était visible à l'œil. Une certaine optimisation a également été nécessaire pour notre stratégie d'injection, afin de garantir l'expression virale à une profondeur corticale moindre.

Perspectives

En profitant de la capacité d'imagerie rapide de 2P-FENDO jusqu'à 100 Hz, notre système serait adapté aux exigences de l'imagerie voltage. Ainsi, il sera possible de mieux comprendre les signaux hyperpolarisants (inhibiteurs) et dépolarisants (excitateurs), ce qui est actuellement limité par l'approche de l'imagerie calcique (Knöpfel et Song, Nature Rev. Neuro. 2019). Par exemple, nous obtiendrions des informations significatives sur les neurones à hypocrétine dans l'hypothalamus latéral, impliqués dans le mécanisme d'éveil (Tyree *et al.* Int. J. Mol. Sci. 2017) où la configuration en mouvement libre est sans nul doute un avantage.

Système visuel

Notre laboratoire étant désormais établi au sein de l'Institut de la Vision, 2P-FENDO peut également constituer un outil puissant pour étudier le système visuel, c'est-à-dire les mécanismes régulant la connectivité fonctionnelle (Guido. J.Neuro. 2018) et le traitement du signal le long du système visuel, du noyau géniculé latéral (LGN) au cortex visuel primaire (V1) chez la souris (Kerschensteiner et Guido Vis. Neuro. 2017). Le modèle de Hubel et Wiesel (J. Physiol. 1962) concernant le champ récepteur du LGN peut être étudié en profondeur grâce à une approche entièrement optique qui remplace les enregistrements électrophysiologiques invasifs. La préférence d'orientation visuelle dans les neurones du dLGN pourrait être mesuré pendant des stimuli visuels, car le dLGN est connu pour transmettre par voie rétinotopique des signaux visuels précis (Roth *et al.* Nature Neuro. 2016). Ainsi, les ensembles activés identifiés peuvent être reproduites avec la technique holographique 2P, directement dans les régions ciblées, au lieu de

dépendre de leurs projections dans les couches corticales supérieures (Sun et al. Nature Neuro. 2016).

Connectivité de deux régions du cerveau

Outre l'implantation directe de la lentille GRIN à l'intérieur du cerveau pour imager les circuits neuronaux plus profonds, l'avantage d'utiliser un microendoscope à base de fibres avec une lentille GRIN de 1,4 mm de largeur reste sur sa petite taille et son poids léger de 2g. Le système est assez léger et petit pour que la souris puisse laisser la place à un autre implant de lentille GRIN. Par conséquent, un double implant de lentilles GRIN permettrait d'imager deux régions du cerveau en même temps et à des profondeurs différentes. De cette façon, la corrélation directe de l'activité neuronale et des connexions fonctionnelles peut être étudiée et manipulée avec 2P-FENDO. Par exemple, décoder l'attention visuelle (cortex visuel, Speed *et al.* Nature Com. 2020) et la réaction au mouvement (cervelet, Muzzu *et al.* PlosOne 2018) de l'animal. Chez l'homme, il a été observé une boucle cérébro-cérébelleuse entre le cortex pariétal postérieur V5 sur la base d'observations par IRM fonctionnel (Kellermann *et al.* Journal of Neuro. 2012) : "Les mécanismes attentionnels semblent souligner les influences pariéto-cérébelleuses sur le traitement du mouvement dans V5". Ils se sont interrogés sur la manière dont ces événements agissent et si d'autres régions sont impliquées dans la prédiction des événements de perception. Par conséquent, l'étude des circuits locaux et la manipulation de deux régions du cerveau à la résolution de la cellule unique peuvent être utiles pour déchiffrer ce mécanisme neuronal. Étant donné que le cervelet ne sert pas seulement au contrôle moteur, mais qu'il soutient également diverses fonctions cognitives, il serait intéressant de tirer parti de la lentille GRIN pour avoir accès à des régions cérébrales plus profondes et observer la connexion fonctionnelle avec d'autres zones afin de décrypter les circuits neuronaux des processus de comportement et de perception chez les animaux se déplaçant librement.

Circuits locaux profonds

Si nous concentrons nos recherches sur un circuit local, 2P-FENDO permet d'accéder à des régions cérébrales plus profondes lorsqu'il est implanté directement dans le tissu cérébral (voir annexe 3) pendant un comportement naturel afin de valider certaines théories récentes. Des publications récentes sur les circuits neuronaux indiquent que le cerveau est capable de plasticité dans ces connexions neuronales et qu'il repose sur l'accomplissement d'un modèle simple : si un groupe de neurones, il suffit d'activer très peu de cellules pour que l'ensemble du circuit s'active, appelé "ensemble de rappel" (Carrillo-Reid *et al.* Science 2016) ou aussi que le contrôle de 14 à 37 neurones suffit à conduire la perception et réactiver les circuits neuronaux (Dalgleish *et al.* eLife 2020). Par conséquent, notre nouveau système de microendoscopie flexible 2P peut permettre de rappeler des ensembles de régions plus profondes impliquées dans des comportements qui nécessitent que l'animal se déplace librement (mémoire, anxiété, prise de décision, etc.).

CONCLUSION

Mon projet de thèse avait pour but de prouver les performances d'un microendoscope flexible 2P nouvellement construit pour l'étude tout-optique des neurones chez des animaux se déplaçant librement. Avec des développements croissants en optique, nous avons réalisé les expériences pilotes des préparations *in vitro* aux préparations *in vivo*. Cela a mis en évidence l'importance d'optimiser les meilleurs paramètres à différentes échelles : du choix du virus comme outil optogénétique efficace, de la stratégie pour tester la capacité d'imagerie en peu de temps avec des tranches organotypiques, des détails des matériaux utilisés (verre couvrant le cerveau plus fin, type de fibre, modèle de lentille GRIN), de l'auto-conception des matériaux (barre de tête, dispositif pour maintenir l'animal, implant), des opérations chirurgicales nombreuses et méticuleuses avec le maintien d'un niveau d'anesthésie optimal et l'optimisation des préparations biologiques *in vivo* (une fenêtre de cerveau propre et stable).

Notre 2P-FENDO, a dépassé les capacités d'imagerie et de photostimulation des systèmes microendoscopiques précédents. Il s'agit du premier microendoscope capable de réaliser simultanément l'imagerie 2P et la stimulation holographique 2P chez des animaux se déplaçant librement, à une vitesse d'acquisition élevée de 100 Hz (>>40 Hz), jusqu'à une profondeur de 200 µm. Nous avons déterminé la meilleure combinaison de fibre et de lentille GRIN pour voir les corps cellulaires (soma) des cellules exprimant jGCaMP7s dans un champ d'imagerie de 250 µm. Les résolutions axiale et latérale sont toutes deux d'environ 7 µm, d'après l'imagerie de la rhodamine. Il a été possible de réaliser l'imagerie calcique à différentes fréquences d'acquisition, de 2 Hz à 100 Hz. Nous avons observé une activité spontanée avec des fluctuations de fluorescence de l'ordre de DF/Fo>100% *in vivo* chez une souris dont la tête était maintenue fixe. Des stimuli sensoriels ont mis en évidence la capacité du système à imager l'activation neuronale dans le cortex visuel et le cortex somatosensoriel à l'aide de stimuli visuels et de stimuli des vibrisses chez des animaux anesthésiés, fixés par la tête. La stimulation simultanée de plusieurs spots holographiques 2P était possible avec 2P-FENDO, où 87% des cellules répondaient à une photostimulation de 30 mW avec une augmentation du DF/Fo d'environ 20%. La résolution latérale de la photostimulation était de 5 µm. Par conséquent, notre système pouvait effectuer la manipulation de multiples neurones. Pour finir, 2P-FENDO peut également réaliser une imagerie et une stimulation robustes chez un animal éveillé et mobile avec l'implantation du microendoscope maintenu avec un support personnalisé sur la barre de tête de la souris.

Nous pensons que notre nouveau 2P-FENDO est un outil prometteur pour l'étude tout-optique des circuits pendant un comportement naturel. Il peut fournir un aperçu direct de l'activité neuronale pendant les stimuli sensoriels en imagerie des somas de multiples cellules avec une résolution suffisante, et en manipulant leur activité avec des outils optogénétiques efficaces. Cette technique ouvrira la voie à des expériences dans lesquelles il sera possible, par exemple, de reproduire avec la lumière des séquences d'activité neuronale, explorant ainsi les mécanismes à l'origine du comportement animal dans l'environnement naturel. Jusqu'à présent, l'étude des circuits neuronaux à l'aide d'un microendoscope flexible était limitée à de faibles vitesse d'imagerie (40 Hz) et à la stimulation 1P, avec une mauvaise section axiale et une imagerie unicolore. Par conséquent, 2P-FENDO dépasse ces limitations pour permettre une imagerie calcique rapide (100 Hz) et une stimulation holographique 2P fiable chez des animaux mobiles. Les expériences pour tester la flexibilité des mouvements de l'animal sont toujours en cours pour prouver la robustesse du système à long terme avec des animaux chroniques. De cette manière, nous sommes convaincus que 2P-FENDO peut être un microendoscope clé pour les investigations

neuronales tout-optique chez les animaux se déplaçant librement, avec une précision à l'échelle de cellule unique. Il pourrait permettre de décrypter les liens entre les circuits neuronaux impliqués dans la perception et le comportement dans un environnement se rapprochant le plus de la réalité.

VI. VADEMECUM

Contents

Basics in physics

I want to expose below the principles of optical concepts that will help to get a turn-key writing support to the chapters related to the development of the new microendoscopy.

VI.1 Light geometric properties

Light is propagating inside tissue (matter) through light rays: beams of electromagnetic wave trains. It can be visible to the human eye or invisible. Visible **spectra** are ranged from 400 to 700nm (blue to red). Invisible spectra go towards infrared (>700nm). **Photons** are the molecules composing the light. The more photons, the greater is the light intensity. The light source, so-called laser is characterized by a specific **wavelength**. It is defined as the shorter distance between two points of the wave curve having the same phase. The light beams are characterized by a speed of propagation and a direction of propagation. The speed of light propagation is about c=3*10^8 m/s in the vacuum otherwise it is highly dependent on the medium. Light polarization defines how the direction of the wave is evolving (linear, circular, random). When light rays pass through a matter, some photons are (1) reflected (2) refracted (3) diffused (4) transmitted (5) absorbed or (6) scattered.

When the light interacts with the matter, the medium matter can be described by a unique property: the **refractive index** (*n*) linked to the wavelength. When the light pass through the interface of two medium with different refractive index, the light ray can be deviated of its initial trajectory with an angle. This deviation angle depends on the wavelength of the light. (1) **Reflection** when the light is bounced off a surface. The amount of reflected light depends on refractive index, incidence angle and polarization. (2) **Refraction** when the light can pass between 2 mediums (3) **Diffusion** or called **diffraction** when the light waves are bending around the edges of the object (4) **Transmission** when all the light passes through the matter without any absorption (5) **Absorption** when the light transfer energy to particles of the matter. Absorbance can vary with the wavelength. To let certain colours passing through it, filters can be used. (6) **Scattering** when the light wave interacts with matter, causing it to move in various directions. The law of Snell-Descartes illustrates those phenomena. n1*sini1=n2*sini2. In addition to those angle beam with various direction propagation, the light can be split by a prism. Each spectral components of the light are deviated; it is called **dispersion**. Indeed, the refractive index depends on the wavelength of the light n(lambda). Cauchy law $n(\lambda)=A+B/(\lambda^2)$. Where A and B are specific from the material. In short, photon can be defined with these parameters: speed, direction, energy, wavelength. Throughout a medium, within a specific refractive index and wavelength, the light rays are either reflected, transmitted or absorbed. Hence the choice of laser source for imaging are highly dependent on reflection coefficient, absorption coefficient of the tissue and the wavelength.

VI.2 Light wavefront properties

Apart from its corpuscular properties, the light has wave properties. By passing through a material (brain tissue), the wave is a deformation of amplitude and trajectory, so called phase. A light wave is characterized by its wavelength (lambda,in nm), its frequency (f, in Hz) and its speed (c, in m/s). c=lambda*f. The laser as light source is a light wave with three properties: (1) monochromatic i.e., a single wavelength or one specific color or frequency (2) unidirectional i.e., the light beam propagates in one direction (3) coherent i.e., the emitted waves are in phase Indeed, if two waves (same wavelength and frequency) are in phase, both wave crests and troughs align. The constructive interference results increase in the wave amplitude: brighter light. In contrary, if two waves are out of phase, the crests will align with the troughs: destructive interference results, a decrease in the amplitude of the combined wave: dimming light. So called **interference** is a phenomenon in which two waves superpose to form a resultant wave of greater, lower, or the same amplitude. Then the sum of wave (interference) is a wave, and its intensity is phase dependent (equation of Alembert). **Huygens's Principle** states that every point on a wavefront is a source of wavelets, which spread forward at the same speed. The emitted waves are semicircular and the new wavefront is tangent to the wavelets. These wavelets spread out in the forward direction, at the same speed as the source wave. When the linear wave meets an opening (slit) or an obstacle where the length is about or smaller than the wavelength, the wave is bended around those edges: a phenomenon of **diffraction** occurs. The smaller the opening or obstacle, the greater is the diffraction. It highlights the property of light as being wave. The optical component to do it is called **diffraction grating**. It has a periodic structure that splits and diffracts light into several beams travelling in different directions. The direction of these beams depends on the spacing of the grating and the wavelength of the light.

VI.3 Imaging resolutions

Diffraction plays a large role in the resolution at which one can see two small distinct objects. Resolution defines the degree of fineness with which an image can be recorded or produced, often expressed as the number of pixels per unit of length. The limit of resolution is the minimal distance that separates two distinct points. The power of resolution is the best resolution that an instrument can reach in the optimal condition of observation. **Diffraction limited spot** (in diameter) is the minimal spot size reachable, depending on a specific laser wavelength, a beam diameter and effective focal length from the lens or objective. It gives an idea of the maximum beam quality. As our object to image is not considered as a flat point but a volumetric object (e.g., cell), we will look at the resolution in xy and z axis. **Lateral resolution** as **Rayleigh critera** is defined as the minimal distance to distinguish two objects in a 2D plan. The objects are said resolved (i.e., easy to distinguish from each other). (Equation Rxy=0.61 (wavelength)/NA). **Axial resolution** is defined as the depth resolution in the direction parallel to the laser beam (Equation $Rz=2*wavelength/(NA^2)$).

When the object is not transparent, the light is diffracted. The diffraction will create interferences of the waves at the site of focal point, so called Airy disks. The **point of spread function (PSF)** defines this phenomenon impacting the optical resolution. PSF is the three-dimensional image of a point-like object under the microscope. PSF varies depending on the wavelength of the light and the numerical aperture (NA) of the objective lens. Shorter wavelength of light (such as blue light,

450nm) result in a smaller PSF; while longer wavelength (such as red light, 650nm) result in a larger PSF and therefore worse resolution. In addition, a high-NA objective gives small PSF and therefore better resolution. The blurring of the PSF in the object is called a **convolution** of the object: Equation Object (X) PSF = Image. The degree of blurring of the point object is a measure for the quality of an imaging system. In 1927, Houston proposed the use of the full width at half maximum (**FWHM**) to quantify resolution, based on the PSF. FWHM is the width of a line shape at half of its maximum amplitude. If two peaks have overlapping FWHMs, the two objects are unresolvable. The smaller the number of FWHM, the better the spatial resolution.

VI.4 Aberrations

The goal of a microscopy is to obtain a precise magnified image on the focal plane i.e., plane that is perpendicular to the axis of a lens or mirror and passes through the focus. Due to technical constraints, optical system should minimize some image deformations, so called aberrations. We cite three of them. First, **spherical aberration** where the focal distance is dependent on the distance from the centre of the lens; second, **chromatic aberration** where the focal distance varies with specific colour and, third, **astigmatism** where the focal change along the xy axis. Historically, the spherical aberration came from the default of polished glass lens. In other terms, the electrons near the lens centre are less deviated from their trajectories compared to the electrons near the edges, therefore the light rays do not converge on the same focal plane. It forms a so-called circle of least confusion, leading to reduced contrast and poorer resolution. To overcome this spherical aberration, there are two methods: either limit the lens edges or use different curved lenses. Chromatic aberration, as its name suggests, emphasize the colours or the light rays. Each of them would not focalize at the same focal point of the optic axis. Causing variations of wavelength, it is caused by different speed of photons or loss of energy. It can be solved by adding divergent lenses.

There are several types of dispersion in the fiber: (a) intermodal dispersion occurring only in multimode fibers, i.e., each mode travels at different time speed inside the fiber so they do not exit the fiber at the same time: different modes propagate at different group velocities (**Fig.A.**) (b) intramodal or chromatic dispersion occurring in all kinds of optical fibers because fiber transmits light of different wavelengths at different speeds (**Fig.B.**) (c) polarization mode dispersion, i.e., different propagation direction of light with different polarization states. (**Fig.C.**)

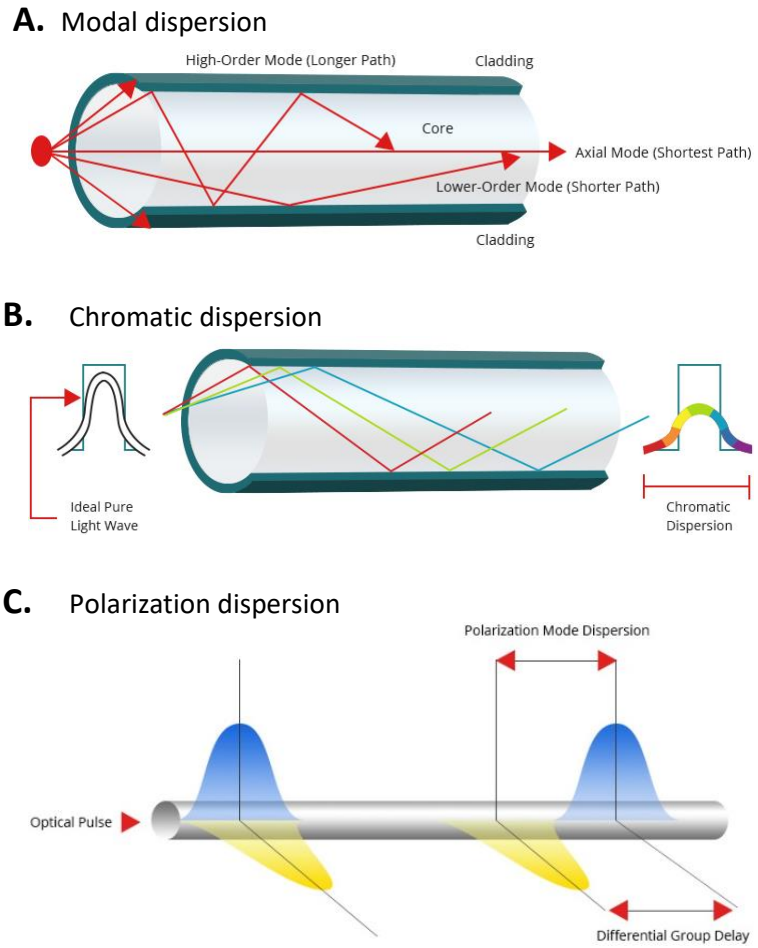

Fig.I.35. Dispersions (from FS website)

VI.5 Microscopy setup

In short, a microscope is an instrument for getting an enlarged image from a small object (magnification), for distinguishing details in the image (resolution) and for making them visible to the eyepiece or camera. Basically, it is composed of a light source (laser), contrast agents, optical components (lens, objective) and a detector (camera). Herewith, I list some optical components that will be used to setup a microscope.

Laser emits light, amplified by stimulated emission of radiation as its acronym indicates.

Lens is a single transparent device to allow the transmission and refraction of light to create either a converging beam (i.e., the light is focused to a point) or diverging beam (i.e., the light is spread out from the lens and does not focus on a point). A converging lens is called convex and diverging one is concave. The lens converges incoming light rays that are parallel to the optical axis toward a single point on the optical axis called the *focal point*. The distance between the focal point and the centre of the lens is called the focal length (f) of the lens. It is a measure of the focusing power of the lens and is related to the radius of curvature (R) and refractive index (n) of the lens as follows: f=R/(2(n-1).

Aperture is the total light-receiving area of the lens. The larger the aperture, the greater amount of light received by the lens from each point in the scene, and hence the brighter the image. The size of the aperture (opening) can be controlled using a diaphragm.

Mirror is an optical device which can reflect light where the angle of reflection equals the angle of incidence. **Dichroic** mirror are mirrors which have different reflection properties for two different wavelengths. Mirror **galvanometer (galvo)** is an electromechanical instrument, it sensed an electric current by deflecting a light beam with a mirror. Its advantages rely on its high speed of movement. The size of the mirror depends on the laser beam. As the diameter and the power of the beam increase so must the diameter of the mirror.

Beam splitter splits a beam of light in two. Polarizing beam splitters split into two beams of orthogonal polarization states. **Polarization** of light is the direction of the electric field oscillation of a light beam.

Waveplate is a transparent plate with a defined amount of birefringence, used for modifying the polarization of light. **Birefringence** is the double refraction of light in a transparent material.

Diffraction grating with a periodic structure splits & diffracts light into several beams travelling in different directions.

PhotoMultiplier Tube (PMT) converts a light pulse into an electrical signal of measurable magnitude. In a vacuum glass tube, the light is absorbed on a photocathode and generates free photoelectrons, those electrons are accelerated with a high voltage to a first electrode and, finally a strongly amplified photocurrent is collected with an anode near the last dynode. It helps to count the numbers of photons to convert to electrical signal before the camera.

Spatial Light Modulator (SLM) is an object that can manipulate light beam by modulation its amplitude, phase, or polarization of the light waves in the two dimensions of space and time.

Optical filter can selectively transmit light in a particular range of wavelengths (colours) while absorbing the remainder. They are longpass (pass long wavelength only) or shortpass (short ones) or bandpass (blocking both longer and shorter).

Camera is used to capture images or video, or to display video on a monitor.

VII. ANNEXES

1. Visual stimuli protocols

References / Parameters	(1)	(2)	(3)	Our lab
Size LCD monitor	X	30*40 cm	30*40 cm	7 inch = 15.5*8.9 cm
Distance from eye	20 cm	25 cm	25 cm	10 cm
Angles of monitor vs eye mouse	45° along axis	30° horizontal and –20° to +30° vertical	(+/–) 38° horiz and 31° vertical	
Blank period	1.4-1.9 sec	4 sec	4-6 sec	4 sec
Cycle per degree (spatial frequency)	0.035	0.05	0.05	0.01 sf == 0.003 cycles per pixel
Cycle per second (temporal frequency Hz)	2 cycles/sec	1Hz	1Hz	1Hz
Nb of directions of drifting gratings	8	8	8	8
Duration of drifting sinusoidal gratings	0.9-1.5 sec	4 sec	4 sec	4 sec
Repetitions of each direction	6	5		
Other comments	100% contrast, 60Hz refresh rate	Optimal grating stimuli = duration 2 sec seperated by 4 sec blank period	0.7 sec before visual stimuli for Fo	Gratingsize = 3600

2. History of fiber-based endoscope

Without a doubt, Medicine is at the origin of many technological breakthrough. The human body is not transparent and at a time, open and close it to safely observe organs was not an easy task. In 1805, Philip Bozzini was the frontrunner of the endoscope. To observe pharynx or rectum, he used a candle and a mirror to guide the light towards deep areas, called the "lichleiter". In 1853, Antonin Jean Desormeaux refined the light source using alcohol and terpentine for providing superior illumination, a mirror to reflect the light and, a condenser lens to raise up the intensity of distribution of the illumination. He was the first to use the term "endoscopy". The first advantages of endoscope lie on (1) easier operating (2) minimization of the pain (3) decreasing size of the system. The first laparoscopy was performed in animal (dog) by Georg Kelling in 1901 and humain patient by Hand Christian Jacobaeus ten years later. In 1948, Harold Hopkins developed zoom lens to reach wider FOV and also created a bundle of glass fibers for better imaging transmission with Narinder Singh Kapany, in 1954 given birth to the first-named fiberscope. In 1956, Basil Hirschowitz and Larry Curtis replaced glass by a more flexible optical fiber (**Fig. Annex 2**.). In 1959, Harold Hopkins created rod-lens system (<5mm). Later, the endoscope is best known to be attached to a camera or video system since 1987. The first report of 3D endoscopic system was published in 1993 by Becker *et al.* Using fiberscope to access deep tissue is daily use in Medicine; for example, to observe human vocal chords through the nose without damaging the body or required anaesthesia, helping the diagnosis of any oral communication troubles prior to decide on the need for heavy surgery or not. Not only for imaging but also for manipulating cells thanks to optogenetic discovery since 2005, microendoscopy using fiber are still evolving. The undeniable advantage is the flexibility of the system that allows awake freely-behaving experiments with small animals such as rodents but also non-human primates such as macaque. Fundamental research laboratories are still working on improving the system to better, faster, stronger microendoscopy (respectively resolution, acquisition rate, optical components).

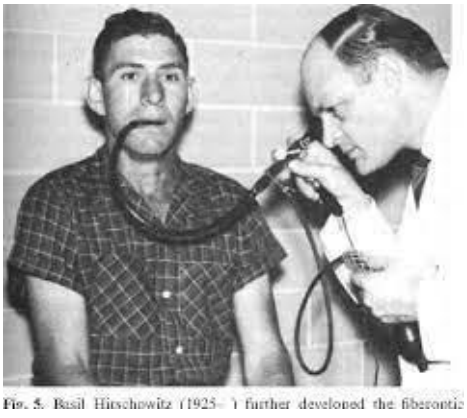

Fig. 5. Basil Hirschowitz (1925–) further developed the fiberoptic

Fig. Annex 2. Fiberscope back in the days for medical use by Hirschowitz (1956)

3. *Implant attempts*

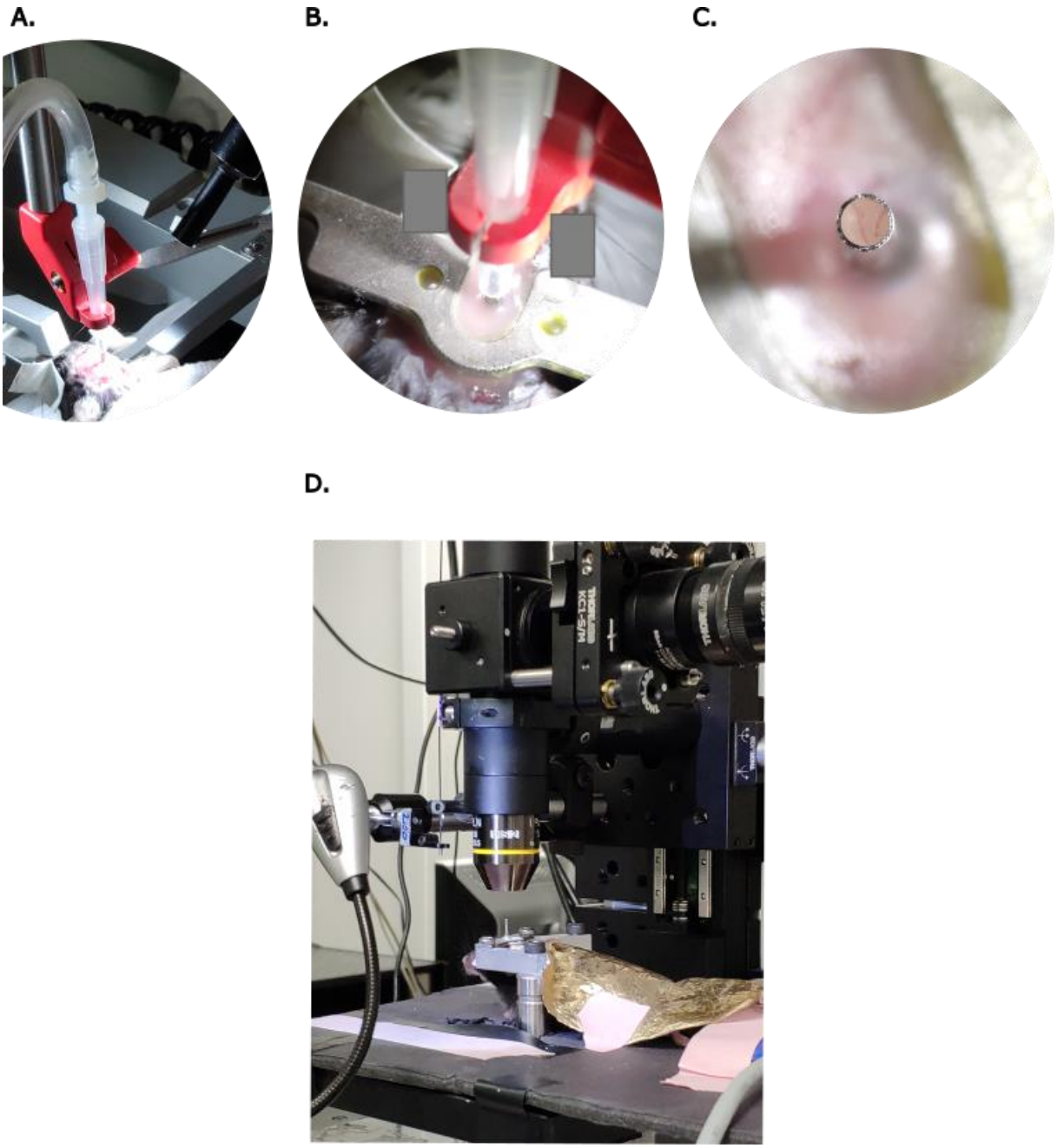

Fig. Annex 3. Implant surgery attempt procedure

A. After craniotomy, GRIN lens is maintained in a custom-tube with negative air pressure
B. Sliding the implant at the willing depth with the z axis of the stereotaxic frame and glue it
C. After waiting few minutes to stabilize the implant, stop the air pressure and check the transparency of the window; here we could visualize blood vessels through the GRIN lens
D. Place the animal under 2P-FENDO with the help of headplate support

VIII. REFERENCES

Accanto N, Chen IW, Ronzitti E, Molinier C, Tourain C, Papagiakoumou E, Emiliani V. Multiplexed temporally focused light shaping through a gradient index lens for precise in-depth optogenetic photostimulation. **Sci Rep.** 9(1):7603 (2019).

Accanto N., Molinier C., Tanese D., Ronzitti E., Newman ZL, Wyart C., Isacoff E., Papagiakoumou E, and Emiliani V. Multiplexed temporally focused light shaping for high-resolution multi-cell targeting. **Optica** 5, 1478-1491 (2018).

Adamantidis AR, Zhang F, Aravanis AM, Deisseroth K, de Lecea L. Neural substrates of awakening probed with optogenetic control of hypocretin neurons. **Nature**. 450(7168):420-4 (2007).

Adamantidis, A., Zhang, F., Aravanis, A. *et al.* Neural substrates of awakening probed with optogenetic control of hypocretin neurons. **Nature** 450, 420–424 (2007).

Aharoni D, Hoogland TM. Circuit Investigations with Open-Source Miniaturized Microscopes: Past, Present and Future**. Front Cell Neurosci.**13:141 (2019)

Ainsworth M, Lee S, Cunningham MO, Traub RD, Kopell NJ, Whittington MA. Rates and rhythms: a synergistic view of frequency and temporal coding in neuronal networks. **Neuron**.75(4):572-83 (2012)

Akerboom J. Optimization of a GCaMP calcium indicator for neural activity imaging. **Journal of Neuroscience** (2012).

Allegra M, Posani L, Gómez-Ocádiz R, Schmidt-Hieber C. Differential Relation between Neuronal and Behavioral Discrimination during Hippocampal Memory Encoding. **Neuron**. 108(6):1103-1112.e6 (2020)

Andrasfalvy BK, Zemelman BV, Tang J, Vaziri A. Two-photon single-cell optogenetic control of neuronal activity by sculpted light**. Proc Natl Acad Sci U S A.** 107(26):11981-6 (2010).

Antonini A, Sattin A, Moroni M, Bovetti S, Moretti C, Succol F, Forli A, Vecchia D, Rajamanickam VP, Bertoncini A, Panzeri S, Liberale C, Fellin T. Extended field-of-view ultrathin microendoscopes for high-resolution two-photon imaging with minimal invasiveness. **Elife**. (2020)

Aoyagi Y., Kawakami R., Osanai H., Hibi T., Nemoto T. A Rapid Optical Clearing Protocol Using 2,2′-Thiodiethanol for Microscopic Observation of Fixed Mouse Brain. **PlosOne** (2015)

Aravanis AM, Wang LP, Zhang F, Meltzer LA, Mogri MZ, Schneider MB, Deisseroth K. An optical neural interface: in vivo control of rodent motor cortex with integrated fiberoptic and optogenetic technology. **J Neural Eng** 4(3): S143-56 (2007).

Attardo A, Fitzgerald JE, Schnitzer MJ. Impermanence of dendritic spines in live adult CA1 hippocampus. **Nature** 523(7562):592-6 (2015).

Bègue A., Papagiakoumou E. et al. Two-photon excitation in scattering media by spatiotemporally shaped beams and their application in optogenetic stimulation. **Biomed. Opt. Express** 4, 2869-2879 (2013).

Baker CA, Elyada YM, Parra A, Bolton MM. Cellular resolution circuit mapping with temporal-focused excitation of soma-targeted channelrhodopsin. **eLife.** 5 e14193 (2016).

Barbera G, Liang B, Zhang L, Gerfen CR, Culurciello E, Chen R, Li Y, Lin DT. Spatially Compact Neural Clusters in the Dorsal Striatum Encode Locomotion Relevant Information. **Neuron** 92(1):202-213 (2016).

Barretto RP, Messerschmidt B, Schnitzer MJ. In vivo fluorescence imaging with high-resolution microlenses. **Nat Methods**. 6(7):511-2 (2009)

Bègue A, Papagiakoumou E, Leshem B, Conti R, Enke L, Oron D, Emiliani V. Two-photon excitation in scattering media by spatiotemporally shaped beams and their application in optogenetic stimulation. **Biomed Opt Express**. 4(12) 2869-79 (2013).

Beier KT, Saunders A, Oldenburg IA, Miyamichi K, Akhtar N, Luo L, Whelan SP, Sabatini B, Cepko CL. Anterograde or retrograde transsynaptic labeling of CNS neurons with vesicular stomatitis virus vectors. **Proc Natl Acad Sci U S A.** .108(37):15414-9 (2011)

Betley JN, Xu S, Cao ZFH, *et al.* Neurons for hunger and thirst transmit a negative-valence teaching signal. **Nature** ;521(7551):180-185 (2015)

Beyeler A, Eckhardt CA, Tye KM. Deciphering memory function with optogenetics. **Prog Mol Biol Transl Sci.**122:341-90 (2014)

Bocarsly ME, Jiang WC, Wang C, Dudman JT, Ji N, Aponte Y. Minimally invasive microendoscopy system for in vivo functional imaging of deep nuclei in the mouse brain. **Biomed Opt Express**.4546-56 (2015).

Bohil CJ, Alicea B, Biocca FA. Virtual reality in neuroscience research and therapy. **Nat Rev Neurosci**. 752-62 (2011).

Boyden, E., Zhang, F., Bamberg, E. *et al.* Millisecond-timescale, genetically targeted optical control of neural activity. ***Nat Neurosci* 8,** 1263–1268 (2005)

Cai, D., Aharoni, D., Shuman, T. *et al.* A shared neural ensemble links distinct contextual memories encoded close in time. **Nature** 534**,** 115–118 (2016)

Carrillo-Reid L, Yang W, Bando Y, Peterka DS, Yuste R. Imprinting and recalling cortical ensembles. **Science**. 353(6300):691-4 (2016)

Carrillo-Reid L, Yuste R. Playing the piano with the cortex: role of neuronal ensembles and pattern completion in perception and behavior**. Curr Opin Neurobiol**. 10.1016/j.conb.03.014. (2020) **Epub** 10 (2020)

Chen G, King JA, Lu Y, Cacucci F, Burgess N. Spatial cell firing during virtual navigation of open arenas by head-restrained mice. **Elife** ;7: e34789 (2018)

Chen IW, Papagiakoumou E, Emiliani V. Towards circuit optogenetics. **Curr Opin Neurobiol**. 50:179-189 (2018)

Chen IW, Ronzitti E., Lee BR., Daigle TL, Dalkara D; Zeng H., Emiliani V., Papagiakoumou E. *In Vivo* Submillisecond Two-Photon Optogenetics with Temporally Focused Patterned Light. **Journal of Neuroscience,** 39 (18) 3484-3497 (2019)

Chen TW, Wardill TJ, Sun Y, Pulver SR, Renninger SL, Baohan A, Schreiter ER, Kerr RA, Orger MB, Jayaraman V, Looger LL, Svoboda K, Kim DS. Ultrasensitive fluorescent proteins for imaging neuronal activity. **Nature**. 499(7458):295-300 (2013)

Corder G, Ahanonu B, Grewe BF, Wang D, Schnitzer MJ, Scherrer G. An amygdalar neural ensemble that encodes the unpleasantness of pain**. Science**. 363(6424):276-281 (2019)

Cossart R., Operational hub cells: a morpho-physiologically diverse class of GABAergic neurons united by a common function. **Current Opinion in Neurobiology**. Volume 26, p51-56 (2014)

Dalgleish HW, Russell LE, Packer AM, Roth A, Gauld OM, Greenstreet F, Thompson EJ, Häusser M. How many neurons are sufficient for perception of cortical activity? **Elife**. 9: e58889 (2020)

Dana H, Chen TW, Hu A, Shields BC, Guo C, Looger LL, Kim DS, Svoboda K. Thy1-GCaMP6 transgenic mice for neuronal population imaging in vivo. **PLoS One** ;9(9) : e108697 (2014)

Dana H, Mohar B, Sun Y, et al. Sensitive red protein calcium indicators for imaging neural activity. ***Elife*** 5:e12727 (2016)

Dana, H., Sun, Y., Mohar, B. *et al.* High-performance calcium sensors for imaging activity in neuronal populations and microcompartments. **Nat Methods** 16, 649–657 (2019)

Deisseroth K. Optogenetics. **Nature Methods** 8, 26-9 (2011)

Denk W, Strickler JH, Webb WW. Two-photon laser scanning fluorescence microscopy. **Science**. 248(4951):73-6. (1990)

Dombeck DA, Harvey CD, Tian L, Looger LL, Tank DW. Functional imaging of hippocampal place cells at cellular resolution during virtual navigation. **Nat Neurosci.** 13(11):1433-40. (2010)

Douglass AM, Kucukdereli H, Ponserre M, Markovic M, Gründemann J, Strobel C, Alcala Morales PL, Conzelmann KK, Lüthi A, Klein R. Central amygdala circuits modulate food consumption through a positive-valence mechanism. **Nat Neurosci.**;20(10):1384-1394 (2017)

Dussaux C, Szabo V, Chastagnier Y, Fodor J, Léger JF, Bourdieu L, Perroy J, Ventalon C. Fast confocal fluorescence imaging in freely behaving mice. **Sci Rep**.8(1):16262. (2018)

Emiliani V., Cohen AE., Deisseroth K. and Michael Häusser. All Optical interrogation of neural circuits. **Journal of Neuroscience** 35 (41) 13917-13926 (2015).

Ernst O, Murcia P, Daldrop P, Tsunoda S, Kateriya S, and Hegemann P. Photoactivation of channelrhodopsin. **J. Biol. Chem.** 283, 1637–1643 (2008)

Fan, J.L., Rivera, J.A., Sun, W. *et al.* High-speed volumetric two-photon fluorescence imaging of neurovascular dynamics. **Nat Commun** 11, 6020 (2020).

Feldbauer K., Zimmermann D., Pintschovius V., Spitz J., Bamann C., Bamberg E. Channelrhodopsin-2 is a leaky proton pump. **Proceedings of the National Academy of Sciences** 106 (30) 12317-12322 (2009)

Flusberg BA, Cocker ED, Piyawattanametha W, Jung JC, Cheung EL, Schnitzer MJ. Fiber-optic fluorescence imaging. **Nat Methods**. 5;2(12):941-50(2005)

Flusberg BA, Nimmerjahn A, Cocker ED, Mukamel EA, Barretto RP, Ko TH, Burns LD, Jung JC, Schnitzer MJ. High-speed, miniaturized fluorescence microscopy in freely moving mice. **Nat Methods**. 5(11):935-8 (2008)

Forli A, Vecchia D, Binini N, Succol F, Bovetti S, Moretti C, Nespoli F, Mahn M, Baker CA, Bolton MM, Yizhar O, Fellin T. Two-Photon Bidirectional Control and Imaging of Neuronal Excitability with High Spatial Resolution In Vivo. **Cell Rep**. 22(11):3087-3098 (2018)

Gardner TJ. An open source, wireless capable miniature microscope system**. J Neural Eng**.14(4):045001. (2017)

Ghosh KK, Burns LD, Cocker ED, Nimmerjahn A, Ziv Y, Gamal AE, Schnitzer MJ. Miniaturized integration of a fluorescence microscope. **Nat Methods**. 8(10):871-8 (2011)

Ginlünas L., Juškaitis R., S.V. Shatalin. Scanning fibre-optic microscope. **Electron Lett.** Vol 27 724-726 (1991)

Goltstein, P. M., Montijn, J. S., and Pennartz, C. M. Effects of isoflurane anesthesia on ensemble patterns of Ca2+ activity in mouse v1: reduced direction selectivity independent of increased correlations in cellular activity. **PLoS ONE** (2015)

Goto Y, Nakajima K, Matsui T, Kurashima T, and Yamamoto F, Influence of Cladding Thickness on Transmission Loss and its Relationship With Multicore Fiber Structure. **J. Lightwave Technol.** 33, 4942-4949 (2015)

Grynkiewicz G, Poenie M, Tsien RY. A new generation of Ca2+ indicators with greatly improved fluorescence properties. **J Biol Chem**. 260(6):3440-50. (1985)

Guido W. Development, form, and function of the mouse visual thalamus. **J Neurophysiol.** 120(1):211-225 (2018)

Haery L, Deverman BE, Matho KS, Cetin A, Woodard K, Cepko C, Guerin KI, Rego MA, Ersing I, Bachle SM, Kamens J and Fan M Adeno-Associated Virus Technologies and Methods for Targeted Neuronal Manipulation. **Front. Neuroanat.** 13:93 (2019)

Havenith, M. N. *et al.* The Virtual-Environment Foraging task enables rapid training and single-trial metrics of attention in head-fixed mice. **Scientific Reports** 8(17371) (2018).

Hayashi, Y., Tagawa, Y., Yawata, S., Nakanishi, S. and Funabiki, K. Spatio-temporal control of neural activity *in vivo* using fluorescence microendoscopy. **European Journal of Neuroscience**, 36: 2722-2732 (2012)

Helmchen, F et al. "Calcium dynamics associated with a single action potential in a CNS presynaptic terminal." ***Biophysical journal*** **vol**. 72, 1458-71 (1997)

Helmchen F, Fee MS, Tank DW, Denk W. A miniature head-mounted two-photon microscope. high-resolution brain imaging in freely moving animals. **Neuron**. 31(6):903-12 (2001)

Helmchen F, Denk W. Deep tissue two-photon microscopy. **Nat Methods**. 2005 2(12):932-40 (2005)

Helmchen F, Denk W, Kerr JN. Miniaturization of two-photon microscopy for imaging in freely moving animals. **Cold Spring Harb Protoc**. (10):904-13 (2013)

Hermes D, Kasteleijn-Nolst Trenité DGA, Winawer J. Gamma oscillations and photosensitive epilepsy. **Curr Biol**. ;27(9): R336-R338 (2017)

Hernandez, O., Papagiakoumou, E., Tanese, D. *et al.* Three-dimensional spatiotemporal focusing of holographic patterns. **Nat Commun** 7, 11928 (2016).

Hires SA, Tian L, Looger LL. Reporting neural activity with genetically encoded calcium indicators. ***Brain Cell Biol.*** 36(1-4):69-86. (2008)

Hontani Y, Xia F, Xu C. Multicolor three-photon fluorescence imaging with single-wavelength excitation deep in mouse brain. **Sci Adv**. 7(12): eabf3531(2021)

Horton, N., Wang, K., Kobat, D. *et al. In vivo* three-photon microscopy of subcortical structures within an intact mouse brain. ***Nature Photon*** **7,** 205–209 (2013).

Hubel DH, Wiesel TN. Receptive fields, binocular interaction and functional architecture in the cat's visual cortex. **J Physiol. ;**160(1) :106-54 (1962)

Huber D., Petreanu L., Ghitani N. *et al.* Sparse optical microstimulation in barrel cortex drives learned behaviour in freely moving mice. ***Nature*** **451,** 61–64 (2008)

Iwai Y, Honda S, Ozeki H, Hashimoto M, Hirase H. A simple head-mountable LED device for chronic stimulation of optogenetic molecules in freely moving mice. **Neurosci Res**.;70(1):124-7 (2011)

Ji N, Milkie DE, Betzig E. Adaptive optics via pupil segmentation for high-resolution imaging in biological tissues. **Nat Methods**. 7(2):141-7 (2010)

Ji N., The Practical and Fundamental Limits of Optical Imaging in Mammalian Brains. **Neuron**, VOLUME 83, ISSUE 6, P1242-1245 (2014)

Ji N, Freeman J, Smith SL. Technologies for imaging neural activity in large volumes. **Nat Neurosci**. 19(9):1154-64. (2016)

Katona G, Szalay G, Maák P, Kaszás A, Veress M, Hillier D, Chiovini B, Vizi ES, Roska B, Rózsa B. Fast two-photon in vivo imaging with three-dimensional random-access scanning in large tissue volumes. **Nat Methods**.9(2):201-8. (2012)

Kerschensteiner D, Guido W. Organization of the dorsal lateral geniculate nucleus in the mouse. **Vis Neurosci.** ;34:E008 (2017)

Khorana HG, Knox BE, Nasi E, Swanson R, Thompson DA. Expression of a bovine rhodopsin gene in Xenopus oocytes: demonstration of light-dependent ionic currents. **Proc Natl Acad Sci U S A.**;85(21):7917-21 (1988)

Kleinfeld D, Mitra PP, Helmchen F, Denk W. Fluctuations and stimulus-induced changes in blood flow observed in individual capillaries in layers 2 through 4 of rat neocortex. **Proc Natl Acad Sci USA**. 95(26):15741-6 (1998)

Klioutchnikov, A., Wallace, D.J., Frosz, M.H. *et al.* Three-photon head-mounted microscope for imaging deep cortical layers in freely moving rats. **Nat Methods** 17, 509–513 (2020)

Knöpfel, T. Genetically encoded optical indicators for the analysis of neuronal circuits. ***Nat Rev Neurosci*** 13**,** 687–700 (2012).

Knöpfel T, Song C. Optical voltage imaging in neurons: moving from technology development to practical tool. **Nat Rev Neurosci.** 20(12):719-727 (2019)

Ko H, Hofer SB, Pichler B, Buchanan KA, Sjöström PJ, Mrsic-Flogel TD. Functional specificity of local synaptic connections in neocortical networks. **Nature**.;473(7345):87-91(2011).

LeChasseur Y, Dufour S, Lavertu G, Bories C, Deschênes M, Vallée R, De Koninck Y. A microprobe for parallel optical and electrical recordings from single neurons in vivo. **Nat Methods**. 8(4):319-25. (2011)

Leila Haery *et al.* Adeno-Associated Virus Technologies and Methods for Targeted Neuronal Manipulation. **Front. Neuroanat.** (2019)

Lein ES *et al.* Genome-wide atlas of gene expression in the adult mouse brain. **Nature**. 445(7124):168-76. (2007)

Lin JY. A user's guide to channelrhodopsin variants: features, limitations and future developments. **Exp Physiol.** 96(1):19-25 (2011)

Lin, M. Beyond the rainbow: new fluorescent proteins brighten the infrared scene. **Nat Methods** 8, 726–728 (2011)

Lin MZ, Schnitzer MJ. Genetically encoded indicators of neuronal activity. **Nat Neurosci**. 1142-53. (2016)

Lissek T, Obenhaus HA, Ditzel DA, et al. General Anesthetic Conditions Induce Network Synchrony and Disrupt Sensory Processing in the Cortex. ***Front Cell Neurosci.*** (2016)

Lutz C, Otis TS, DeSars V, Charpak S, DiGregorio DA, Emiliani V. Holographic photolysis of caged neurotransmitters. **Nat Methods**. 5(9):821-7 (2008)

Madisen L, Mao T, Koch H, Zhuo JM, Berenyi A, Fujisawa S, Hsu YW, Garcia AJ 3rd, Gu X, Zanella S, Kidney J, Gu H, Mao Y, Hooks BM, Boyden ES, Buzsáki G, Ramirez JM, Jones AR, Svoboda K, Han X, Turner EE, Zeng H. A toolbox of Cre-dependent optogenetic transgenic mice for light-induced activation and silencing. **Nat Neurosci.** 15(5):793-802. (2012)

Mager T, Lopez de la Morena D, Senn V, Schlotte J, D Errico A, Feldbauer K, Wrobel C, Jung S, Bodensiek K, Rankovic V, Browne L, Huet A, Jüttner J, Wood PG, Letzkus JJ, Moser T, Bamberg E. High frequency neural spiking and auditory signaling by ultrafast red-shifted optogenetics. **Nat Commun**. 9(1):1750 (2018)

Malvaut S, Constantinescu VS, Dehez H, Doric S, Saghatelyan A. Deciphering Brain Function by Miniaturized Fluorescence Microscopy in Freely Behaving Animals. **Front Neurosci**. 14:819 (2020)

Marshel JH, Kaye AP, Nauhaus I, Callaway EM. Anterior-posterior direction opponency in the superficial mouse lateral geniculate nucleus. **Neuron**. 76(4):713-20 (2012)

Marshel JH, Kim YS, Machado TA, Quirin S, Benson B, Kadmon J, Raja C, Chibukhchyan A, Ramakrishnan C, Inoue M, Shane JC, McKnight DJ, Yoshizawa S, Kato HE, Ganguli S, Deisseroth K. Cortical layer-specific critical dynamics triggering perception. **Science**. 365(6453): eaaw5202 (2019)

Meyer CA, Liu XS. Identifying and mitigating bias in next-generation sequencing methods for chromatin biology. **Nat Rev Genet**. 15(11):709-21 (2014)

Mizrahi A., Crowley JC, Shtoyerman E., Katz LC. High-Resolution In Vivo Imaging of Hippocampal Dendrites and Spines. **Journal of Neuroscience,** 24 (13) 3147-3151 (2004)

Moretti C, Antonini A, Bovetti S, Liberale C, Fellin T. Scanless functional imaging of hippocampal networks using patterned two-photon illumination through GRIN lenses. **Biomed Opt Express**. 7(10):3958-3967. (2016)

Moser MB, Rowland DC, Moser EI. Place cells, grid cells, and memory. **Cold Spring Harb Perspect Biol**. 7(2):a021808 (2015)

Moser, E., Moser, MB. & McNaughton, B. Spatial representation in the hippocampal formation: a history. **Nat Neurosci 20**, 1448–1464 (2017).

Mrsic-Flogel TD, Hofer SB, Ohki K, Reid RC, Bonhoeffer T, Hübener M. Homeostatic regulation of eye-specific responses in visual cortex during ocular dominance plasticity. **Neuron**. 54(6):961-72(2007)

Nagel G., Szellas T., Huhn W., Kateriya S., Adeishvili N., Berthold P., Ollig D., Hegemann P., Bamberg E. Channelrhodopsin-2, a directly light-gated cation-selective membrane channel **Proceedings of the National Academy of Sciences**, 100 (24) 13940-13945 (2003)

Niell CM, Stryker MP. Highly Selective Receptive Fields in Mouse Visual Cortex **Journal of Neuroscience** 28 (30) 7520-7536 (2008)

Nieman, B. J., van Eede, M. C., Spring, S., Dazai, J., Henkelman, R. M., & Lerch, J. P. MRI to assess neurological function. **Current Protocols in Mouse Biology**, 8, e44 (2018)

Nikolic, K., Grossman, N., Grubb, M.S., Burrone, J., Toumazou, C. and Degenaar, P. Photocycles of Channelrhodopsin-2. Photochemistry and Photobiology, 85: 400-411 (2009)

Oheim M, Beaurepaire E, Chaigneau E, Mertz J, Charpak S. Two-photon microscopy in brain tissue: parameters influencing the imaging depth. **J Neurosci Methods**. 111(1):29-37(2001).

Oron D, Silberberg Y. Spatiotemporal coherent control using shaped, temporally focused pulses. **Opt Express**. 13(24):9903-8 (2005)

Ouzounov DG, Wang T, Wang M, Feng DD, Horton NG, Cruz-Hernández JC, Cheng YT, Reimer J, Tolias AS, Nishimura N, Xu C. In vivo three-photon imaging of activity of GCaMP6-labeled neurons deep in intact mouse brain. **Nat Methods**. 14(4):388-390 (2017)

Ozbay BN, Futia GL, Ma M, Bright VM, Gopinath JT, Hughes EG, Restrepo D, Gibson EA. Three dimensional two-photon brain imaging in freely moving mice using a miniature fiber coupled microscope with active axial-scanning. **Sci Rep**. 8(1):8108. (2018)

Packer, Adam M et al. "Simultaneous all-optical manipulation and recording of neural circuit activity with cellular resolution in vivo." ***Nature methods*** **vol**. 12,2 (2015): 140-6.

Papagiakoumou E, Anselmi F, Bègue A, de Sars V, Glückstad J, Isacoff EY, Emiliani V. Scanless two-photon excitation of channelrhodopsin-2. **Nat Methods.** 7(10):848-54. (2010)

Papagiakoumou E, de Sars V, Emiliani V, Oron D. Temporal focusing with spatially modulated excitation. **Opt Express**. 17(7) :5391-401. (2009)

Papagiakoumou, E., Bègue, A., Leshem, B. *et al.* Functional patterned multiphoton excitation deep inside scattering tissue. ***Nature Photon* 7,** 274–278 (2013)

Papagiakoumou E., Ronzitti E., Chen IW, Gajowa M., Picot A. Emiliani V. Two-Photon Optogenetics by Computer-Generated Holography in Book "Optogenetic Roadmap". **Springer Protocols** 2018

Pastor WA, Pape UJ, Huang Y, Henderson HR, Lister R, Ko M, McLoughlin EM, Brudno Y, Mahapatra S, Kapranov P, Tahiliani M, Daley GQ, Liu XS, Ecker JR, Milos PM, Agarwal S, Rao A. Genome-wide mapping of 5-hydroxymethylcytosine in embryonic stem cells. **Nature**. 473(7347):394-7 (2011)

Pégard NC, Mardinly AR, Oldenburg IA, Sridharan S, Waller L, Adesnik H. Three-dimensional scanless holographic optogenetics with temporal focusing (3D-SHOT). **Nat Commun** 8(1):1228 (2017)

Picot A, Dominguez S, Liu C, Chen IW, Tanese D, Ronzitti E, Berto P, Papagiakoumou E, Oron D, Tessier G, Forget BC, Emiliani V. Temperature Rise under Two-Photon Optogenetic Brain Stimulation. **Cell Rep.** 24(5):1243-1253 (2018)

Prakash R, Yizhar O, Grewe B, Ramakrishnan C, Wang N, Goshen I, Packer AM, Peterka DS, Yuste R, Schnitzer MJ, Deisseroth K. Two-photon optogenetic toolbox for fast inhibition, excitation and bistable modulation. **Nat Methods**. 9(12):1171-9. (2012)

Prasher DC, Eckenrode VK, Ward WW, Prendergast FG, Cormier MJ. Primary structure of the Aequorea victoria green-fluorescent protein. **Gene**. 111(2):229-33. (1992)

Reutsky-Gefen I, Golan L, Farah N, Schejter A, Tsur L, Brosh I, Shoham S. Holographic optogenetic stimulation of patterned neuronal activity for vision restoration. **Nat Commun**. 4:1509 2013)

Rickgauer JP, Deisseroth K, Tank DW. Simultaneous cellular-resolution optical perturbation and imaging of place cell firing fields. **Nat Neurosci** 17(12):1816-24 (2014)

Robinson NTM, Descamps LAL, Russell LE, Buchholz MO, Bicknell BA, Antonov GK, Lau JYN, Nutbrown R, Schmidt-Hieber C, Häusser M. Targeted Activation of Hippocampal Place Cells Drives Memory-Guided Spatial **Behavior. Cell**. 183(6):1586-1599.e10.(2020)

Romoser VA, Hinkle PM, Persechini A. Detection in living cells of Ca2+-dependent changes in the fluorescence emission of an indicator composed of two green fluorescent protein variants linked by a calmodulin-binding sequence. A new class of fluorescent indicators. **J Biol Chem**. 272(20):13270-4 (1997)

Ronzitti E., Conti R. *et al.* Submillisecond Optogenetic Control of Neuronal Firing with Two-Photon Holographic Photoactivation of Chronos. **J. Neuro.** (2017)

Ronzitti, E., Ventalon, C., Canepari, M., Forget B. & Papagiakoumou E. and Emiliani, V. Recent advances in patterned photostimulation for optogenetics. **Journal of Optics.** 19. 2040-8986 (2017)

Roth MM, Dahmen JC, Muir DR, Imhof F, Martini FJ, Hofer SB. Thalamic nuclei convey diverse contextual information to layer 1 of visual cortex. **Nat Neurosci.** 19(2):299-307 (2016)

Russell Lloyd E., Yang Zidan, Pei Lynn Tan, Fişek Mehmet, Packer Adam M., Dalgleish Henry W.P., Chettih Selmaan , Harvey Christopher D. and Häusser Michael . The influence of visual cortex on perception is modulated by behavioural state. bioRxiv (2019)

Russell Lloyd E., Dalgleish Henry W. P., Nutbrown Rebecca, Gauld Oliver M., Herrmann Dustin, Fişek Mehmet, Packer Adam M., Häusser Michael. All-optical interrogation of neural circuits in behaving mice. **bioRxiv** (2021)

Sawinski J, Wallace DJ, Greenberg DS, Grossmann S, Denk W, Kerr JN. Visually evoked activity in cortical cells imaged in freely moving animals. **Proc Natl Acad Sci U S A**. 106(46):19557-62. (2009)

Schmidt-Hieber C, Häusser M. Cellular mechanisms of spatial navigation in the medial entorhinal cortex. **Nat Neurosci**. 16(3):325-31. (2013)

Schneider F, Grimm C, Hegemann P. Biophysics of Channelrhodopsin. Annu Rev Biophys. 2015; 44:167-86.

Schneider-Warme, F. The power of optogenetics. ***Herzschr Elektrophys*** 29, 24–29 (2018).

Schwenkgrub J, Harrell ER, Bathellier B, Bouvier J. Deep imaging in the brainstem reveals functional heterogeneity in V2a neurons controlling locomotion. **Sci Adv**. 6(49): eabc6309. (2020)

Seibel EJ, Smithwick QY. Unique features of optical scanning, single fiber endoscopy**. Lasers Surg Med**. 30(3):177-83 (2002)

Shemesh OA *et al.* Precision Calcium Imaging of Dense Neural Populations via a Cell-Body-Targeted Calcium Indicator. **Neuron**. 107(3):470-486.e11 (2020)

Shemesh OA, Tanese D, Zampini V, Linghu C, Piatkevich K, Ronzitti E, Papagiakoumou E, Boyden ES, Emiliani V. Temporally precise single-cell-resolution optogenetics. **Nat Neurosci.** 20(12):1796-1806 (2017)

Shimomura O. The discovery of aequorin and green fluorescent protein. **J Microsc.** 217(Pt 1):1-15(2005)

Speed, A., Del Rosario, J., Mikail, N. *et al.* Spatial attention enhances network, cellular and subthreshold responses in mouse visual cortex. ***Nat Commun*** 11**,** 505 (2020).

Sridharan S., Gajowa M., Ogando MB, Jagadisan U, Abdeladim L., Sadahiro M., Bounds H., Hendricks WD, Tayler I., Gopakumar K., Oldenburg IA, Brohawn SG, Adesnik H. High performance microbial opsins for spatially and temporally precise perturbations of large neuronal networks **bioRxiv** 04.01.438134 (2021)

Srivastava A. In vivo tissue-tropism of adeno-associated viral vectors. **Curr Opin Virol.** 21:75-80 (2016)

Stringer C. Michaelos M., Tsyboulski D., Lindo SE, Pachitariu M. High precision coding in visual cortex. **Cell** 184 (10): 2767-2778.e15 (2021)

Subach OM, Sotskov VP, Plusnin VV, *et al.* Novel Genetically Encoded Bright Positive Calcium Indicator NCaMP7 Based on the mNeonGreen Fluorescent Protein**. Int J Mol Sci.** 21(5) :1644 (2020)

Sun W, Tan Z, Mensh BD, Ji N. Thalamus provides layer 4 of primary visual cortex with orientation- and direction-tuned inputs. **Nat Neurosci.** 19(2):308-15 (2016)

Szabo V, Ventalon C, De Sars V, Bradley J, Emiliani V. Spatially selective holographic photoactivation and functional fluorescence imaging in freely behaving mice with a fiberscope. **Neuron** (2014)

Theis L, Berens P, Froudarakis E, Reimer J, Román Rosón M, Baden T, Euler T, Tolias AS, Bethge M. Benchmarking Spike Rate Inference in Population Calcium Imaging. **Neuron** 90(3):471-82 (2016)

Thurley K, Ayaz A. Virtual reality systems for rodents. ***Curr Zool.*** 63(1):109-119 (2017)

Tian, L., Hires, S., Mao, T. *et al.* Imaging neural activity in worms, flies and mice with improved GCaMP calcium indicators. ***Nat Methods*** 6**,** 875–881 (2009)

Tyree SM, de Lecea L. Optogenetic Investigation of Arousal Circuits. **Int J Mol Sci.** 18(8):1773 (2017)

Vance, M. A., Mitchell, A., and Samulski, R. J. Gene Therapy - Principles and Challenges. **IntechOpen** (2015)

Vanderver A, Hathout Y, Maletkovic J, Gordon ES, Mintz M, Timmons M, Hoffman EP, Horzinski L, Niel F, Fogli A, Boespflug-Tanguy O, Schiffmann R. Sensitivity and specificity of decreased CSF asialotransferrin for eIF2B-related disorder. **Neurology** 70(23):2226-32 (2008)

Villette V, Chavarha M, Dimov IK, Bradley J, Pradhan L, Mathieu B, Evans SW, Chamberland S, Shi D, Yang R, Kim BB, Ayon A, Jalil A, St-Pierre F, Schnitzer MJ, Bi G, Toth K, Ding J, Dieudonné S, Lin MZ. Ultrafast Two-Photon Imaging of a High-Gain Voltage Indicator in Awake Behaving Mice. **Cell**. 179(7):1590-1608.e23 (2019)

Vo-Dinh, T. Biomedical photonics: Handbook. (2003).

Wang C, Ji N. Characterization and improvement of three-dimensional imaging performance of GRIN-lens-based two-photon fluorescence endomicroscopes with adaptive optics. **Opt Express**. 21(22):27142-54 (2013)

Wang C, Liu R, Milkie DE, Sun W, Tan Z, Kerlin A, Chen TW, Kim DS, Ji N. Multiplexed aberration measurement for deep tissue imaging in vivo. **Nat Methods**. 11(10):1037-40 (2014)

Wang T, Ouzounov DG, Wu C, Horton NG, Zhang B, Wu CH, Zhang Y, Schnitzer MJ, Xu C. Three-photon imaging of mouse brain structure and function through the intact skull. **Nat Methods.** 15(10):789-792 (2018)

Wang T. and Xu C. Three-photon neuronal imaging in deep mouse brain. **Optica** 7, 947-960 (2020)

Watakabe A, Ohtsuka M, Kinoshita M, Takaji M, Isa K, Mizukami H, Ozawa K, Isa T, Yamamori T. Comparative analyses of adeno-associated viral vector serotypes 1, 2, 5, 8 and 9 in marmoset, mouse and macaque cerebral cortex. **Neurosci Res** 93:144-57 (2015)

Xu Y, Zou P, Cohen AE. Voltage imaging with genetically encoded indicators. **Curr Opin Chem Biol**. 39:1-10 (2017)

Xu Yongxian, Peng Zou and Adam E. Cohen, Voltage imaging with Genetically Encoded Indicators. **Current Opinion Chem. Biol.** (2017)

Yaroslavsky AN, Schulze PC, Yaroslavsky IV, Schober R, Ulrich F, Schwarzmaier HJ. Optical properties of selected native and coagulated human brain tissues in vitro in the visible and near infrared spectral range. **Phys Med Biol**. 47(12):2059-73. (2002)

Zemelman BV, Lee GA, Ng M, Miesenböck G. Selective photostimulation of genetically chARGed neurons. **Neuron**. 33(1):15-22 (2002)

Zhang, T. *et al.* Kilohertz two-photon brain imaging in awake mice. ***Nat. Methods*** 16, 1119–1122 (2019)

Zheng C., Baum B.J. Evaluation of Promoters for Use in Tissue-Specific Gene Delivery. In: Le Doux J.M. (eds) **Gene Therapy Protocols**. Methods in Molecular Biology™, vol 434. Humana Press (2008)

Zhu G, van Howe J, Durst M, Zipfel W, Xu C. Simultaneous spatial and temporal focusing of femtosecond pulses. **Opt Express** 13(6):2153-9 (2005)

Zipfel WR, Williams RM, Webb WW. Nonlinear magic: multiphoton microscopy in the biosciences. **Nat Biotechnol**. 21(11):1369-77 (2003)

Zong W, Wu R, Li M, Hu Y, Li Y, Li J, Rong H, Wu H, Xu Y, Lu Y, Jia H, Fan M, Zhou Z, Zhang Y, Wang A, Chen L, Cheng H. Fast high-resolution miniature two-photon microscopy for brain imaging in freely behaving mice. **Nat Methods**. 14(7):713-719 (2017)

Zuend M, Saab AS, Wyss MT, Ferrari KD, Hösli L, Looser ZJ, Stobart JL, Duran J, Guinovart JJ, Barros LF, Weber B. Arousal-induced cortical activity triggers lactate release from astrocytes. **Nat Metab**. 2(2):179-191 (2020)

HOLOGRAPHIC INVESTIGATION OF VISUAL CIRCUITS

"Proof-of-concept of a new flexible two-photon microendoscopy system for all-optical interrogation of neuronal circuits for freely-moving animals"

Abstract

Understanding how the brain encodes information is one of the grand challenges of our times. Over the past decades, Neuroscience has made exponential progress towards neural communication. Geneticists developed light-activated microbial proteins "opsin" to manipulate it. Optogenetic enables us to drive and read neural circuits and determine how it gives rise to sensation, perception, and cognitive function.

To decipher the neural code, it is necessary to have a closer look at how individual neurons in the circuits collaborate to establish behaviour. To reach such fine resolution and to mimic activity at the millisecond scale, V. Emiliani's lab has been developing cutting-edge optical tools based on wavefront shaping approaches such as computer-generated holography (Papagiakoumou *et al.* Optic Exp. 2008) to control multiple neurons (Hernandez *et al.* Nature Com. 2016; Accanto, Molinier *et al.* Optica 2018, Chen *et al.* JNeuro. 2019).

Microendoscopes were developed mainly to image neuronal activity in freely-moving rodents (Ghosh *et al.* Nature Met. 2011, Szabo *et al.* Neuron 2014, Aharoni *et al.* Front. C. Neuro. 2019, Helmchen *et al.* Cold Spr. Harb. Prot. 2013, Zong *et al.* Nature Met. 2017, Ozbay *et al.* Sc. Rep. 2018) with single- (1P) and two-photon (2P) approaches. Nevertheless, they presented some limitations. Current systems are limited in imaging speed to 3-40Hz. To cite the most important drawback: with no 2P stimulation at the single cell level. For the brain exploration, precise measurements, and the capability to precisely induce spiking activity in selected cells are essential.

Hence, a new flexible 2P microendoscope "2P-FENDO" was built. We validated *in vivo* morphological imaging of single cells with high axial resolution and two-colour imaging to ~200µm depth in the mouse brain. With jGCaMP7s (Dana *et al.* Nature Met. 2019), we achieved fast activity imaging using 2P imaging (50-100Hz) in large FOV (250*250*200 µm3) and 2P holographic stimulation in freely-moving mice.

Keywords: Neuroscience, optogenetics, calcium imaging, 2P photostimulation, microendoscopy, freely-moving mice

INVESTIGATION HOLOGRAPHIQUE DES CIRCUITS VISUELS

"Preuve de concept d'un nouveau microendoscope deux-photons flexible pour l'étude tout-optique des circuits neuronaux chez les animaux mobiles"

Résumé

Comprendre comment le cerveau code les informations est l'un des grands défis de notre époque. Au cours des dernières décennies, les neurosciences ont fait des progrès exponentiels pour la communication neuronale. Les généticiens ont développé des protéines microbiennes "opsines" activables par la lumière. Ainsi, l'optogénétique permet de lire et contrôler les circuits neuronaux et de déterminer comment ils encodent nos sensations, perceptions et cognition.

Pour décrypter le code neuronal, il est nécessaire d'examiner comment les neurones individuels des circuits collaborent pour établir le comportement. Pour atteindre une résolution fine et imiter l'activité à la milliseconde, le laboratoire de V. Emiliani a développé des outils optiques de pointe basés sur des approches de front d'onde telles que l'holographie générée par ordinateur (Papagiakoumou *et al.* Optic Exp. 2008) pour contrôler de multiples neurones (Hernandez *et al.* Nature Com. 2016 ; Accanto, Molinier *et al.* Optica 2018, Chen *et al.* JNeuro. 2019).

Les microendoscopes ont été développés principalement pour imager l'activité neuronale chez des rongeurs agiles (Ghosh *et al.* Nature Met. 2011, Szabo *et al.* Neuron 2014, Aharoni *et al.* Front. C. Neuro. 2019, Helmchen *et al.* Cold Spr. Harb. Prot. 2013, Zong *et al.* Nature Met. 2017, Ozbay *et al.* Sc. Rep. 2018) avec des approches à un et deux photons. Néanmoins, ses systèmes sont limités en vitesse d'imagerie à 3-40Hz et ne permettent pas de stimulation de cellule unique. Pour l'exploration du cerveau, des mesures précises et la capacité d'induire l'activité sont essentielles.

Un nouveau microendoscope 2P flexible "2P-FENDO" a donc été construit. Nous avons validé l'imagerie *in vivo* bicolore de cellules uniques avec une haute résolution jusqu'à une profondeur de ~200µm dans le cerveau de la souris. Avec jGCaMP7s (Dana *et al.* Nature Met. 2019), l'imagerie 2P rapide est démontrée (50-100Hz) dans un grand champ (250*250*200 µm3) et permet la stimulation holographique chez la souris agile et mobile.

Mots-clés : Neurosciences, optogénétique, imagerie calcique, photostimulation 2P, microendoscope, souris mobile